



# Comparison of API & IEC Standards for Offshore Wind Turbine Applications in the U.S. Atlantic Ocean: Phase II

**March 9, 2009 – September 9, 2009**

A. Jha, D. Dolan, T. Gur, S. Soyoz, and  
C. Alpdogan  
*MMI Engineering*  
*Houston, Texas*

NREL Technical Monitor: Walt Musial

NREL is a national laboratory of the U.S. Department of Energy, Office of Energy Efficiency & Renewable Energy, operated by the Alliance for Sustainable Energy, LLC.

**Subcontract Report**  
NREL/SR-5000-49688  
January 2013

Contract No. DE-AC36-08GO28308

# **Comparison of API & IEC Standards for Offshore Wind Turbine Applications in the U.S. Atlantic Ocean: Phase II**

**March 9, 2009 – September 9, 2009**

A. Jha, D. Dolan, T. Gur, S. Soyoz, and  
C. Alpdogan  
*MMI Engineering  
Houston, Texas*

NREL Technical Monitor: Walt Musial  
Prepared under Subcontract No. LEE-7-66518-01

**NREL is a national laboratory of the U.S. Department of Energy, Office of Energy  
Efficiency & Renewable Energy, operated by the Alliance for Sustainable Energy, LLC.**

**This publication received minimal editorial review at NREL.**

### **NOTICE**

This report was prepared as an account of work sponsored by an agency of the United States government. Neither the United States government nor any agency thereof, nor any of their employees, makes any warranty, express or implied, or assumes any legal liability or responsibility for the accuracy, completeness, or usefulness of any information, apparatus, product, or process disclosed, or represents that its use would not infringe privately owned rights. Reference herein to any specific commercial product, process, or service by trade name, trademark, manufacturer, or otherwise does not necessarily constitute or imply its endorsement, recommendation, or favoring by the United States government or any agency thereof. The views and opinions of authors expressed herein do not necessarily state or reflect those of the United States government or any agency thereof.

Available electronically at <http://www.osti.gov/bridge>

Available for a processing fee to U.S. Department of Energy and its contractors, in paper, from:

U.S. Department of Energy  
Office of Scientific and Technical Information  
P.O. Box 62  
Oak Ridge, TN 37831-0062  
phone: 865.576.8401  
fax: 865.576.5728  
email: <mailto:reports@adonis.osti.gov>

Available for sale to the public, in paper, from:

U.S. Department of Commerce  
National Technical Information Service  
5285 Port Royal Road  
Springfield, VA 22161  
phone: 800.553.6847  
fax: 703.605.6900  
email: [orders@ntis.fedworld.gov](mailto:orders@ntis.fedworld.gov)  
online ordering: <http://www.ntis.gov/help/ordermethods.aspx>

Cover Photos: (left to right) PIX 16416, PIX 17423, PIX 16560, PIX 17613, PIX 17436, PIX 17721



Printed on paper containing at least 50% wastepaper, including 10% post consumer waste.

## List of Acronyms and Abbreviations

API	American Petroleum Institute
BSEE	Bureau of Safety and Environmental Enforcement (formerly Minerals Management Service)
CAP	Capacity Analysis Program
FAST	Fatigue, Aerodynamics, Structures, and Turbulence (software)
IEC	International Electrotechnical Commission
JIP	Joint Industry Project
NREL	National Renewable Energy Laboratory
OCS	U.S. Outer Continental Shelf
OTM	overturning moment
OWT	offshore wind turbine

## List of Symbols

A	Area (projected or cross section)
c	Shear strength of clay
C	Wave celerity
$C_D$	Viscous drag coefficients
$C_{ds}$	Steady state flow drag coefficient at post-critical Reynolds numbers
$C_M$	Inertia coefficient
$C_S$	Shape coefficient
$C_X$	Water height above mean still water at numerical limit for Stream Function theory
$C_Y$	Water height above mean still water at physical limit for wave breaking condition
D	Diameter
$D_{mp}$	Monopile diameter
E	Young's modulus
G	Shear modulus or limit state function
$H_b$	Wave height at the breaking location
$H_{max}$	Maximum wave height
$H_s$	Significant wave height
$H_X$	Wave height at numerical limit for Stream Function wave theory
$H_Y$	Wave height at physical limit for wave breaking condition
I	Moment Inertia
K	Keulegan-Carpenter Number
L	Load
$L_{BW}$	Aerodynamic blade load and the hydrodynamic wave load
$L_{Corr}$	Additional load where a correction to Stream function is warranted
$L_{Slam}$	Wave slam load

$L_{\text{tower}}$	Wind load on the tower
$M$	Bending moment
$M_b$	Base over-turning moment
$M_t$	Tower top over-turning moment
$N$	Axial load
$R_{\text{mp}}$	Radius of the monopile
$R$	Resistance (or capacity)
$t$	Thickness
$T_{\text{max}}$	Zero crossing wave period corresponding to maximum wave height in a storm
$T_z$	Average zero crossing wave period
$u$	Velocity (water particle or wind)
$U_m$	Maximum water particle velocity normal to the cylinder axis
$V$	Displaced volume of the cylinder per unit length
$V$	Shear force
$V_b$	Base shear force
$V_t$	Tower top shear force
$W_s$	Average wind speed
$X_{\text{BW}}$	Model uncertainty and variability for aerodynamic load on blade and hydrodynamic load from drag and inertia from wave particle kinematics acting on the foundation.
$X_{\text{Corr}}$	Model uncertainty for the load correction applied to Stream Wave theory
$X_{\text{Slam}}$	Model uncertainty for slam loads from breaking waves
$X_{\text{Tower}}$	Model uncertainty on tower wind load
$\eta_b$	Maximum elevation of the free water surface above the still water level
$\lambda$	Curling factor
$\rho$	Density (water or air)

## Executive Summary

The National Renewable Energy Laboratory (NREL) contracted MMI Engineering to conduct Phase II of the Joint Industry Project on Comparison of two design standards for offshore wind turbines (OWTs) in the United States Outer Continental Shelf waters. The two standards were the American Petroleum Institute (API) RP – 2A *Recommended Practice for Planning, Designing, and Constructing Fixed Offshore Platforms* and the International Electrotechnical Commission (IEC) 61400-3 *Design Requirements for Offshore Wind Turbines*.

In Phase I, two structure types (a monopile and a tripod) were studied at two sites – offshore Texas at 24-m water depth and offshore Massachusetts at 15-m water depth. This study provided insights into the loads imposed on the structures caused by wind and ocean forces, and also provided insights into the strength (capacity) of the structures subject to these loads. The resulting reliability (annual failure probability for ultimate strength) for the two structures at the two sites were generally governed by turbine and blade resonance avoidance for designing the structure, and not by ultimate strength needs to resist extreme loads. The conclusions drawn from Phase I were based on these limited numbers of case studies. This limitation prompted the need to conduct this second phase to study two new designs, the monopile and a jacket (space frame) substructure, at the same site where ultimate strength would likely also influence design and resonance avoidance.

The site selected for Phase II was the offshore Massachusetts site, but with a water depth of 25 m (instead of 15 m as in Phase I). This selection permitted the use of the same meteorological and oceanographic (metocean) parameters, with the breaking wave criteria altered as a result of the increased water depth.

Preliminary designs for the monopile and the jacket structure were developed based on insights into 50-year loads (for the IEC based design; loads exceeding on average once every 50 years) and 100-year loads (for the API-based design) from Phase I. These two structures were then analyzed carefully to include coupled aerodynamic blade loads and hydrodynamic loads on the support structure, and breaking wave loads in extreme storms. The design was then finalized using these loads to ensure the utilization of the members remained below allowable stress thresholds, according to API and IEC design codes. Once the design was finalized, which resulted in few changes to the preliminary design, the structure was analyzed to calculate its capacity to resist strength failure for operating loads, as well as for loads during 50- and 100-year storm conditions.

The final step of the study was to conduct a reliability analysis to find the annual probability of ultimate strength failure. This step was done by calculating the annual probability of the imposed loads on OWTs that exceed the ultimate strength capacity, including the probability distribution of the key parameters to model their randomness.

The key conclusion upon comparison of API and IEC results reinforced the observations in Phase I, in which the resulting reliabilities from the API and IEC methods were similar for both the monopile and the tripod substructure for ultimate strength failure. Note the reliability against fatigue failure was not the focus of this study or of Phase I. The monopile design was largely driven by resonance avoidance conditions; however, the tripod design was also impacted by consideration of ultimate strength failure.

Further study is recommended on overall system reliability to include fatigue consideration, especially from breaking waves. Another critical recommended step is the development of an acceptable target reliability level for OWTs in U.S. waters, and inclusion of this target reliability via specific partial safety factors for the design guidelines that would include considerations of turbine size, regional hurricane risk, and water depth.

# Table of Contents

<b>List of Acronyms and Abbreviations .....</b>	<b>v</b>
<b>List of Symbols .....</b>	<b>vi</b>
<b>Executive Summary .....</b>	<b>viii</b>
<b>List of Tables .....</b>	<b>xii</b>
<b>List of Figures .....</b>	<b>xiii</b>
<b>1 Introduction.....</b>	<b>1</b>
1.1 Overview.....	1
1.2 Report Structure.....	1
1.3 Background.....	1
1.4 Objective.....	2
<b>2 Methodology .....</b>	<b>4</b>
2.1 Structure Type.....	4
<b>3 Turbine and Site Characterization .....</b>	<b>6</b>
3.1 Turbine Specifications .....	6
3.1.1 Turbine Size.....	6
3.1.2 Tower Properties.....	7
3.1.3 Turbine Operation Requirements.....	8
3.2 Site Location and Water Depth.....	9
3.3 Support Structure Configuration.....	10
3.3.1 Monopile.....	10
3.3.2 Jacket .....	11
3.4 Meteorological and Oceanographic Data.....	13
3.4.1 Breaking Waves.....	16
3.4.2 Metocean Data for the Site .....	16
3.5 Other Site Assumptions .....	17
<b>4 Analysis Methodology .....</b>	<b>18</b>
4.1 Coupled Wave and Wind Load Analyses .....	20
4.1.1 Wind Load on Blades .....	20
4.1.2 Wave Load on Monopile .....	21
4.1.3 Wind Load on Tower.....	22
4.2 Equivalent Monopile Properties for FAST Analyses .....	22
4.3 Coupled Wave and Wind Load Analyses with FAST .....	23
4.4 Breaking Wave Forces.....	24
4.5 Additional Drag and Inertia .....	28
<b>5 Monopile Substructure Analysis.....</b>	<b>30</b>
5.1 Wind and Wave Load Analyses with FAST.....	30
5.2 Total Wind and Wave Load Demand .....	34
5.3 Strength Checks .....	36
5.4 Capacity Analysis .....	38
5.5 Monopile Reliability Analysis.....	40
<b>6 Jacket Substructure Analysis .....</b>	<b>48</b>
6.1 Design Requirements for Resonance Avoidance.....	48
6.2 Wind and Wave Load Analyses with FAST.....	48
6.3 Total Wind and Wave Load Demand .....	50
6.4 Strength Checks .....	52
6.5 Capacity Analysis .....	55
6.6 Jacket Reliability Analysis.....	58
<b>7 Comparison of Monopile and Jacket.....</b>	<b>64</b>
7.1 Monopile Results, 25-m versus 15-m water depth .....	64

7.2 Jacket versus Monopile at 25-m water depth site .....	66
7.3 Overall Comparison .....	68
<b>8 Summary and Conclusions .....</b>	<b>69</b>
8.1 Key Findings .....	69
8.1.1 Effect of Breaking Waves .....	69
8.1.2 Effect of Change in Water Depth on Monopiles .....	69
8.1.3 Effect of Structure Type on Loads, Design, and Reliability .....	69
8.2 Recommendations .....	70
<b>References .....</b>	<b>71</b>
<b>Appendix A: Soil Springs in the Analyses .....</b>	<b>72</b>
<b>Appendix B: Drag and Inertia Coefficients for Large Diameter Turbine Components .....</b>	<b>75</b>
<b>Appendix C: Study on Sensitivity of Load Results to the Number of Simulations .....</b>	<b>77</b>

# List of Tables

- Table 1. Properties of the NREL 5-MW Baseline Wind Turbine..... 7
- Table 2. Undistributed Blade Structural Properties ..... 7
- Table 3. Tower Dimensions..... 8
- Table 4. Metocean criteria for site (offshore Massachusetts) ..... 17
- Table 5. FAST input data for monopile ..... 34
- Table 6. Monopile design loads at mudline section ..... 36
- Table 7. Monopile Design Loads at Critical Section (Highest Bending Stress) Below Mudline ..... 37
- Table 8. Member Utilization Ratios for Monopile ..... 38
- Table 9. Lateral Load and Overturning Capacity for the Monopile ..... 39
- Table 10. FAST Input Data for Jacket Structure ..... 50
- Table 11. Jacket Design Loads at Mudline Section ..... 52
- Table 12. Jacket Design Loads per IEC/ISO ..... 53
- Table 13. Jacket Design Loads per API ..... 54
- Table 14. Utilization Ratio Summary for Jacket ..... 55
- Table 15. Capacity Analysis Results for Jacket..... 58
- Table 16. Design Load Comparison for Monopile in 25-m Depth to 15-m Depth (from Phase I)..... 66
- Table 17. Utilization Ratio Comparison for Monopile in 25-m Depth to 15-m Depth (from Phase I) 66

# List of Figures

Figure 1. Types of support structures: three-legged space frame structure on left, and a monopile structure on the right. (Illustration from MMI Engineering) .....	5
Figure 2. Campbell diagram .....	8
Figure 3. Location of site.....	9
Figure 4. Soil-strength profile .....	10
Figure 5. Monopile with 4-second period. (Illustration from MMI Engineering) .....	11
Figure 6. Jacket with 4-second period. (Illustration from MMI Engineering).....	12
Figure 7. Correlation of wind speed $W_s$ and significant wave height $H_s$ for tropical storms .....	14
Figure 8. Relation of maximum wave height to significant wave height $H_s$ in a tropical storm.....	14
Figure 9. Relation of average zero-crossing period $T_z$ to significant wave height $H_s$ in a storm ...	15
Figure 10. Surge height as a function of significant wave height for MA site.....	16
Figure 11. Methodology flowchart.....	19
Figure 12. Grid points for the wind velocity data and force components acting on a blade. (Illustrations from NREL) .....	21
Figure 13. Tower and monopile model properties. (Illustration from MMI Engineering).....	23
Figure 14. Breaking waves at the site. ( $T_{app}$ is the apparent wave period.).....	25
Figure 15. Impact load from a breaking wave. (Illustration from MMI Engineering) .....	26
Figure 16. Impulse force on structure from a breaking wave of height 17.4 m.....	27
Figure 17. Response of the monopile to the impulse force from a breaking wave of height 17.4 m .....	27
Figure 18. Comparison of impact forces from breaking waves on monopile and jacket structures (member diameters shown in parenthesis) .....	28
Figure 19. Additional drag and inertia forces for modeling missing effects in wave theory near a breaking wave. (Illustration from MMI Engineering).....	29
Figure 20. Comparison of CAP and FAST results in the frequency domain for the monopile .....	31
Figure 21. Effect of damping on monopile structure (“target” is from CAP; numbers in legend denote FAST analyses with different overall damping values) .....	33
Figure 22. Coupled wind and wave loads for monopile for blade loads and hydrodynamic loads. (Illustration from MMI Engineering).....	35
Figure 23. Monopile model in CAP.....	37
Figure 24. Results of a typical capacity analysis. (Left: Load-displacement curve; Right: deflected shape with nonlinear events.) .....	39
Figure 25. Mudline overturning moment (OTM) versus wind speed for the smallest storm analyzed. (There is no breaking wave phenomenon for this small storm.) .....	41
Figure 26. Mudline OTM vs. wind speed for the largest storm analyzed. (Includes breaking wave effect.).....	42
Figure 27. Loads on blade and wave loads only as a function of $W_s$ , shown for all $H_s$ values analyzed.....	43
Figure 28. Loads on blade and wave load as a function of $H_s$ .....	44
Figure 29. Total loads (including all applicable components) vs. wind speed. (1-hour average, at 10-m reference height.).....	45
Figure 30. Mudline overturning moment (including all load components) of monopile as a function of $H_s$ .....	46
Figure 31. Total load and capacity for monopile as a function of wind speed. (Failure mechanism is different for operating vs. parked modes.) .....	47
Figure 32. Total load and capacity for monopile as a function of significant wave height.....	47
Figure 33. Effect of damping on jacket structure .....	49
Figure 34. Coupled wind and wave loads for a jacket-type structure for blade (top) and hydrodynamic (bottom) loads .....	51
Figure 35. Jacket model in CAP. (Illustration from MMI Engineering) .....	53
Figure 36. Results of a typical capacity analysis under operating storms (Bottom: load-displacement curve; Top: deflected shape with nonlinear events at important steps.).....	56
Figure 37. Results of a typical capacity analysis for a 50-year wave (Bottom: load-displacement curve; Top: deflected shape with nonlinear events at important steps.) .....	57

Figure 38. Mudline overturning moment (OTM) versus wind speed for the smallest storm analyzed.....	59
Figure 39. Mudline OTM vs. wind speed for the largest storm analyzed. (Includes breaking wave effect.).....	59
Figure 40. Mudline overturning moment due to aerodynamic wind load and hydrodynamic wave loads. (No breaking wave effect included yet.) .....	60
Figure 41. Loads from aerodynamic and hydrodynamic effects (excluding breaking wave effects) vs. $H_s$ .....	60
Figure 42. Total load (including all effects) vs wind speed for different $H_s$ values .....	61
Figure 43. Total load (including all effects) vs $H_s$ for different wind speed values .....	61
Figure 44. Total load and capacity for jacket as a function of wind speed.....	62
Figure 45. Total load and capacity of jacket as a function of $H_s$ .....	63
Figure 46. Monopile loads for 15-m and 25-m depth as a function of wind speed and significant wave height .....	65
Figure 47. Jacket vs. monopile loads for 25-m water depth for key return periods as a function of wind speed .....	67
Figure 48. Jacket vs. monopile loads for 25-m water depth for key return periods as a function of significant wave height .....	68

# 1 Introduction

## 1.1 Overview

This report documents the results of the project that was undertaken to address design standards needed for offshore wind turbines (OWTs) in the United States. This is Phase II of the joint industry project (JIP) that was funded by several organizations and executed by MMI Engineering. This second phase was sponsored by the National Renewable Energy Laboratory (NREL). It will help the reader to first review the JIP results as background to this report.

## 1.2 Report Structure

The report is structured as follows:

- Section 2 provides a summary of the general approach to the work.
- Section 3 details the turbine specification, provides a description of the substructure types studied, and summarizes the meteorological, oceanographic, and site characteristics of the location for the OWTs.
- Section 4 provides the methodology for calculating the loads imposed on the structure from wind and hydrodynamic loads.
- Section 5 presents load, capacity, and reliability results for the monopile.
- Section 6 presents load, capacity, and reliability results for the jacket.
- Section 7 compares the monopile results to the jacket results at the site.
- Section 8 offers the key findings and recommendations for further work.

## 1.3 Background

The Bureau of Safety and Environmental Enforcement (BSEE), formerly known as the Minerals Management Service or MMS, has regulatory authority over offshore wind power developments in the U.S. Outer Continental Shelf (OCS). There are codes and standards that have been developed for overseas offshore wind power development; however, no standards have yet been adopted for use in the U.S. OCS by the BSEE or other local U.S. regulatory agencies. The standards that are being considered include the:

- American Petroleum Institute (API) recommended practice, which is currently used for the design and regulatory review of structures used for oil and gas development in the U.S. OCS, titled *Recommended Practice for Planning, Designing, and Constructing Fixed Offshore Platforms, Working Stress Design, RP-2A*.
- International Electrotechnical Commission (IEC) 61400 requirements, which have been developed specifically for the design of OWT generators, titled *Part 3: Design Requirements for Offshore Wind Turbines*.

NREL and BSEE have a common interest in the definition of a standard that can be applied for design of OWT support structures in U.S. OCS waters. This new standard could include an adapted form of API RP2A [4], the IEC 61400-3 [3], or some other standard that has been

developed specifically for OWT design. In the selection of any standard, both the BSEE and the U.S. wind power industry need to have confirmation that the standards applied will fulfill the requirements for both safety and reliability over the intended service life of any facility.

Under a separate JIP (referred to as Phase I in this report), that was partially sponsored by NREL and conducted over the past two years, MMI investigated the relative level of safety provided by each of these standards using two sites and two different support structures for a 5-MW reference wind turbine developed by NREL. Under Phase I it was revealed that the IEC and API designs have comparable levels of safety, but the conditions upon which this conclusion was reached were limited to the two cases investigated under the JIP. Those investigations were insufficient to characterize all the possible differences between the standards. To increase the number of case studies to validate these conclusions, Phase II looked at two additional cases – a monopile and a jacket (space frame) substructure at a relatively deeper water depth at one of the Phase I sites. More details of Phase I can be found in the MMI Engineering report [5]. The reader can also refer to a conference paper based on this report [6].

## 1.4 Objective

The previous study indicated that the levels of reliability generated with the use of the API and IEC codes are dependent upon region (tropical or nontropical), wind load, wave load, structure type, and water depth. Specifically, the API refers to the American Petroleum Institute Recommended Practice 2A, Working Stress Design, 21<sup>st</sup> Edition [4]. The IEC refers to the International Electrotechnical Commission (IEC), IEC 61400-3 Ed.1, Wind Turbines – Part 3: Design requirements of OWTs, IEC TC 88 WG3 Committee Draft, December 2005 [3]. This Phase I study provided specific calibration data for two very specific conditions (e.g., a shallow-water monopile at a Northeast Atlantic site and a medium-water depth tripod at a Gulf of Mexico site). In deep open ocean, the height of the extreme storm-generated waves generally grow increasingly larger with storm intensity. However, when the wave height and the water depth are near the same magnitude, the waves begin to break, but are simultaneously attenuated by interaction with the sea bed. These shallow-water effects have first-order impact on the magnitude of the extreme loads. The breaking waves impart a much different and generally more severe force on the support structures, but this effect is offset by reduced wave height. As a result, the turbine reliability index computed in shallow water (15 m) off the Massachusetts coast for a monopile foundation was found to be virtually unaffected by the difference between the 50-year and the 100-year return period that distinguishes the API and IEC standards. This result occurred because the wave heights could not grow beyond about 10 m in height due to the shallow-water depth limitation. Therefore, extreme loading on this structure is dominated by wind-driven operational loads (blades rotating and generating power) rather than the extreme wave loading (blades parked, no power generation) from rare tropical storms.

The objective of this current study is to expand the matrix of conditions analyzed in order to provide a more complete representation of actual applications to U.S. wind farms.

The study will compare API and IEC guidelines for OWTs with jacket and monopile foundations at the same Massachusetts site analyzed under the previous study. The same metocean data were applied for the Phase II study, with the assumption that the water depth at this site is now 25 m

versus 15 m, which was considered under the previous study. This change in water depth will provide an understanding of the following:

- Effect of change in water depth on the monopile loads, design, and reliability for API and IEC calculations
- Effect of structure type (a monopile versus a jacket structure, which is more transparent in a wave action zone) on the load, design, and reliability for API and IEC calculations
- Shallow-water effects on the most critical load components.

## 2 Methodology

Monopile and jacket-type structures were compared to establish both their similarities and differences with respect to their applicability to OWT support structures in U.S. OCS waters, based on API and IEC guidelines. The IEC guideline has been developed specifically for OWT support structures (safety levels seem to reflect European metocean conditions). This guideline addresses many design requirements that are specific to OWT support structures, which are not addressed within API RP2A, given API's focus on offshore oil and gas platforms. The API design guideline suggests use of 100-year storm specifications for developing the design of a structure. The IEC guideline does not specifically address the requirements for OWT support structures in regions subject to hurricanes. Also, the IEC guideline utilizes a 50-year storm condition to define the loads that are required to establish the minimum strength requirements for the support structure.

The approach in executing this study was the following:

- Utilize for this site, the same metocean data directly from the previous Phase I study, but assume a new water depth of 25 meters for the Massachusetts site and apply appropriate consideration of the shallow-water effects for this 25-m water depth.
- Develop designs for a jacket-type and a monopile foundation for the turbine at this site, applying the necessary resonance-avoidance constraints and the design guidelines, as suggested in API and IEC documents.
- Compare the loads, capacities, and reliability of the jacket and monopile at this site.
- Address the shallow-water effects and consequent loads on structure. A representative soil profile modeling variation of soil properties with depth below mudline was assumed for this site (similar to Phase I).
- Investigate the impact of API and IEC guidelines on overall reliability (probability of failure).

### 2.1 Structure Type

There are a number of different types of support structures that may be used for OWTs. These include monopiles, gravity base structures, tripods, jackets, and various floating concepts. Different design standards will very likely produce levels of reliability that vary for these different concept types. The study focused on the structure types that will most likely be used in the near-term development of offshore wind farms in the United States. These types included a monopile and a jacket (a three-legged space frame structure), as illustrated in Figure 1.

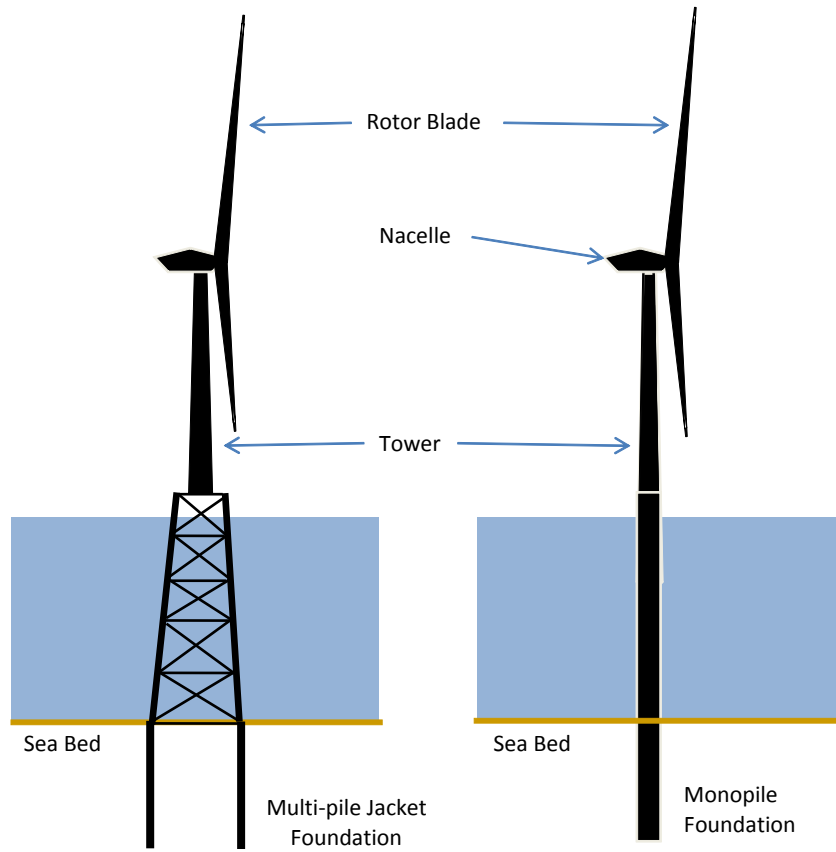


**Figure 1. Types of support structures: three-legged space frame structure on left, and a monopile structure on the right. (Illustration from MMI Engineering)**

## 3 Turbine and Site Characterization

This section summarizes the turbine characteristics, the site parameters, and the metocean characteristics at the site. The turbine type utilized is the same as in Phase I, and the details of the section below are largely repeated from the Phase I report for convenience.

The designs presented herein are representative of a monopile and a three-legged jacket-type structure. The wind turbine utilized is an upwind rotor or a horizontal axis turbine with the blade turned towards the incoming winds. The results presented in this document may not directly apply to other turbine configurations, such as a downwind rotor or a vertical axis wind turbine.

### 3.1 Turbine Specifications

#### 3.1.1 Turbine Size

The size of the wind turbine (i.e., the megawatt rating of the turbine system) predominantly determines both the magnitude of the wind load and the elevation of the centroid of effective wind pressure. Together, these two factors have a significant effect on the base overturning moment (OTM), which may control the design of many of the components of any support structure configuration. The demand (predominantly the wind load) on the support structure increases with increasing turbine size; however, it is not clear what effect turbine size may have on the relative levels of reliability that are achieved with API and IEC. The reason for this complexity relates to the relative significance of wind and wave loading and how these forces vary for both operating and extreme loading conditions. It is intuitive, however, to assume that the 100-year wind and wave load would generally be higher than the 50-year wind and wave load for the same structural system. The specific loads and resulting reliability are discussed in more detail in the subsequent sections of this report.

A 5-MW turbine was used as the basis of the study, as in Phase I, to permit comparisons of the results of this phase to prior phase results. The most significant factor in selecting the 5-MW turbine was the availability of models that were needed to define wind and wave loads for all of the conditions required during the case study analysis. Wind and wave force simulations were performed using the FAST<sup>1</sup> software provided by NREL. NREL also provided the model data for its reference-level turbine and this became the basis for all wind and wave force calculations performed for this study.

The properties of the turbine and blades used in the analysis are summarized in Table 1 and Table 2. These specifications are obtained from the NREL Offshore 5-MW baseline wind turbine as described in NREL/TP-500-41958 technical report [1].

---

<sup>1</sup> Fatigue, Aerodynamics, Structures, and Turbulence. An Aeroelastic Design Code for Horizontal Axis Wind Turbines. Jason Jonkman, National Wind Technology Center. <http://wind.nrel.gov/designcodes/simulators/fast/>.

**Table 1. Properties of the NREL 5-MW Baseline Wind Turbine**

Rating	5 MW
Rotor Orientation, Configuration	Upwind, 3 Blades
Control	Variable-Speed, Collective Pitch
Drivetrain	High-Speed, Multiple-Stage Gearbox
Rotor, Hub Diameters	126 m, 3 m
Hub Height	90 m
Cut-In, Rated, Cut-Out Wind Speed	3 m/s, 11.4 m/s, 25 m/s (10-minute average, at hub height)
Cut-In, Rated Rotor Speed	6.9 rpm, 12.1 rpm
Rated Tip Speed	80 m/s
Overhang, Shaft Tilt, Precone	5 m, 5°, 2.5°
Rotor Mass	110,000 kg
Nacelle Mass	240,000 kg
Tower Mass	347,460 kg
Coordinate Location of Overall Center of Mass	(-0.2 m, 0.0 m, 64.0 m)

**Table 2. Undistributed Blade Structural Properties**

Length (w.r.t Root Along Preconed Axis)	61.5 m
Overall (Integrated) Mass	17,740 kg
Second Mass Moment of Inertia (w.r.t. Root)	11,776,047 kg-m <sup>2</sup>
First Mass Moment of Inertia (w.r.t. Root)	363,231 kg-m
CM Location (w.r.t. Root along Preconed Axis)	20.475 m
Structural Damping Ratio (All Modes)	0.477465 %

### 3.1.2 Tower Properties

The tower, which is the column that spans the height from the top of the support structure to the nacelle, was included in all of the wind and wave load response analyses; however, the design of the tower was not varied for the IEC and API design conditions. The tower used in this study is identical with the one used by NREL for the analyses of a 5-MW baseline wind turbine [1]. Some of the key dimensions of the tower are provided in Table 3.

**Table 3. Tower Dimensions**

Tower base outer diameter (m)	6.0
Tower base wall thickness (m)	0.03
Tower top outer diameter (m)	3.87
Tower top wall thickness (m)	0.02
Tower length (from tower base to yaw bearing) (m)	77.6

### 3.1.3 Turbine Operation Requirements

The support structure must be designed to avoid resonant response with the rotor. If a resonance condition happens, the amplification of motion will likely cause significant damage to the rotor and the blades and would also lead to premature fatigue distress in the support structure. Turbine manufacturers provide frequency resonance criteria for their specific turbines that are based on the operating speed of the rotor and the number of blades. These data are typically represented in a Campbell diagram, such as that shown in Figure 2 for the reference 5-MW turbine. The Campbell diagram defines both rotor and blade passing frequencies (i.e., the frequency with which any of the three blades pass the central support column) for a range of rotor speeds up to the operating speed of the turbine (i.e., the range between the two vertical lines). The normal range of rotor operating speeds can thus be used to establish a range of structure frequencies that will avoid resonant behavior for either of these two inputs. As seen in the diagram, resonance conditions would occur for structural frequencies of 0.1 to 0.2 (Hertz) Hz; and 0.34 to 0.6 HZ as shown in the shaded areas of the figure. A frequency of 0.25 Hz (4-second period) was defined as the target frequency for the first structural mode frequency for all support structure configurations at both sites.

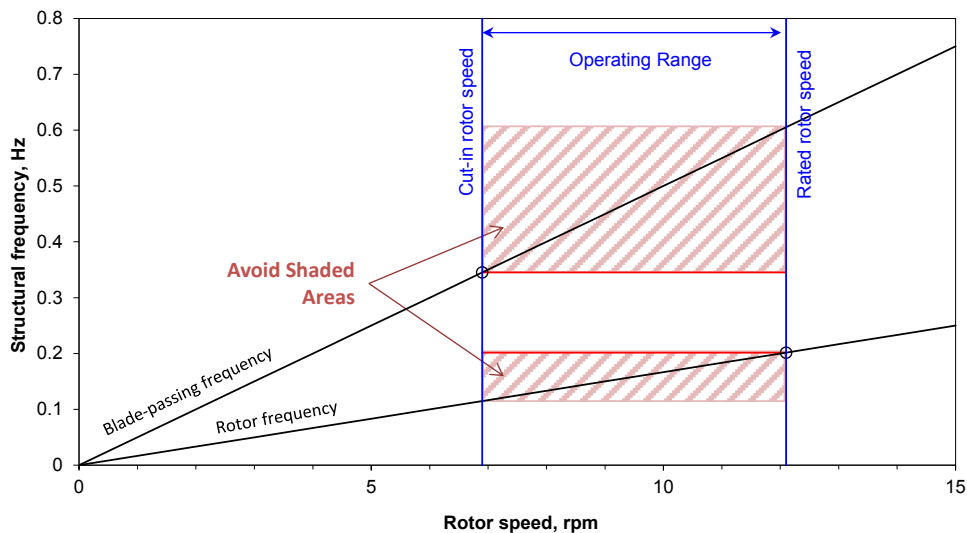


**Figure 2. Campbell diagram**

### 3.2 Site Location and Water Depth

The location of the site is shown in Figure 3. The site is located south of Massachusetts and Rhode Island between Martha's Vineyard and Block Island, which is at  $41^{\circ}15' N$   $71^{\circ}15' W$ . The water depth at the site was assumed to be 25 m, instead of the actual water depth of 15 m used in Phase I. The water depth was increased artificially to permit the study of an increased water depth effect (especially wave breaking effects) on structure design and resulting reliability. This change in depth would also provide for an understanding of results with variation of water depth for monopile design when compared to Phase I results.

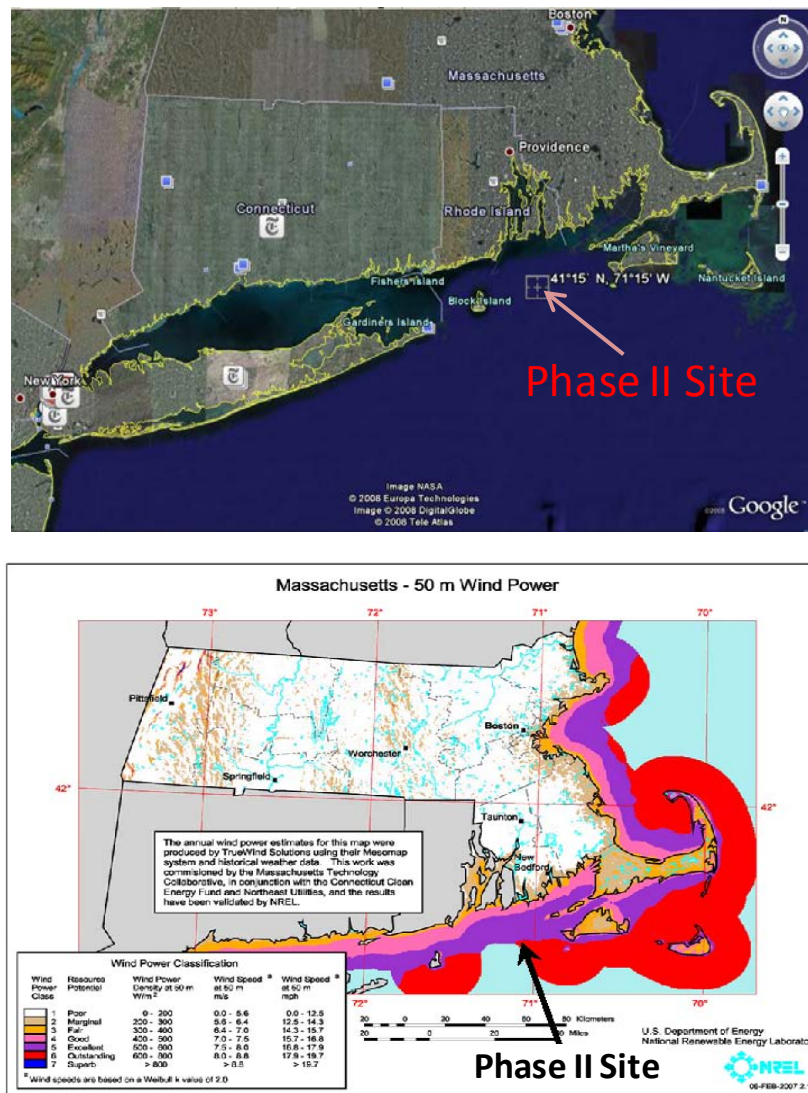


Figure 3. Location of site<sup>2</sup>

<sup>2</sup> Note that these maps are publicly available on the Internet and were simply annotated with the site labels to indicate approximate location [http://www.windpoweringamerica.gov/wind\\_maps.asp](http://www.windpoweringamerica.gov/wind_maps.asp).

### 3.3 Support Structure Configuration

#### 3.3.1 Monopile

The monopile is the most basic of configurations. It includes a large single pile that is driven to a penetration depth that provides the necessary mudline fixity to resist the large OTMs caused by wind and wave loads. The monopile is assumed to extend to a distance of 10 m above water line. At this point, there is a transition to the tower, which is connected to the monopile either by a bolted flange or with a grouted sleeve connection, which accounts for any transition in pile diameter to tower diameter. It is assumed that the tower tapers in diameter from this transition point to the upper flange that supports the nacelle. The yaw bearing that provides support to the nacelle is supported on the tower and located 87.6 m above the water line.

Phase I monopile section properties were used to establish an initial definition of the gross properties of the monopile. In Phase I, a parametric study was performed to evaluate the sensitivity of the structural period to the monopile diameter. In this analysis, the monopile was assumed to have a constant diameter-to-section-thickness ( $D/t$ ) ratio. Given this assumption, all of the key properties of the monopile could be defined as a function of monopile diameter. This includes the variables that control pile structural mass and stiffness and soil-pile interaction. Figure 4 shows that a uniform soil-strength profile was considered. Soil-pile interaction was represented explicitly using soil springs to model the lateral bearing ( $p-y$ ), shaft friction ( $t-z$ ) and end bearing ( $q-z$ ) reaction of the soil. The soil spring properties were developed based on the formulations recommended by API RP2A, as shown in Appendix A.

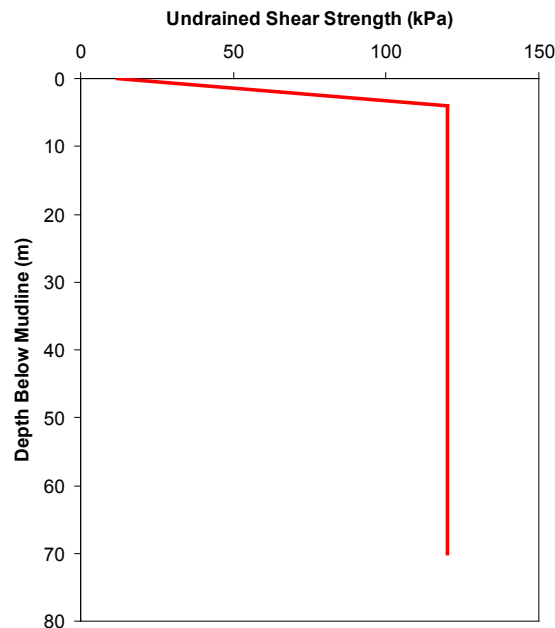


**Figure 4. Soil-strength Profile**

A monopile diameter  $D_{mp}$  of 6.5 m was selected because this generated the 4-second target maximum period. The corresponding wall thickness is 65 mm.

The basic properties of the monopile are illustrated in Figure 5. The fixed attributes of the monopile configuration included the flange elevation, nacelle height, and tower top diameter. The attributes of the monopile that were considered to be primary variables include its diameter, wall thickness, and penetration depth. Note that the pile wall thickness was assumed to be uniform through the depth of the pile for simplicity.

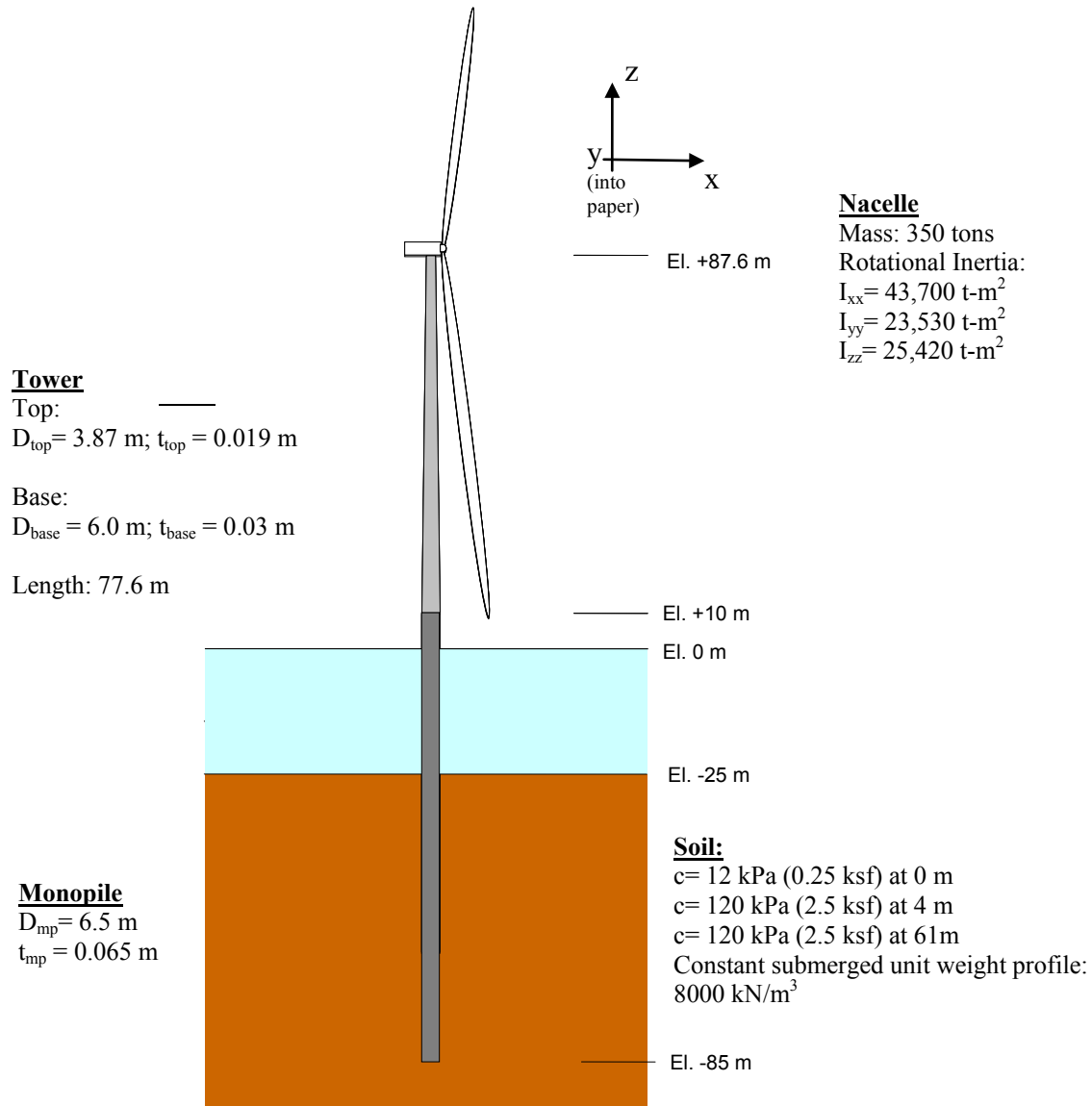


Figure 5. Monopile with 4-second period. (Illustration from MMI Engineering)

### 3.3.2 Jacket

As a second substructure type, a jacket configuration was used. The jacket concept is one of several multi-piled configurations. The basic difference between the multi-pile concepts and the monopile is their ability to resist overturning forces through the couple of pile axial tension and compression forces, rather than bending as in the case of a monopile. These configurations can

provide greater strength and stiffness for systems in deeper water where the large monopile diameter may become prohibitive, both in terms of material and installation costs. For this study, a three-leg jacket structure, illustrated in Figure 6, was considered as sufficient for the water depth at this site.

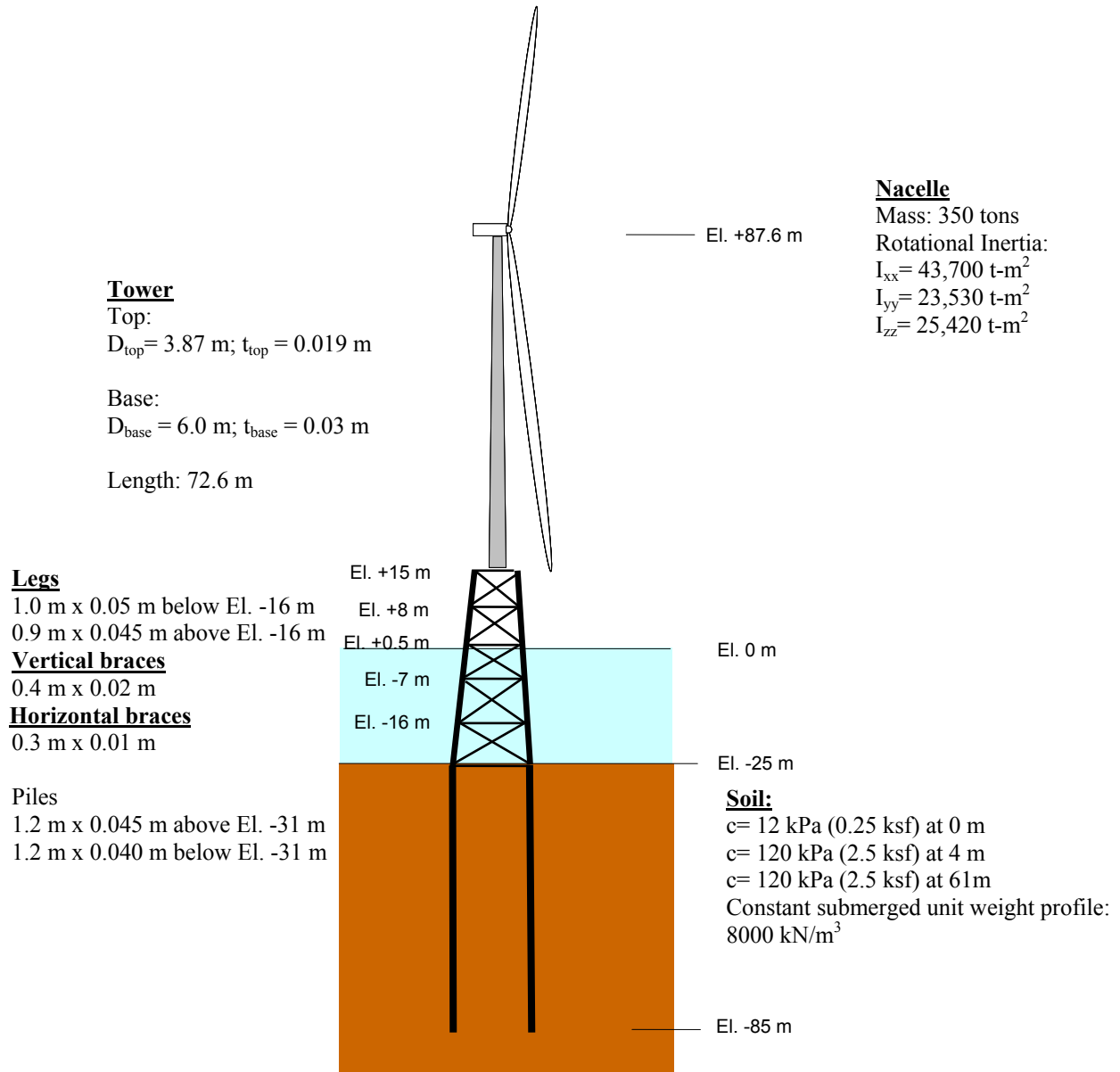


Figure 6. Jacket with 4-second period. (Illustration from MMI Engineering)<sup>3</sup>

<sup>3</sup> Tower length is 5 m shorter than the monopile case because the top of the jacket is up to an elevation of 15 m to keep the junction of the top of the jacket and the base of the tower clear of the extreme storm crests.

### 3.4 Meteorological and Oceanographic Data

Site-specific wind, wave, and current data from Phase I were used for this study. A 25-m water depth was imposed on this data set (instead of 15 m in Phase I) to account for wave breaking and shallow-water depth effects.

The raw data were available to MMI Engineering from Phase I study. These data are referred to as hindcast data and similar data have also been used by the oil and gas industry for much of the reliability work for offshore structures in the Gulf of Mexico. The hindcast data are generated by metocean models that have been calibrated to observed data from past storms.

The metocean data included the following:

- Wind speed for 1-hour-average duration at 10 m above sea level
- Significant wave height,  $H_s$
- Average zero-crossing wave period,  $T_z$
- Current velocity
- Surge height.

The data that were available to define the metocean conditions are as follows:

- Tropical: covering tropical storms from 1900 to 2005
- Extratropical and Continuous storms: metocean statistics provided from analysis of Extratropical storms from 1957 to 2000, and Continuous storms from 1990 to 2005.

The key metocean parameters for OWTs are wind speed and significant wave height,  $H_s$ . The remaining parameters are defined based on  $H_s$ . For example, given a storm with a specific  $H_s$  value, the data regression provides the associated wave period, maximum wave height, current velocity, and surge height. Given an  $H_s$  value, the remaining ocean parameters are modeled as deterministic, with the value obtained through regression functions that define the parameter as a function of  $H_s$ .

Figure 7 conveys the level of correlation seen in wind speed and  $H_s$  values. The correlation for these data was about 85%. This correlation is included<sup>4</sup> in the reliability analysis to calculate the reliability index.

---

<sup>4</sup> The annual maximum wind speed (1 hour average at 10-m reference height) and the annual maximum significant wave height are each specified by a Gumbel probability distribution; a correlation coefficient of 0.85 is additionally specified to model the observed correlation in the hindcast data. For the design storms (i.e., 50-year storm for the IEC and 100-year storm for the API), the associated 50-year and 100-year estimates are used to define the storm. This is a minor enhancement in the approach to Phase I to now account for the joint occurrences of metocean parameters that define a 50-year or a 100-year design storm.

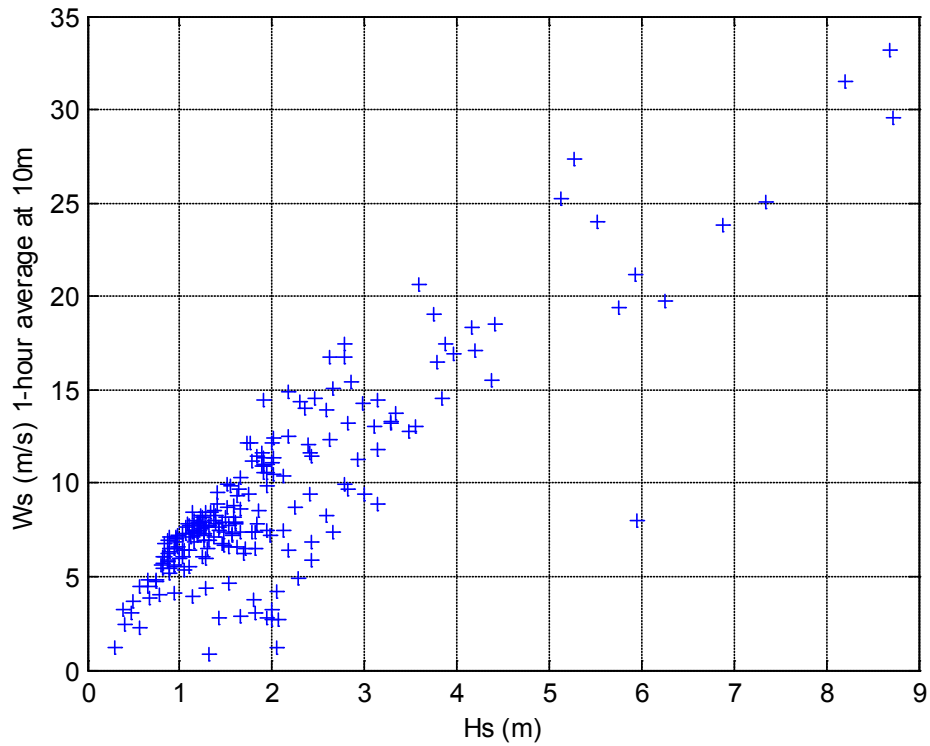


**Figure 7. Correlation of wind speed  $W_s$  and significant wave height  $H_s$  for tropical storms**

Figures 8 and 9 convey the deterministic regression functions used to relate the associated ocean parameters to  $H_s$ . Although not relevant, in these figures, the GP number refers to the grid point used in the hindcast models to generate the meteocean parameters. The Massachusetts site is referred to as GP 3468.

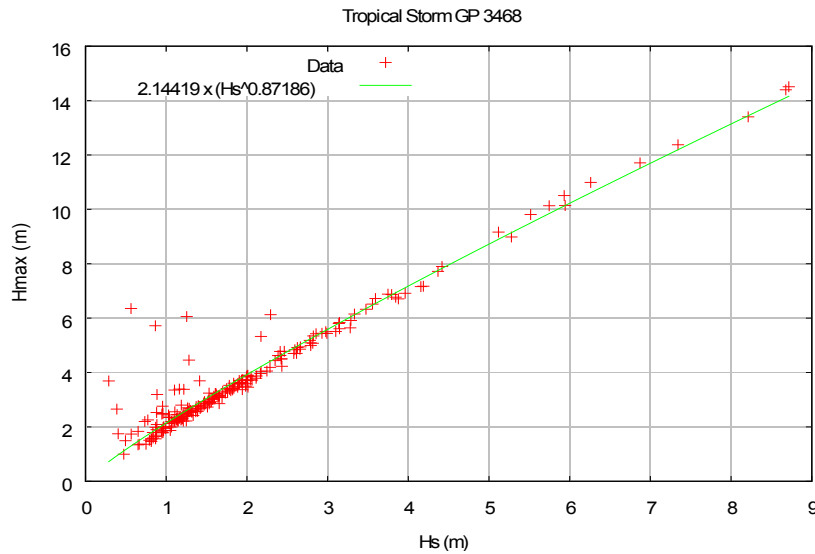


**Figure 8. Relation of maximum wave height to significant wave height  $H_s$  in a tropical storm**

The hindcast data from Oceanweather does not account for breaking wave consideration. The large  $H_{\max}$  values represent “unbroken” waves. Later we discuss the breaking wave limit and how the wave heights were reduced to account for this effect.

The scatter observed in  $T_z$  values for small  $H_s$  values (Figure 9) causes only a nominal change in the wave load on the OWT structure. The load also generally decreases as the wave period increases. Therefore, a conservative simplification was adopted in which the median  $T_z$  value was used as the associated  $T_z$  (and hence the associated  $T_{\max}$ ) for small values of  $H_s$ . Small wave heights do not generally cause ultimate strength failure, so this assumption was considered reasonable. The data for large  $H_s$  values are limited and does not show a large scatter around the median  $T_z$  value.  $T_{\max}$  is assumed to  $1.2 \times T_z$  for this study.

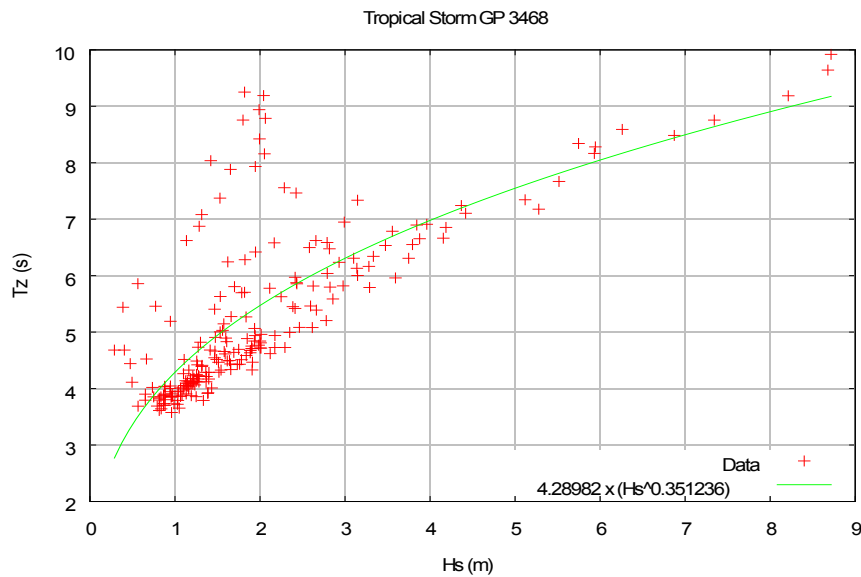


**Figure 9. Relation of average zero-crossing period  $T_z$  to significant wave height  $H_s$  in a storm**

Figure 10 shows the relationship of surge height to significant wave height. The hindcast data indicate scatter in the surge height; however, as the regression line indicates, the surge height generally increases with  $H_s$ . This regression line was used to calculate the surge height to be used for storms with different  $H_s$  values.

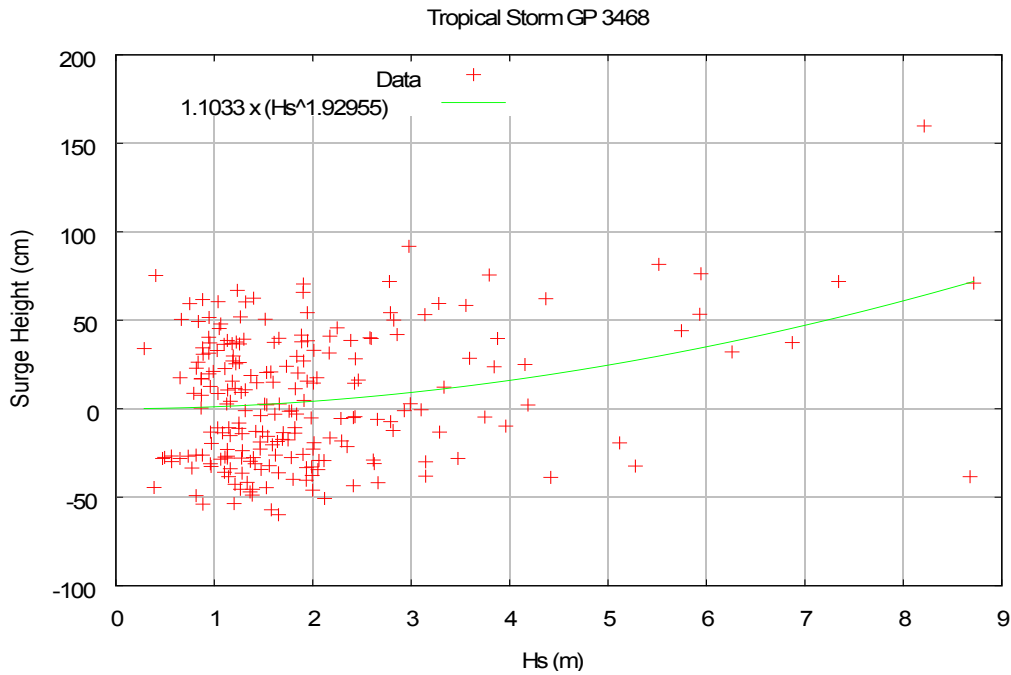


**Figure 10. Surge height as a function of significant wave height for MA site**

### 3.4.1 Breaking Waves

The wave data provided by Oceanweather (data vendor for Phase I of the study) do not specifically address breaking waves; therefore, wave heights defined using this model for shallow-water conditions may be significantly greater than the breaking wave limits. To address this limitation in the data, wave heights were reduced when required to equal the associated breaking wave limit corresponding to the specific water depth. This correction also required special attention to the wave slam forces associated with breaking waves. Additional details on this issue are presented in Section 4.4.

### 3.4.2 Metocean Data for the Site

The wave and wind data that were developed for the Massachusetts site are summarized in Table 4. This summary includes the conditions used for the Power Generation (Operating), 50-year, and 100-year storm conditions.

**Table 4. Metocean criteria for site (offshore Massachusetts)**

Return Period		Ws 10m, 1hr (m/s)	Ws 90m, 10 min (m/s)	H <sub>s</sub> (m)	T <sub>z</sub> (sec)	H <sub>max</sub> (m)	T <sub>max</sub> (sec)	Surge (m)	Current (m/sec)
Max. Wave	Wind Speed								
1	<1	10.99	11.4	3.99	6.97	7.17	8.37	0.159	0.146
A	50	46.3	49.47	7.48	8.7	12.4	10.4	1.346	0.393
50	A	40.42	42.98	8.67	9.16	14.1	10.9	0.945	0.381
A	100	51.85	55.62	8.32	9.03	13.6	10.8	1.644	0.447
100	A	45.29	48.35	9.81	9.57	15.7	11.4	1.172	0.441

Note: "A" stands for associated. For example, for a 50-year storm defined as the one with largest maximum wave height (referred to as wave with 50-year return period), the wind speed chosen is the associated wind speed for the 50-year storm with the largest wave height. Also, for wind speed columns, the two quantities qualifying the definition are elevation above sea level and duration, over which the average wind speed is provided. So, Ws 10 m, 1 hr (m/s) refers to average wind speed meters per second observed at an elevation of 10 m above sea level, with the averaging performed over a 1-hour duration. The water current on the right-most column is assumed to be a uniform current through the water depth.

### 3.5 Other Site Assumptions

To permit easier comparison of results, a stiff clay profile was selected to represent the site. The shear strength profile selected for the analyses is shown in Figure 4. Additional soil details are in Appendix A.

No special site conditions, including seafloor slope, seafloor irregularity, and scour, were part of the study.

## 4 Analysis Methodology

The methodology adopted for the analyses in this study is summarized in Figure 11. Due to the complexity of the formulation of steep and breaking wave forces and some limitations of the FAST simulation software in this regard, a sequential process was developed to determine loads and structural response. The gross dimensions of each structure were developed based on the dynamic performance considerations described in Section 3.3. Using FAST to define the wind and wave force time-histories and to specifically represent the change in blade wind forces caused by motions in the system generated by wave loading, a coupled model of the turbine, tower, and support structure was developed. The FAST analysis does not determine the impulsive forces caused by breaking wave slam on the tower. The FAST analysis is also restricted to some extent by the limits in particle kinematic theories that are used to define wave drag and inertia forces. Lastly, FAST does not determine the wind force applied directly to the tower shaft through drag. These additional forces were estimated using CAP<sup>5</sup> and other calculations, and were added to the FAST results to define the complete set of physical loads.

Once the total wind and wave forces were defined, a second CAP model was developed and used for both the structural design calculations (e.g., member utilization checks) and nonlinear capacity analysis. Member sizes were evaluated and modified as required to meet the minimum IEC or API requirements for each case study.

---

<sup>5</sup> CAP is the Capacity Analysis Program, which provides the capability for the rapid assessment of the ultimate strength and for nonlinear dynamic (wave and earthquake) analysis of the offshore structure. This program permits nonlinear modeling of the structure and the ability to capture soil-structure interaction. This tool is licensed by MMI, and has been in use in the offshore industry for more than a decade.

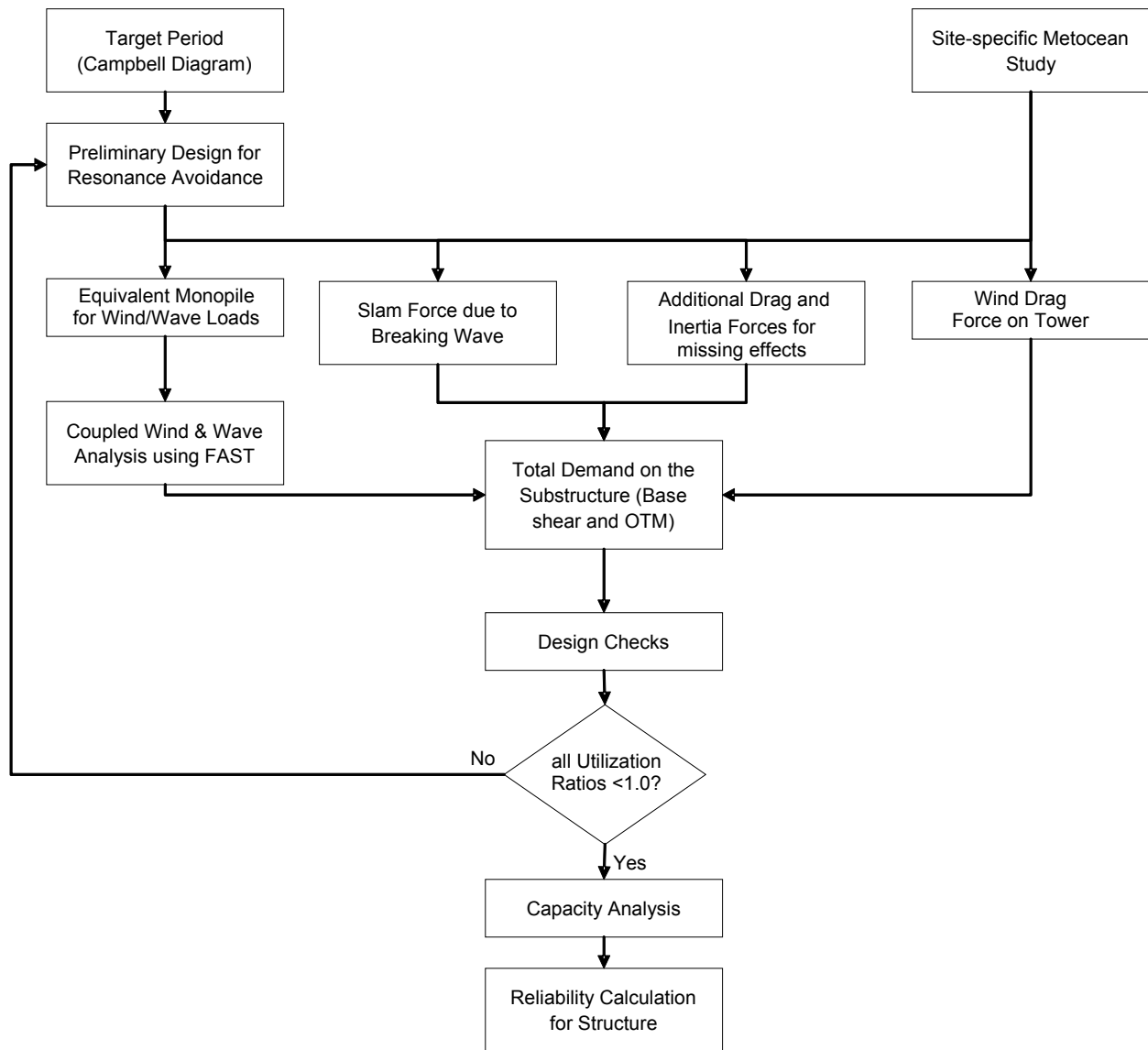


**Figure 11. Methodology flowchart**

## 4.1 Coupled Wave and Wind Load Analyses

In order to evaluate the demand for a range of site-specific environmental conditions, a series of dynamic, coupled wind and wave analyses were performed. The FAST code developed by the NREL was used for the analysis. FAST is a comprehensive, aerodynamic/hydrodynamic simulator that is capable of calculating the response of an onshore or OWT under operational and extreme metocean conditions, with some limitations as mentioned earlier.

As in Phase I, a coupled analysis for aerodynamic and hydrodynamic loads was targeted to model any cross effects of the two loads in a time-history analysis of the loads in different storm conditions. A coupled analysis seeks to include the dynamic effects of simultaneous application of aerodynamic and hydrodynamic loads. This analysis includes effects of damping and any phasing (in time) associated with the two loads, especially if the phasing were to reinforce the two loads' components, and results in higher than simple addition of loads.

Each load case was defined with a combination of maximum wave height and average wind speed for storms of different return periods with associated current and surge. Each case was examined with a number of different wind/wave simulations to assess the effect of variation of wind turbulence and to provide a converged estimate of maximum structural response in these storms. A sensitivity study was performed to assess the number of simulations that are necessary to obtain a converged estimate of the maximum demand for different turbulent wind flow models. (Appendix C presents these results.) Each analysis that was performed included 10-minute time-history simulations for 10 different stochastic simulations of turbulent wind flow. From each 10-minute simulation, the maximum OTM and base shear values were extracted. The mean and standard deviation of these maximum values were then calculated for design and capacity analysis and for reliability calculations.

The following subsections categorize the wind turbine loads and describe how each are modeled and analyzed.

### 4.1.1 Wind Load on Blades

The calculation of blade wind load requires the definition of full-field, wind-flow time histories that are defined at grid points that cover the vertical plane of turbine blades (Figure 12). TurbSim<sup>6</sup> was used to develop wind turbulence time histories. A stochastic turbulence model (extreme turbulence model for wind-turbine class 1, according to IEC 61400-1 Edition 3 standard) was applied for a given mean wind velocity at hub-height. Due to the stochastic nature of the turbulence model, 10 different simulations were performed for a single mean wind velocity specified at hub-height. The vertical mean wind profile was obtained by applying a power law over the rotor disk and a logarithmic profile below the disk. The power law exponent as stated in the IEC guidelines is 0.14 for normal wind conditions and 0.11 for extreme winds. Below the rotor disk, API suggests use of a logarithmic vertical-wind profile that is consistent with IEC.

---

<sup>6</sup> A stochastic, full-field, turbulent-wind simulator for use with the AeroDyn-based design codes (YawDyn, FAST, and MSC.ADAMS®) <http://wind.nrel.gov/designcodes/preprocessors/turbsim/>.

The aerodynamic calculations were based on two-dimensional airfoil-data coefficients (pitch, drag, and pitching moment coefficients), with corrections for three-dimensional behavior. These calculations were performed within the AeroDyn module of FAST software. The structural properties (summarized in Table 1) and aerodynamic properties of blades were obtained from an NREL report by Jonkman [1].

In the aerodynamic load calculation for extreme storms, it is assumed that the blades are able to yaw into the incoming winds. IEC refers to this as the “normal” condition. An “abnormal” condition would be one where the yaw mechanism is ineffective during severe weather, leaving the blades in some other orientation. This abnormal condition would result in potentially greater loads than when the blades are facing the incoming winds. The IEC permits use of a lower safety factor (of 1.1) for the 50-year load in an abnormal extreme load condition. A safety factor of 1.35 is used for a normal extreme condition.

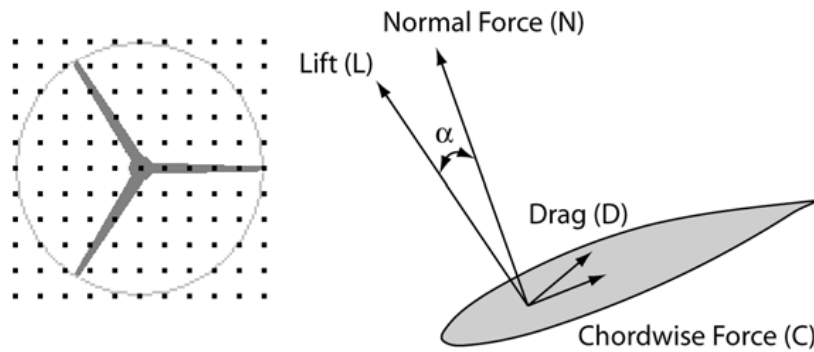


Figure 12. Grid points for the wind velocity data and force components acting on a blade. (Illustrations from NREL)<sup>7</sup>

#### 4.1.2 Wave Load on Monopile

A coupled dynamic wave and wind analysis requires the time-history of wave forces to be applied along the depth of the structure. Incident wave kinematics were modeled with Stream function wave theory. To calculate the drag and inertia forces on the monopile, the relative velocity form of Morison’s equation (Eq. 1) was used:

$$F = -C_A \rho V \ddot{q} + (1 + C_A) \rho V \frac{\delta u}{\delta t} + \frac{1}{2} C_D \rho A (u - \dot{q}) |u - \dot{q}| \quad (1)$$

where

$A$  is the projected area

$V$  is the displaced volume of the cylinder per unit length

$q$  is the displacement degree of freedom of tower/monopile node

$u$  is the water particle velocity

$C_A$  is the normalized hydrodynamic-added-mass coefficient

$C_M$  is the inertia coefficient given by  $1+C_A$

<sup>7</sup> The figure showing the grid points is from *Turbsim User’s Guide for version 1.40*, NREL, September 12, 2008. The figure showing the forces on the blade is from *AeroDyn Theory Manual*, NREL/EL-500-36881, Dec. 2005

$C_D$  is the normalized viscous drag coefficient  
 $\dot{q}$  is the particle velocity  
 $\ddot{q}$  is the particle acceleration

The drag and inertia coefficients used for each type of substructure are listed in Table 5 and Table 10, and the calculation of these coefficients is provided in Appendix B.

Morison's equation becomes less accurate for member diameters that are large relative to the length of the wave. A typical wave length of the incident storm waves used in the analysis is about 100 meters. For the monopile diameter of 6.5 meters, the ratio of wave length to the member diameter is well above the limiting value of 5 as suggested by API RP2A for Morison's equation applicability.<sup>8</sup>

A series of analyses were performed to verify the wave force formulation included in FAST. Various comparisons were completed to assess time-histories of monopile base shear and overturning to those generated with CAP and through other independent wave force calculations.

#### 4.1.3 Wind Load on Tower

The FAST program does not represent the drag load on the tower caused by wind. This drag force was calculated independently following Eq. (2.3.2-8) in API RP-2A (see also Eq. 2 below), using a logarithmic vertical wind profile and mean wind speed at hub-height. This static force was then superimposed with the aerodynamic loads obtained by FAST.

$$F = (\rho/2)u^2 C_S A \quad (2)$$

where

$u$  is wind velocity  
 $C_S$  is shape coefficient (0.5 for cylindrical sections)  
 $A$  is the projected area of the tower facing the incoming wind.

Note that both API and IEC suggest modeling all physical loads; the API formulation was used only as a matter of convenience.

## 4.2 Equivalent Monopile Properties for FAST Analyses

The FAST program is limited to the modeling of fixed monopile support structure configurations. For monopiles, the program represents the supporting structure both in terms of applied wind and wave load, and more importantly, also in terms of the structural vibration characteristics that affect the resulting turbine wind loads. Any support structure other than a fixed monopile requires an equivalent representation to capture at least the first mode of vibration, wave drag, and inertial loading. An equivalent fixed-base monopile was "tailored" to match the desired structural period for each case study by changing the depth of fixity and also calibrating the system damping. The target structural period was selected to avoid resonance caused by the turbine rotor rotation and the aerodynamic effect of the blade passing in close

---

<sup>8</sup> This limitation will be more important for the smaller waves that contribute to fatigue.

proximity to the support tower. This concept is explained in detail in Section 3.1.3, with the use of a Campbell diagram. The equivalent representation of the monopile is illustrated in Figure 13.

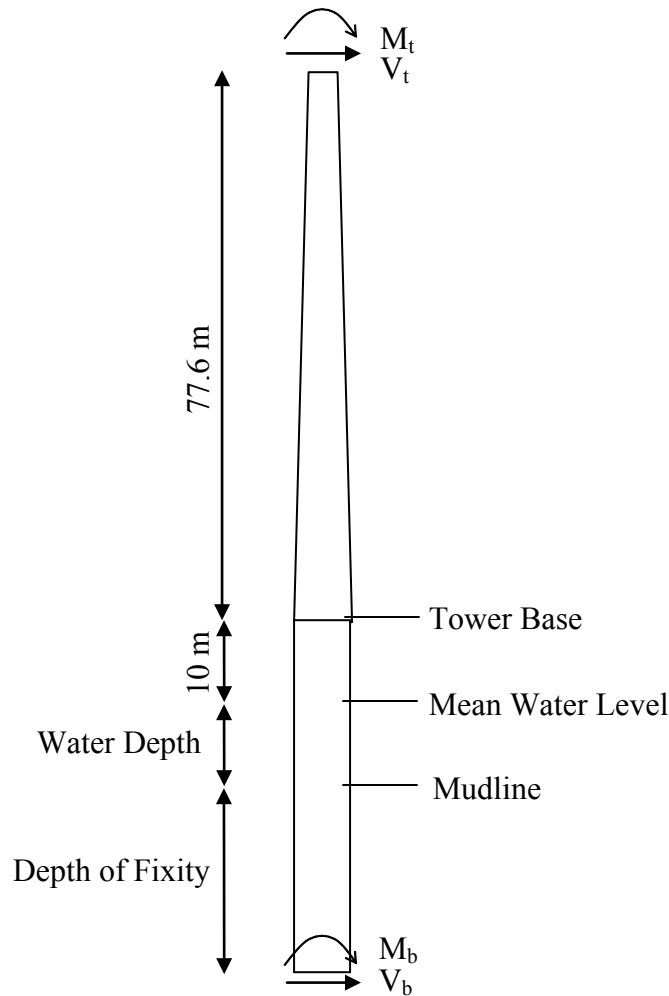


**Figure 13. Tower and monopile model properties. (Illustration from MMI Engineering)**

### 4.3 Coupled Wave and Wind Load Analyses with FAST

The numerical results for the load analysis are presented in Sections 5.1 and 6.2. This section provides a general description of the analysis method.

A range of wave and wind conditions were specified for the site. Ten simulations were performed for each case using a combination of wind and wave conditions. For each simulation, a different turbulent field was specified for the mean wind speed. It was determined through an additional set of parametric analysis that 10 simulations provide a stable representation of the wind force, specifically the mean value of the maximum wind force.

The FAST program can model both the operating (rotating blades) and parked (stationary blades) conditions. During extreme wind conditions (for mean hub-height, 10-minute average wind

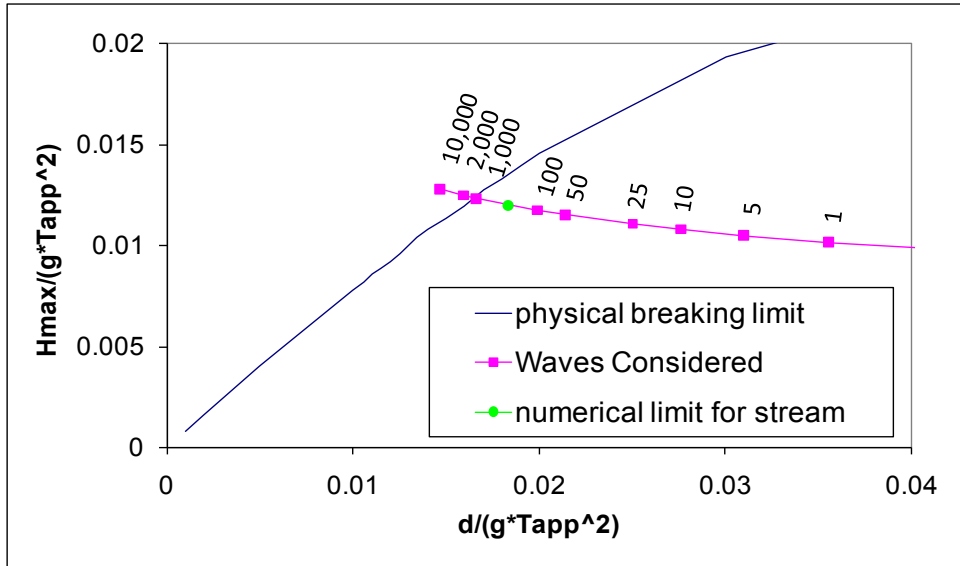
speeds above 25 m/s) the turbine is positioned as parked. The value of 25 m/s is the cut-out wind speed specified in NREL's 5-MW baseline wind turbine.

Four internal force and moment components were obtained for each analysis (or case) in the form of a time-history; namely, tower top shear and over-turning moment ( $V_t$  and  $M_t$  in Figure 13), and monopile base shear and over-turning moment ( $V_b$  and  $M_b$ ). The maximum values of these components were recorded for each simulation. The mean of these maxima were calculated over the 10 simulations. The mean of these maximum force components were then used for the reliability assessment of each structure.

#### 4.4 Breaking Wave Forces

The breaking wave limit identifies the combination of wave height, wave period, water depth, and seafloor slope that causes instability in the wave form that leads to the breaking wave condition. For this study, a flat sea bed is assumed. A zero seafloor slope produces a spilling breaking wave condition. Impact forces were calculated in cases where wave instability was indicated. If the wave was numerically unstable prior to wave breaking, additional drag-inertia forces were also calculated using Stream function particle kinematic theory. To obtain the total base shear and OTM, these forces were added to what was calculated by the FAST analysis and with the wind forces on the tower.

Figure 14 shows the wave conditions for the site along with the breaking wave limit. It also shows the numerical limit to the range of applicability for Stream function.



$H_{max}$ (m)	$T_{max}$ (sec)	Physically Stable <sup>9</sup>	Numerically Stable <sup>10</sup>	Return Period (years)
3.92	6.56	Yes	Yes	<1
7.17	8.37	Yes	Yes	1
8.54	8.98	Yes	Yes	5
9.91	9.54	Yes	Yes	10
11.24	10.03	Yes	Yes	25
13.85	10.92	Yes	Yes	50
15.27	11.35	Yes	Yes	100
19.72	12.58	Yes	No	1,000
21.01	12.91	No	No	2,000
23.97	13.61	No	No	10,000

**Figure 14. Breaking waves at the site. ( $T_{app}$  is the apparent wave period.)**

Below is the procedure to calculate impact forces caused by wave breaking. A conceptual illustration of the problem is provided in Figure 15. The breaking wave impact force was calculated based on the guidelines provided in IEC [3] using Equation 3.

<sup>9</sup> Physically stable implies whether wave breaking has occurred or not

<sup>10</sup> Numerically stable implies whether Stream Function Wave theory is numerically well behaved and provides results or not

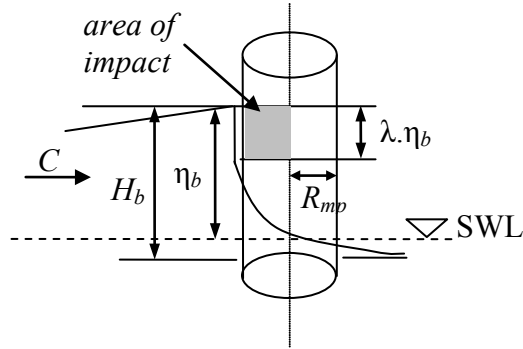


**Figure 15. Impact load from a breaking wave. (Illustration from MMI Engineering)**

where

$C$ : wave celerity

$H_b$ : wave height at the breaking location

$\eta_b$ : maximum elevation of the free water surface above the still water level

$R_{mp}$ : radius of the cylinder (also referred to as  $R$  here)

$\lambda$ : curling factor (approximately 0.5)

$\rho$ : water density

SWL: Still water level

The impact force is given by

$$F(t) = \lambda \eta_b \rho R C^2 \left( 2\pi - 2\sqrt{\frac{Ct}{R}} \operatorname{Arctan} \sqrt{1 - \frac{Ct}{4R}} \right) \quad (3a)$$

$$\text{for } 0 \leq t \leq \frac{R}{8C}$$

$$F(t) = \lambda \eta_b \rho R C^2 \left( \pi \sqrt{\frac{R}{6Ct'}} - 4\sqrt{\frac{8Ct'}{3R}} \operatorname{Arctan} \sqrt{1 - \frac{Ct'}{4R} \sqrt{\frac{6Ct'}{R}}} \right) \quad (3b)$$

$$\text{for } \frac{3}{32} \frac{R}{C} \leq t' \leq \frac{12}{32} \frac{R}{C} \quad \text{where } t' = t - \frac{1}{32} \frac{R}{C}$$

The first term in Equation 3a is the maximum value; the second term is the decay of force with time. The maximum value is twice that given using API guidelines.

A representative impact force time-history is provided in Figure 16 for a maximum wave height of 20.07 m (17.37 m after breaking).

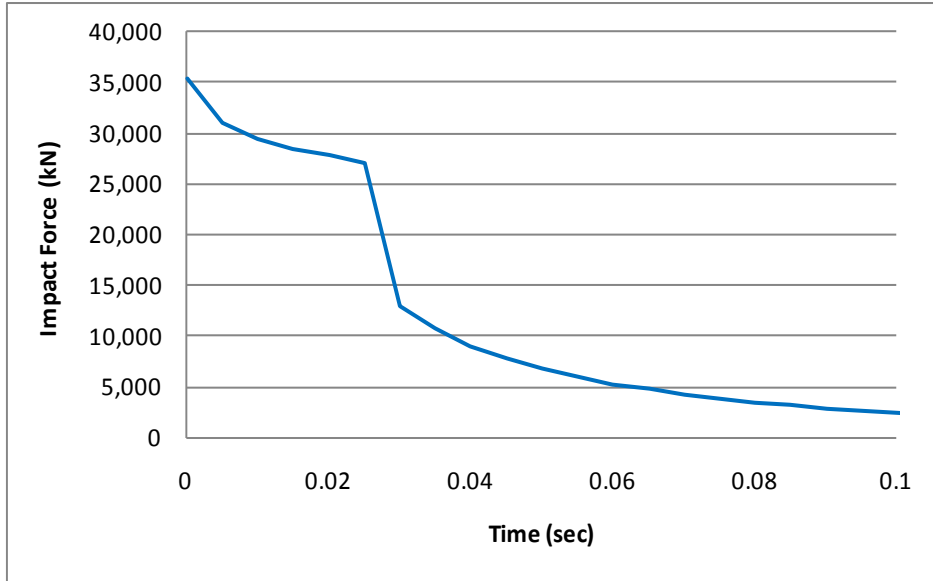


**Figure 16. Impulse force on structure from a breaking wave of height 17.4 m**

A CAP analysis was performed to calculate the dynamic response of the monopile to this impulse loading. The mudline OTM time-history is provided from this analysis in Figure 17. This response shows significant transient behavior in the monopile. This behavior is caused by the instantaneous nature of the loading. The peak at 208 MN-m is the OTM caused by impulse loading from the breaking wave that is added to other load components to calculate the overall mudline OTM.

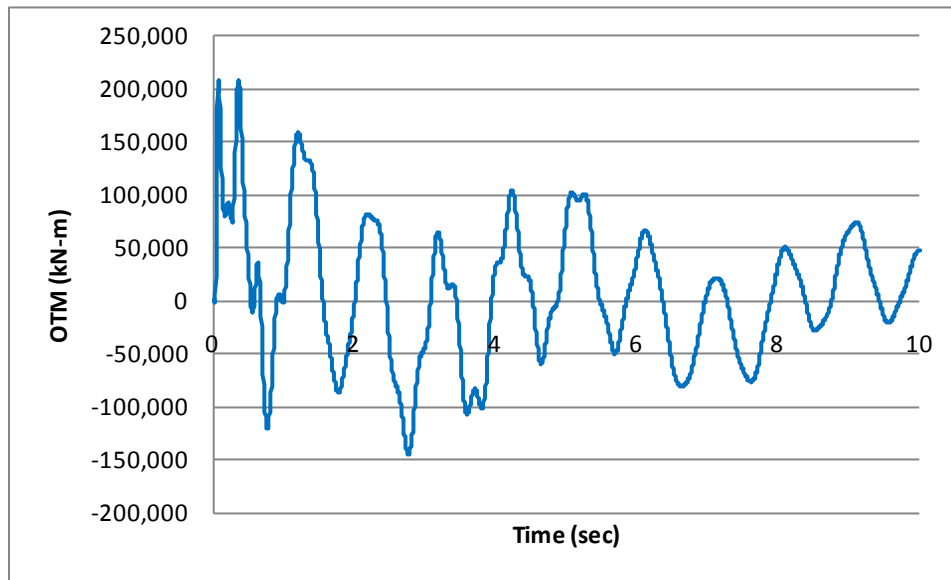


**Figure 17. Response of the monopile to the impulse force from a breaking wave of height 17.4 m**

Based on Equation 3, the amplitude and the effective duration of the impact force is a function of the structural member diameter (or radius  $R$ ). Figure 18 shows that for jacket members, which are smaller than the monopile in diameter, both the amplitude and the duration of the impact force is less compared to those for the monopile. As a result, the input energy, which is the area

under the curves, is significantly less for the jacket structure. This means that the response of the jacket structure to the impulse loading is significantly less, compared to the response of the monopile. Therefore, jacket structures, being more transparent, are less sensitive to the impact loading from breaking waves.

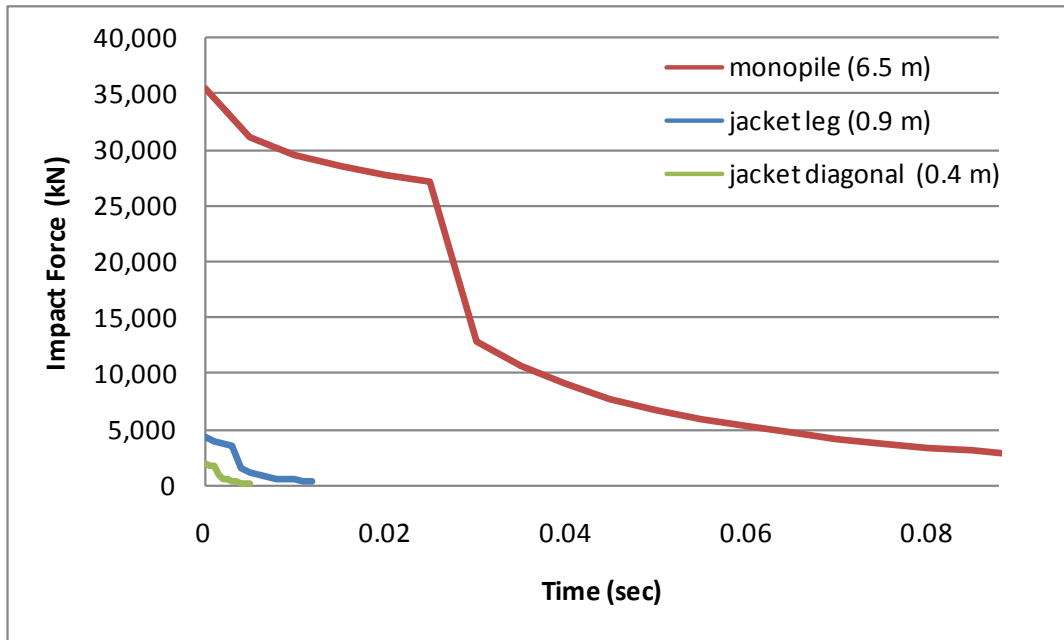
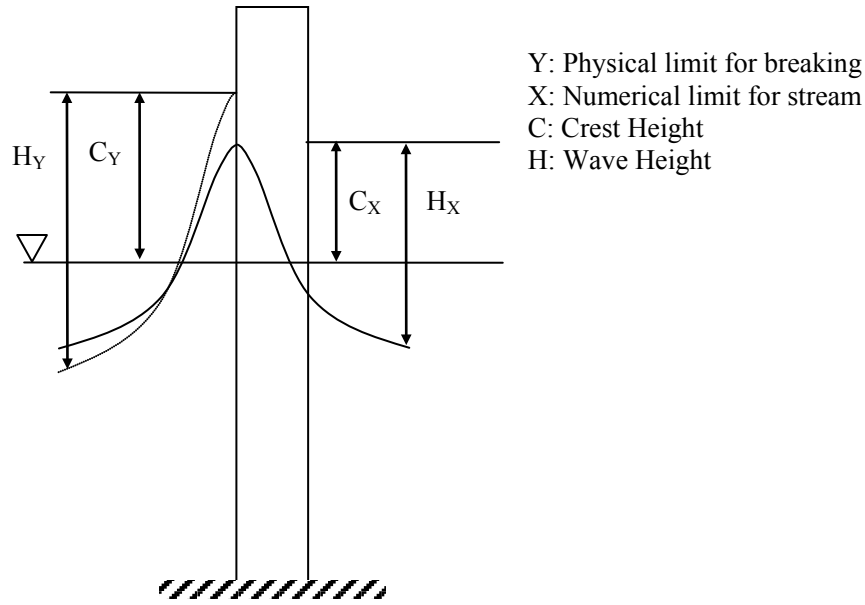


Figure 18. Comparison of impact forces from breaking waves on monopile and jacket structures (member diameters shown in parenthesis)

#### 4.5 Additional Drag and Inertia

For wave heights that exceed the numerical applicability of Stream Function wave theory (see Figure 14), drag and inertia forces from Stream theory can only be calculated up to the indicated limit. Above this limit, drag and inertia forces still exist and were calculated using the approach discussed in this section.

Figure 19 shows the concept of how this force is treated. We assume that  $C_X/H_X = C_Y/H_Y$  (i.e., the wave steepness remains the same above the Stream limit) and the velocity profile stays constant above  $C_X$ . The kinematic wave profile is calculated for  $C_X$  using Stream theory, and the kinematics above  $C_X$  (up to  $C_Y$ ) are assumed to be constant. This is a reasonable approach to incorporate this small correction effect.



**Figure 19. Additional drag and inertia forces for modeling missing effects in wave theory near a breaking wave. (Illustration from MMI Engineering)**

The formulation is provided for a maximum wave height of 17.22 m and the corresponding surge of 1.50 m. Based on stream function, one calculates  $C_X$  as 13.07 m, maximum horizontal velocity as 13.04 m/sec, and maximum horizontal acceleration as  $5.51 \text{ m/sec}^2$ . The equivalent drag and inertia coefficients are 1.03 and 1.30. The maximum stable wave height  $H_Y$  is 74% of the effective water depth. The effective water depth of 26.5 m results from the actual water depth of 25 m plus surge of 1.5 m during the analyzed storm.

$$H_Y = 0.74 \times 26.50 = 19.72 \text{ m}$$

$$\Rightarrow C_Y = 19.72 \times 13.07 / 17.22 = 14.96 \text{ m}$$

The base shear caused by additional drag and inertia is:

$$\text{Additional Base Shear} = F_D + F_I$$

$$F_D = C_D \frac{\rho}{2g} A u |u|$$

$$F_I = C_m \frac{\rho}{g} V \frac{\partial u}{\partial t}$$

$$F_D = C_D \frac{\rho}{2g} \times 6.5 \times (14.96 - 13.07) \times 13.04^2 = 1,076 \text{ kN}$$

$$F_I = C_m \frac{\rho}{g} \times \pi \times 3.25^2 \times (14.96 - 13.07) \times 5.51 = 450 \text{ kN}$$

$$\Rightarrow \text{Additional Base Shear} = 1,526 \text{ kN}$$

$$\text{Additional OTM} = 1526 \times \left( 39.57 + \frac{(14.96 - 13.07)}{2} \right) = 62 \text{ MNm}$$

## 5 Monopile Substructure Analysis

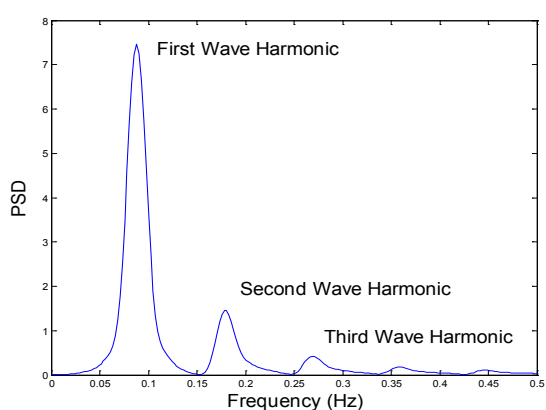
A series of wave and wind load analyses were performed at the start of the development of the monopile concept to assess the variation in load as a function of projected area of the monopile, its stiffness, and the corresponding first mode of vibration. These analyses indicated clearly that the basic properties of a monopile (i.e., base diameter and thickness) at its critical section (i.e., the location of maximum bending moment immediately below mudline) would be controlled by the allowable range in the first mode period that was established to avoid accelerated fatigue. This assessment was applicable for both the IEC and API conditions, because it was found that the required minimum section properties to provide adequate strength for the 50- or 100-year design conditions were significantly less than those required to achieve a maximum first mode vibration period of 4 seconds.

There are a number of combinations of monopile diameter and wall thicknesses that can be used to achieve the required maximum 4-second vibration period. Generally speaking, in terms of stiffness, greater overall efficiency is achieved with larger diameter and smaller wall thickness. Other factors that must be considered include the feasibility and cost of driving large-diameter piles, the larger drag and inertia wave forces, local buckling, soil-pile interaction, and foundation stiffness. A monopile diameter of 6.5 meters with a mudline wall thickness of 65 mm was found to provide a reasonable balance of all design parameters. Additional detail on this design is provided in Figure 5. This configuration was used for the remainder of the calculations.

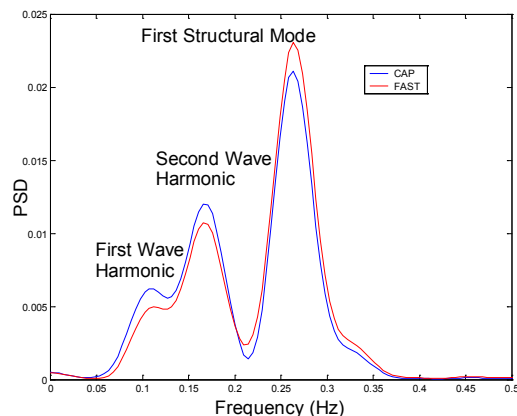
### 5.1 Wind and Wave Load Analyses with FAST

FAST is configured to model monopile support structures; therefore, most of the properties of the structure were represented directly. FAST does not model soil-pile interaction and the additional flexibility that occurs from lateral soil strain. This soil-pile interaction was represented in the model by changing the depth of fixity. FAST is not capable of formulating variable drag and inertia coefficients that would be appropriate for conditions where marine fouling would occur underwater. An equivalent set of drag and inertia coefficients were determined through a separate set of wave load time-history analyses using the Capacity Analysis Program (CAP) software, which does address variable drag and inertia coefficients (Appendix B). A few parameters, such as assumption of fixity depth, overall damping of the system, modulus of elasticity, and coefficients for drag and inertia coefficients, formed part of the “tuning” exercise so as to represent in FAST the physical effects available in CAP.

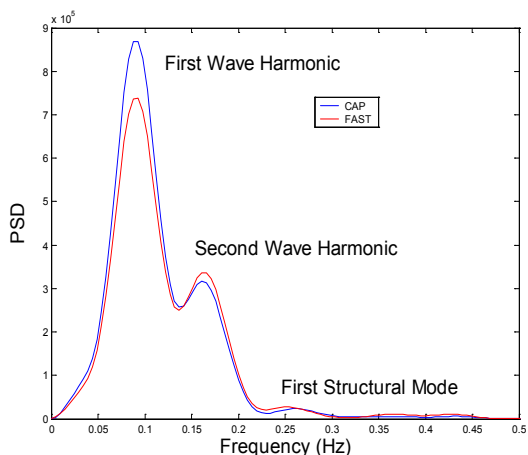
To verify the structural modeling in two different programs, i.e., CAP and FAST, frequency analyses were performed on the response values. Three different response quantities were considered: displacement, base shear, and OTM. The wave frequencies were also needed to understand the “forcing” frequencies. Therefore, first the frequency analyses of the input waves were performed. Figure 20 shows the first and the higher harmonics of the input wave. One can observe the first structural frequency and the wave harmonics from the frequency analyses of the nacelle displacement in the figure. The same peaks are visible on the frequency response analyses of the base shear and the OTM. Some of the important observations based on Figure 20 are listed below.



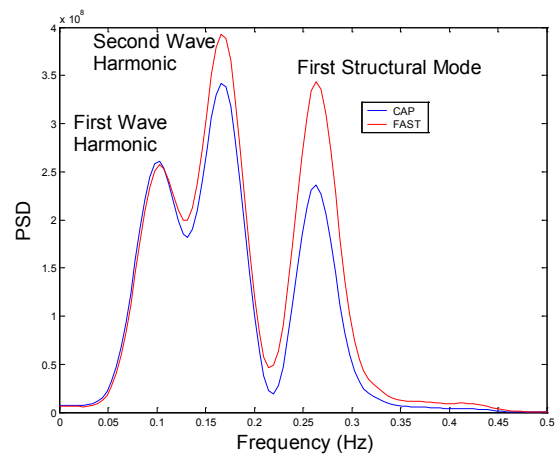
Wave Input



Nacelle Displacement



Base Shear



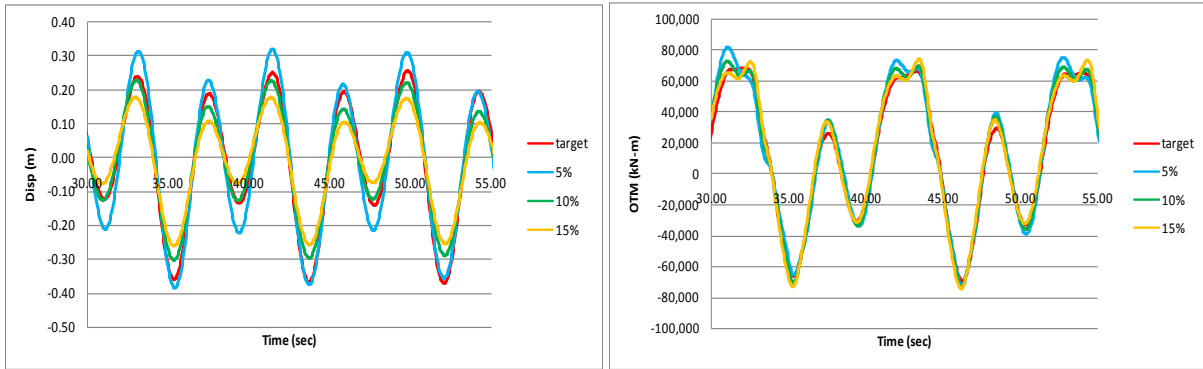
Overturning Moment

**Figure 20. Comparison of CAP and FAST results in the frequency domain for the monopile**

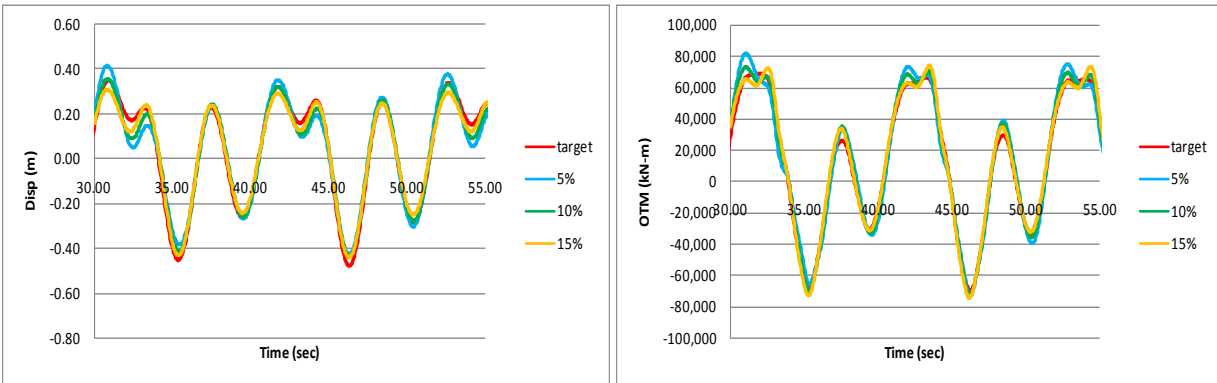
- The first structural mode frequency obtained from the CAP and FAST models match closely.
- There is no higher mode contribution observed beyond the second mode. Therefore, modeling the turbine by the first two modes suffices for the purposes of this study.
- The first structural mode is away from the first wave harmonic (first modal frequency is different from first wave harmonic frequency); however it is closer to the second wave harmonic. Although the energy from the second wave harmonic is less than from the first wave harmonic, resonance at the first structural mode may still occur from the second wave harmonic.
- If the frequency responses of the displacement and the base shear are compared, one can observe that structural response (energy) is higher in displacement response, whereas

wave energy is higher for base shear. This means that displacement response is dominated mostly by structural characteristics, whereas base shear is mostly dominated by wave loading characteristics. One can see that these two effects (i.e., contribution of the loading itself and the response of the structure) are comparable to each other in the frequency response of the OTM. This is because overturning moment is a function of both the wave loading and the response of the nacelle mass. Response of the nacelle mass is influential for the base overturning moment because of the long moment arm (height of the turbine above the mudline).

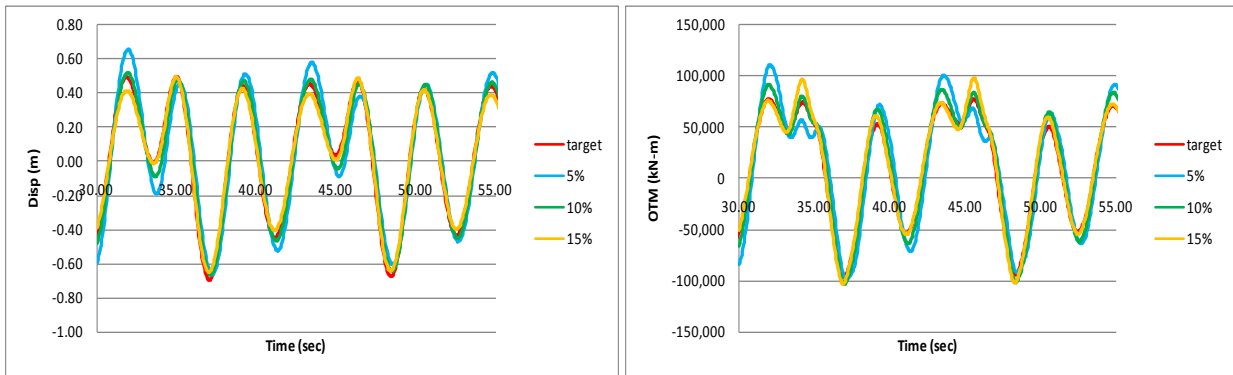
Structural damping, soil damping, aerodynamic damping, and hydrodynamic damping form components of overall damping that reduce the response of a structure once the imposed load is removed. In the CAP analysis, these components are modeled implicitly or explicitly, and an attempt was made to capture the overall damping via a single parameter within FAST to mimic the physical effects in CAP. Figure 21 shows the effect of damping on both nacelle displacement and OTM for the monopile structure. Note that this is an overall “damping” parameter to permit FAST to mimic physical effects in CAP and is not to be confused with the physical structural damping in the system. The structural damping is usually on the order of a percent or so. The target nacelle displacement and the overturning moment time-histories were obtained by explicit CAP analysis. A parametric study for the damping values of the tower was performed in the FAST analysis to replicate the target time histories from CAP. The priority was given to match the maximum or minimum values (i.e., the extremes) obtained from two different analyses, the CAP and FAST analyses, because the maximum OTM is the main parameter of interest for structure design and reliability analysis in this study. One can conclude that 10% is a good representation of the damping in the system for all the ranges of the heights, i.e., 1 year-, 50 year-, and 100-year waves.



**Operating Case (1-Year Wave)**



**50-Year Wave**



**100-Year Wave**

**Figure 21. Effect of damping on monopile structure (“target” is from CAP; numbers in legend denote FAST analyses with different overall damping values)**

The resulting equivalent monopile properties that were used for the FAST analyses are summarized in Table 5.

**Table 5. FAST input data for monopile**

Monopile thickness (m)	0.065
Tower base outer diameter (m)	6.5
Tower base wall thickness (m)	0.03
Tower top outer diameter (m)	3.87
Tower top wall thickness (m)	0.02
Steel density (effective) (kg/m <sup>3</sup> )	8,500.00
Steel Young's modulus (E) (MPa)	2.100E+5
Steel shear modulus (G) (MPa)	8.080E+4
Water depth, d (m)	25
Height monopile extends above MSL (m)	10
Length of tower + monopile (m)	112.6
C <sub>d</sub>	1.03
C <sub>m</sub>	1.30
Damping	10%*
Structural fore-aft period (s)	4.08

\*This is a “tuning” number and includes all sources of damping so that the response of the structures match from two different analyses programs: CAP and FAST. In this sense it is an overall “tuned” damping number to permit FAST software to mimic the physical effects missing in FAST that are captured explicitly in CAP (e.g., soil structure interaction).

## 5.2 Total Wind and Wave Load Demand

Figure 22 presents the results of coupled wind and wave analyses with FAST in terms of base shear and OTM. One can observe that for a constant wave height, base shear and the overturning moment first increase and then decrease. Prior to the cut-out wind speed, the range of wind speed values are those at which the turbine operates and generates power. After the cut-out wind speed, the response values (base shear and the overturning moment) increase because of the increase in the wind speed itself. Another observation is that for larger waves and under operating wind speeds the response values get magnified due to the interaction between the wave and wind loading. Although the response surfaces for base shear and OTM are shown for all of the wave heights and wind speeds are presented in the figure, one should focus on the response values that lie on the diagonal, i.e., wind speed and wave height with the same return periods. These response values are the most probable ones to happen in reality because the wave height and the wind speed are correlated. Table 6 provides the results for the metocean loads used in the design checks. These results are nominal loads and do not include any load factors.

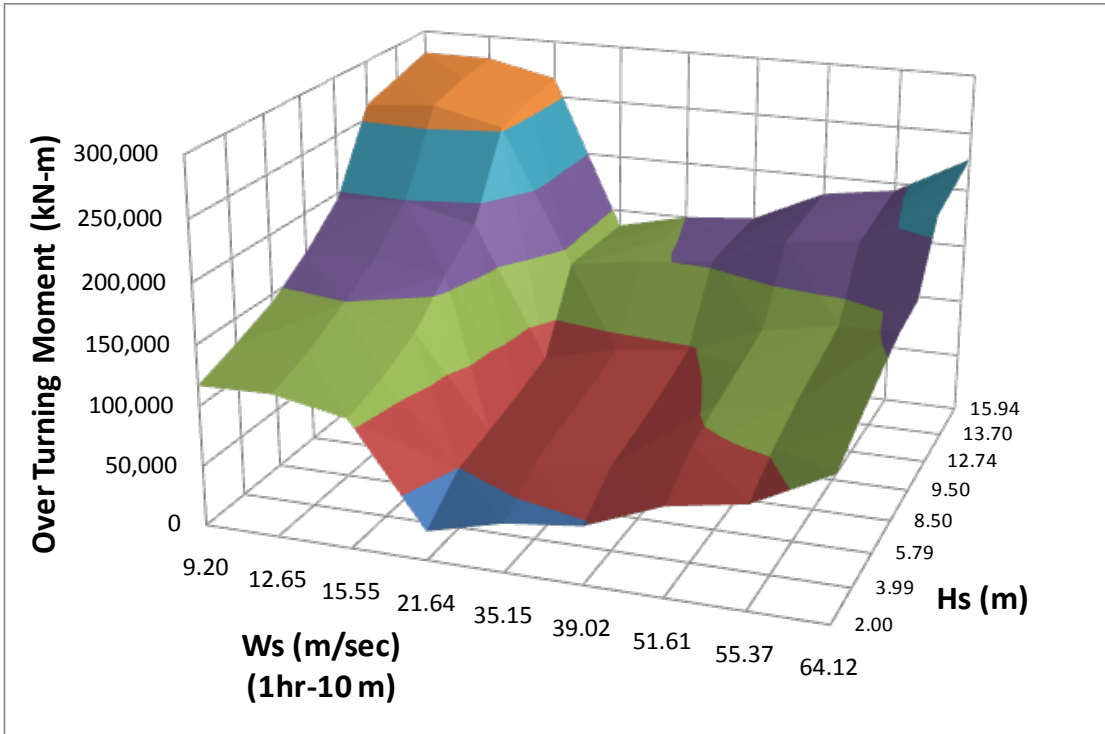
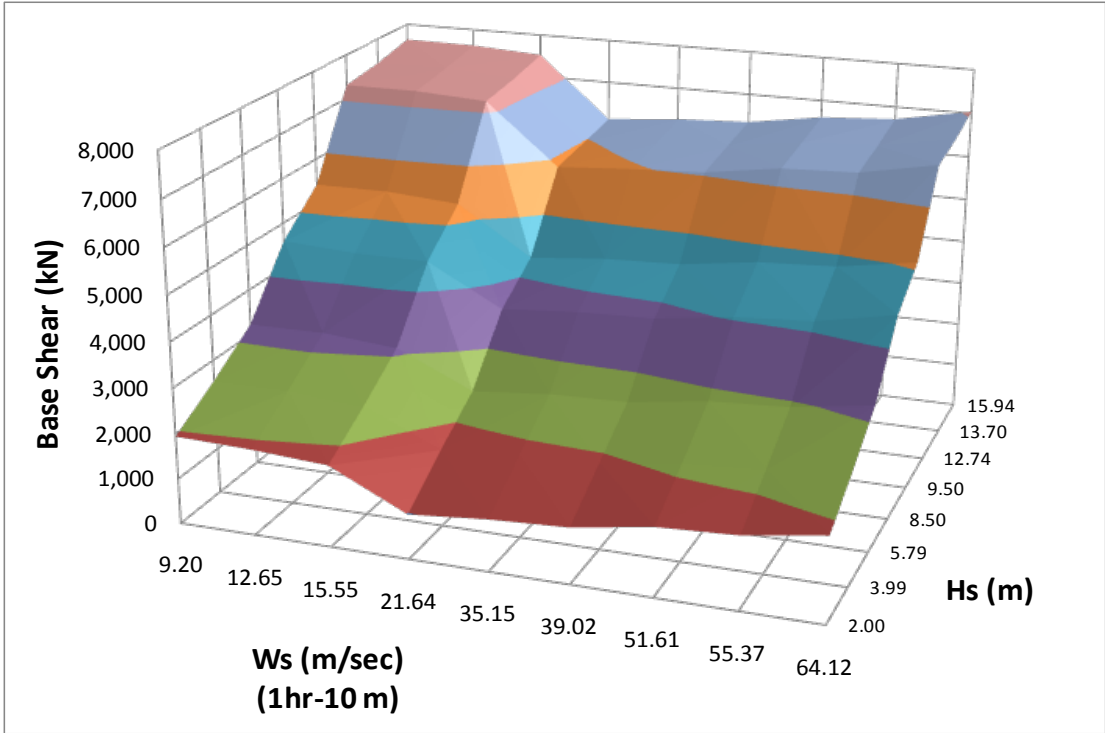


Figure 22. Coupled wind and wave loads for monopile for blade loads and hydrodynamic loads. (Illustration from MMI Engineering)

**Table 6. Monopile design loads at mudline section**

<b>Base Shear (kN)</b>			
Storm Type	Coupled Wind-Wave	Tower Wind	Total*
Operating Storm	2,542	7.26	2,549
50-year Storm (Wind Driven)	3,455	117	3,572
50-year Storm (Wave Driven)	4,046	90	4,136
100-year Storm (Wind Driven)	4,035	145	4,180
100-year Storm (Wave Driven)	5,152	112	5,264
<b>Mudline Overturning Moment (MN-m)</b>			
Storm Type	Coupled Wind-Wave	Tower Wind	Total*
Operating Storm	130	0.51	130
50-year Storm (Wind Driven)	90	8.66	99
50-year Storm (Wave Driven)	84	6.64	91
100-year Storm (Wind Driven)	101	10.8	112
100-year Storm (Wave Driven)	104	8.30	112

\* Note: There are no breaking wave effects in these storms

Superimposing the different components of load (aerodynamic and hydrodynamic loads from FAST, tower wind, as well as slam, and stream correction, if present) is conservative. The intent is to estimate the annual maximum load in a storm; more specifically, the maximum combined wind and maximum wave load in a storm with a given frequency (return period). The conservatism comes from algebraically adding peak value of each component, which assumes these peaks occur at the same time. In reality, there is a lag between the different component peaks, depending on whether a component is drag dominated or inertia dominated. The drag components are driven by wind or wave velocity, while the inertia components are dominated by wind or wave acceleration. The velocity and accelerations achieve their maximum values at different times. The FAST analysis includes this effect for the wind and wave force components that are modeled explicitly (i.e., rotor wind and normal substructure wave), but the maximum values for remaining components are simply added; the time phase lag between the components is ignored. It is reasonable to make this conservative assumption for the objectives of this study because it has a consistent effect for both the API and IEC analyses.

### 5.3 Strength Checks

Structural response was assessed for each load condition (i.e., unfactored mudline base shear and OTM) using the CAP model. CAP includes a pile-soil interaction capability (Figure 23) and thus properly represents the effect of soil bearing on both pile fixity and bending moment.

The maximum demand in the monopile generally occurs below the mudline and Table 7 lists the unfactored design loads used in the CAP analyses at the most critical cross-section within the monopile. API RP2A utilizes these unfactored loads, whereas IEC/ISO requires the application of load factors (1.1 for gravity loads, and 1.35 for extreme environmental loads) prior to the

structural response analysis. These loads are compared to the monopile loads for the 15-m water depth case (from Phase I) in Section 7.1. A material strength of 250 MPa (36 ksi) was assumed for the initial utilization ratio check for the monopile. The analyses indicate that higher-strength steel is not needed for this case.

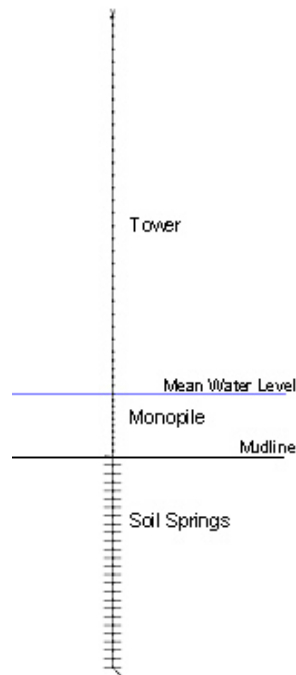


Figure 23. Monopile model in CAP

Table 7. Monopile Design Loads at Critical Section (Highest Bending Stress) Below Mudline

Load Cases	Unfactored Loads			Design Loads per API (no load factors)			Design Loads per IEC/ISO		
	Gravity Analysis	Wind/Wave Analysis					(1.1 Gravity + 1.35 Environmental)		
	Axial Load (kN)	Shear (kN)	Moment (MN-m)	Axial Load (kN)	Shear (kN)	Moment (MN-m)	Axial Load (kN)	Shear (kN)	Moment (MN-m)
Power Production	10,020	4,770	141	10,020	4,770	141	11,020	6,430	191
Parked (50-yr Metocean Criteria / Wave-driven)	10,020	4,150	113	/	/	/	11,020	5,600	152
Parked (50-yr Metocean Criteria / Wind-driven)	10,020	3,910	116	/	/	/	11,020	5,280	156
Parked (100-yr Metocean Criteria / Wave-driven)*	10,020	5,280	141	10,020	5,280	141	/	/	/

\*The wind-driven 100-year storm generates similar or smaller loads for both shear and overturning, so only the 100-year wave-driven storm was used as the design storm load.

The monopile cross-section was evaluated using both the API and IEC design formulations. The maximum utilization ratios (i.e., ratio of stress demand by external loads to allowable stress according to API; ratio of the stress demand by factored external loads to factored strength according to IEC/ISO) for the monopile are summarized in Table 8. The utilization ratios for shear do not govern design of the section.

**Table 8. Member Utilization Ratios for Monopile**

	Based on API RP2A		Based on IEC / ISO	
	Power Production <sup>a</sup>	Parked/Idling	Power Production <sup>b</sup>	Parked/Idling
<b>Combined Axial Load and Bending</b>	0.529	0.395	0.402	0.343
<b>Shear</b>	0.073	0.06	0.071	0.062

<sup>a</sup> Without one-third allowable stresses increase factor

<sup>b</sup> With the same load and material factors from parked/idling condition

The results shown above indicate that the design is well within the acceptable limits for both API and IEC. There were no changes.

These results confirm that the design of the monopile is predominantly controlled by the maximum first mode period of vibration (i.e., resonance avoidance for rotor and blade-passing frequency).

A perfectly tuned design would achieve utilization ratios of 1.0 for all components of the structure using factored loads and factored strength. Such a design would achieve the reliability implicit in a given design code. The utilization ratios for this design are significantly less than 1.0 (the largest utilization is 0.53). Therefore, this structure will generate a very high level of reliability (or very high beta values, presented later).

These results indicate very clearly that the basic properties of the monopile (i.e., base diameter and thickness) at its critical section (i.e., the location of maximum bending moment immediately below mudline) are controlled by the resonance avoidance criteria. The minimum section properties required to provide adequate strength for the 50- or 100-year design conditions were significantly less than those required to achieve a maximum first mode vibration period of 4 seconds. Thus, this assessment was applicable for both the IEC and API conditions.

## 5.4 Capacity Analysis

A series of structural capacity analyses were performed using CAP software to determine the total capacity of the monopile design. The capacities were determined for each pair (each design storm) of base shear and base OTM separately. These capacities were then input to the reliability analysis.

The monopile was modeled in CAP to establish the effect of the soil-pile response and to determine the location of maximum pile bending below mudline. CAP includes an explicit representation of both material and geometric nonlinear behavior.

In the capacity analysis, the lateral load on the monopile is increased incrementally until the structure reaches its ultimate point. Figure 24 shows the results from the capacity analysis with the API extreme load case as an example. As the lateral load is increased, the elements below mudline are forced beyond their initial yielding level. The lateral capacity was assumed to be reached when the first full plastic hinge developed in the monopile below mudline. Table 9 presents the monopile capacity for each load case.

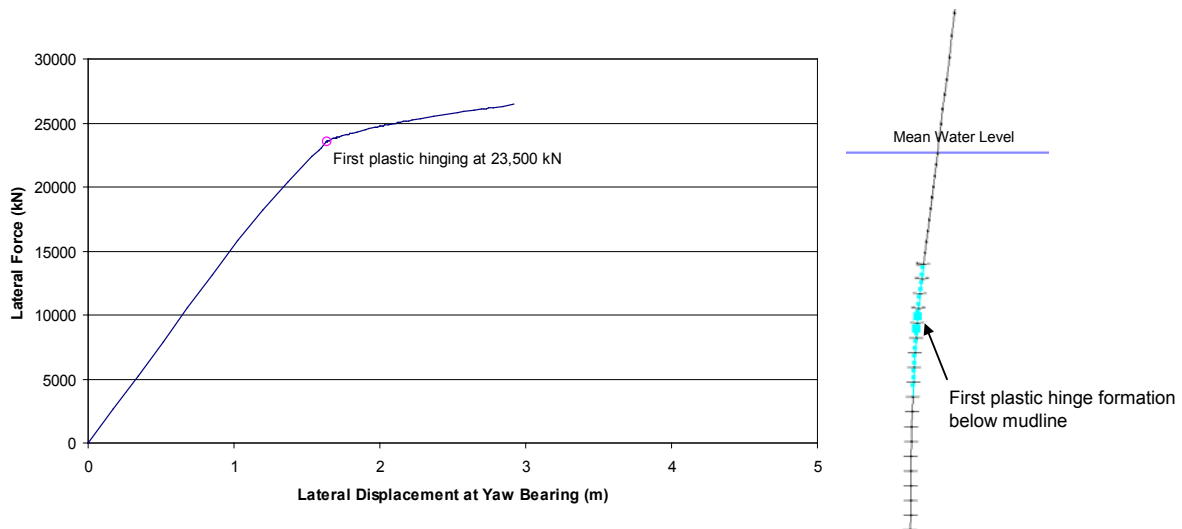


**Figure 24. Results of a typical capacity analysis.**  
(Left: Load-displacement curve; Right: deflected shape with nonlinear events.)

**Table 9. Lateral Load and Overturning Capacity for the Monopile**

Load Case	Capacity		Capacity/Demand Ratio	
	Base Shear (kN)	Base OTM (MN-m)	Base Shear	Base OTM
Power Production	11,500	586	4.5	4.5
Parked/Idling (50-yr Extreme / Wave-driven )	23,100	508	5.58	5.58
Parked/Idling (50-yr Extreme/ Wind-driven)	19,600	537	5.48	5.48
Parked/Idling (100-yr Extreme)	23,500	505	4.47	4.47

The ratios of the capacity-to-design-load, which are far greater than 1, provide a clear indication of the reliability implicit in the design. If the ratio of the capacity to design load is greater than the “net” safety factor, then the design would result in a higher safety factor than suggested by the design guide. The ratio of capacity to design load is about 4.5 for the operating case, about 5.5 for the 50-year cases, and about 4.5 for the 100-year case.

## 5.5 Monopile Reliability Analysis

The reliability formulation utilized here is adopted from Phase I and is repeated below for convenience.

To calculate the reliability of the monopile, the following simple limit state function was used:

$$G() = R/L - 1 \quad (4)$$

When  $G()$  is less than zero, failure is assumed to happen in the ultimate strength. The resistance or capacity is modeled as a lognormal random variable with a CoV of 15%, and a 5-percentile value equal to  $C$  (=505 MNm)

The load  $L$  is modeled as  $L=L_{BW} X_{BW} + L_{tower} X_{Tower} + L_{Slam} X_{Slam} + L_{Corr} X_{Corr}$

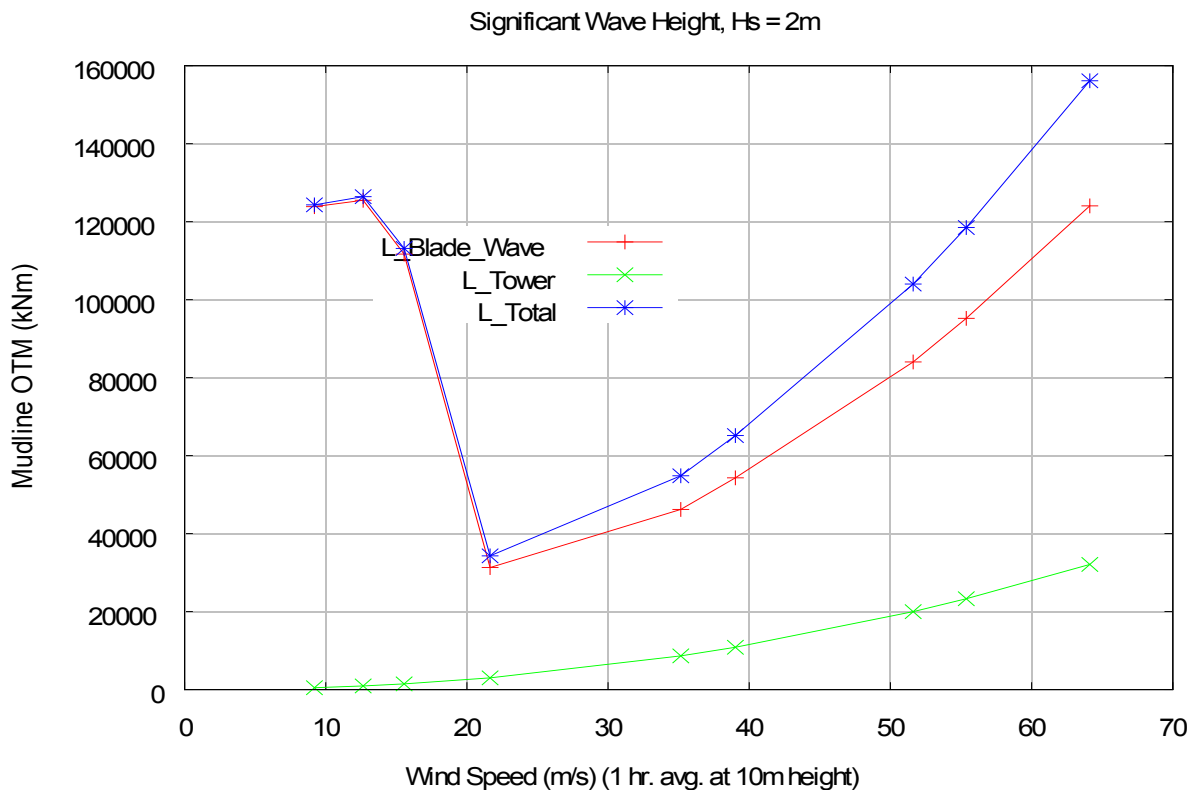
where

- $L_{BW}$  is the aerodynamic blade load and the hydrodynamic wave load, which is calculated using FAST and is a function of wind speed and wave height.
- $X_{BW}$  is the model uncertainty and variability for the aerodynamic load on the blade and the hydrodynamic load from drag and inertia from wave particle kinematics acting on the foundation. This factor is assumed to have a lognormal probability distribution with a mean value of 1 and CoV of 7% (7% CoV was obtained from the FAST analysis of  $L_{BW}$ ).
- $L_{tower}$  is the wind load on the tower, and is a function of wind speed.
- $X_{Tower}$  is the model uncertainty on the tower wind load and is assumed to be Lognormally distributed with a mean of 1 and CoV of 5%.
- $L_{Slam}$  is the wave slam load, if any, on the structure's portion below water, and is a function of wave height and total water depth (i.e., surge height plus water depth).
- $X_{Slam}$  is the model uncertainty for slam loads and is assumed to be lognormally distributed with a mean of 1 and CoV of 20%. Note this CoV is relatively large to represent the uncertainty associated with the breaking wave forces on large-diameter structures.
- $L_{Corr}$  is the additional load associated with the Stream function correction, and is a function of wave height and total water depth.
- $X_{Corr}$  is the model uncertainty for the load correction  $L_{Corr}$ . This factor is assumed to be lognormally distributed with a mean of 1 and CoV of 5%

In this formulation, the metocean parameters that drive the load calculations are the wind speed and significant wave height for the annual maximum storm condition. The significant wave height implicitly defines the zero-crossing wave period, current velocity, and the surge height experienced for different storm severities (return periods). The wind speed and significant wave height are in turn correlated for the site. The metocean data at the site indicate that the wind speed ( $W_s$ ) and significant wave height ( $H_s$ ) have a correlation coefficient of 84%. In the reliability analysis,  $W_s$  and  $H_s$  are each modeled using the Gumbel distribution for tropical storms as found from the site-specific data for this site, and the correlation between  $W_s$  and  $H_s$  is

modeled as 84%. The alternate approach would be to model either  $W_s$  or  $H_s$  as an independent distribution and the second parameter as conditional on the first distribution of the wave. This approach was not used because of limitations on the probability distribution of the conditioned parameter. Also, generally for fixed offshore platforms,  $H_s$  is selected as the independent variable and  $W_s$  is chosen as the conditioned variable. However, for OWTs,  $W_s$  may be far more critical and thus should be used as the independent variable, while  $H_s$  may be critical when slam loads come into effect for extreme storms. Therefore, the correlation coefficient approach was adopted to give equal weight to  $W_s$  and  $H_s$  in the reliability calculation.

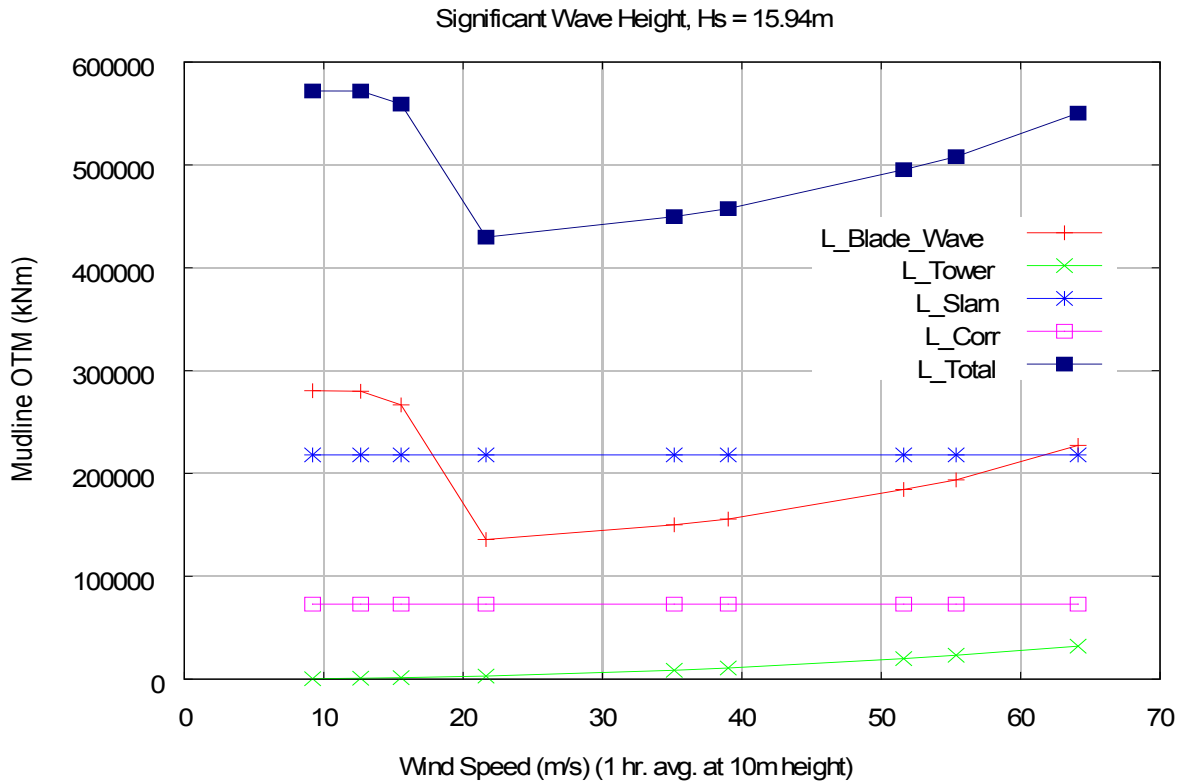
The variation of OTM with  $W_s$  and  $H_s$  is shown in the figures below. In the analysis performed, the aerodynamic load on the blade and the hydrodynamic load on the monopile are analyzed in FAST using simulated wind time-histories and a Stream nonlinear wave-elevation profile. The data provide average values of the maximum load (mudline OTM) for each simulated case. The load that is most relevant to the reliability analysis is the annual mean maximum OTM at mudline.



**Figure 23. Mudline overturning moment (OTM) versus wind speed for the smallest storm analyzed.**  
**(There is no breaking wave phenomenon for this small storm.)**

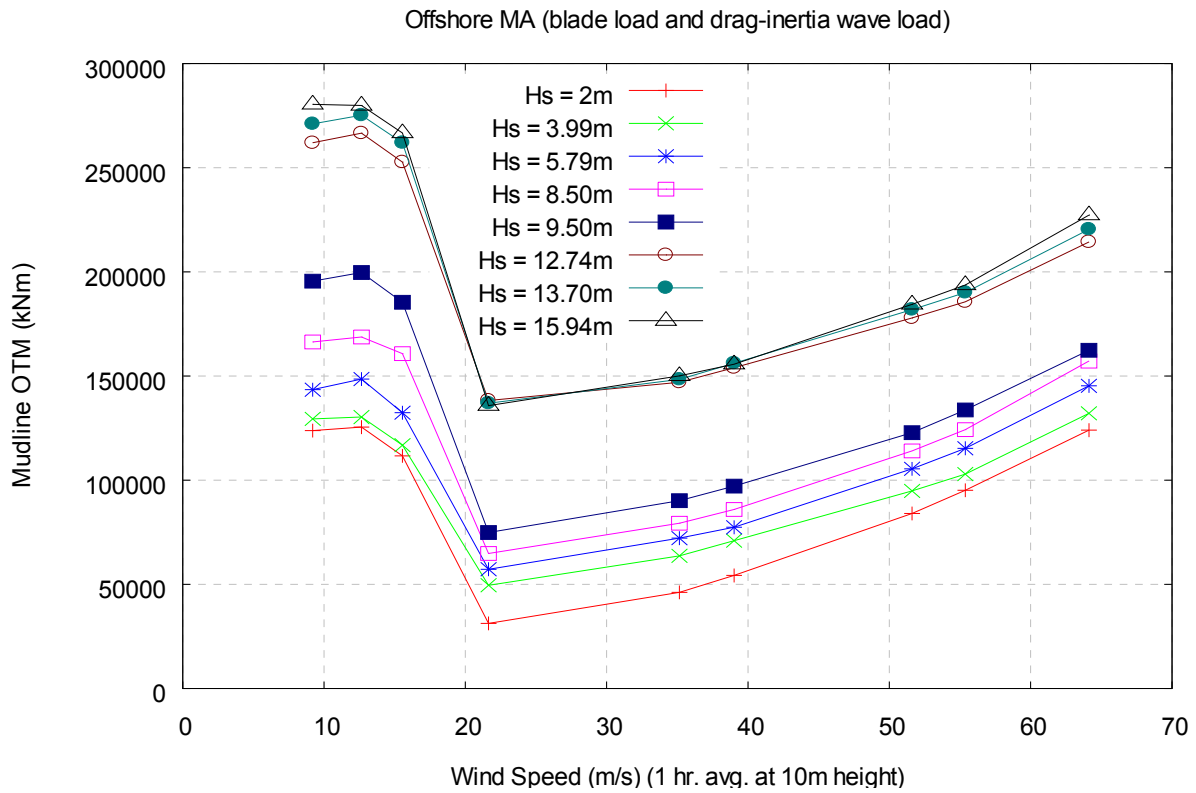
For wind speeds less than about 19 m/s at a 10-m height (i.e., cut-out wind speed of 25 m/s at a hub height of 90 m) the turbine is operating, so the aerodynamic loads are high. As the wind speed becomes greater than 19 m/s, the turbine is assumed to be in parked mode, where the blades are “feathered” into the wind to reduce wind forces on blades. The wind load drops considerably as wind speed goes from an operating range (< 25 m/s at a 90-m height) to a parked

range (> 25 m/s at a 90-m height). Beyond wind speeds of 25 m/s, the load gradually increases with increasing wind speed.



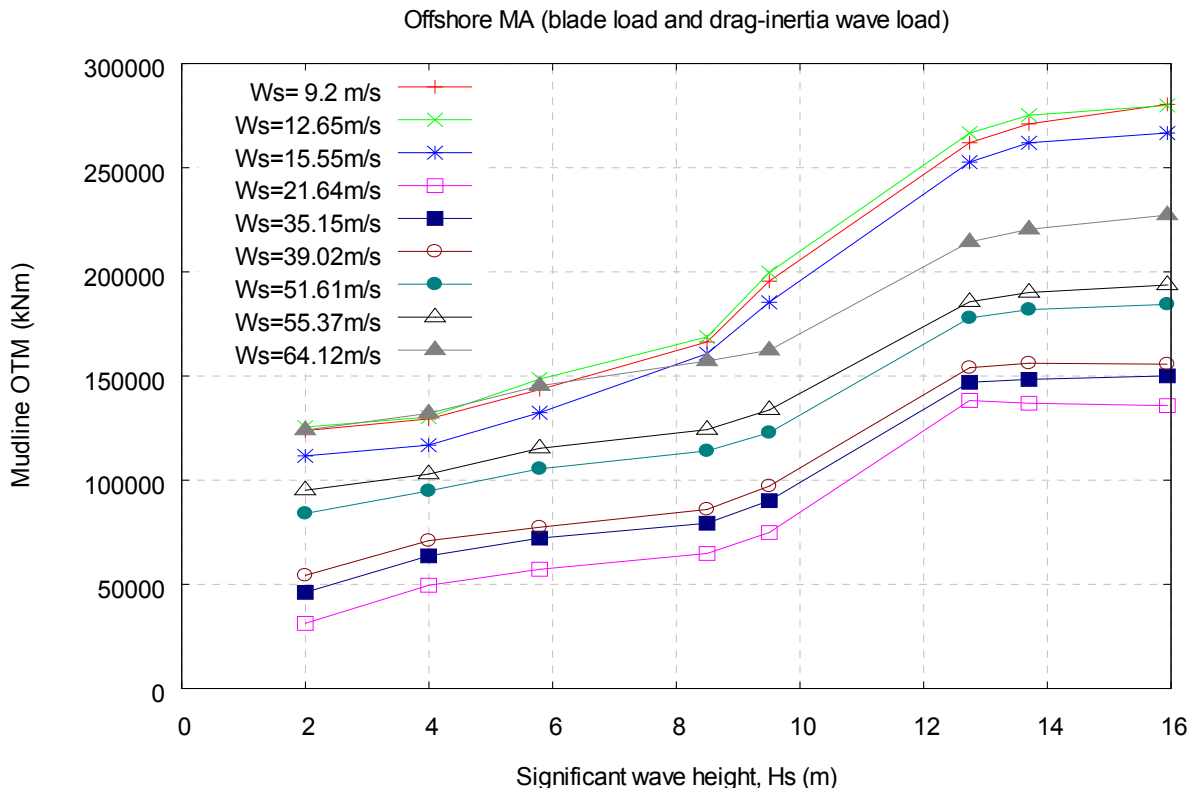
**Figure 26. Mudline OTM vs. wind speed for the largest storm analyzed. (Includes breaking wave effect.)**

The preceding figure shows the contribution from different effects on the total load imposed on the structure. Note that the slamming load is in a similar order of magnitude as the wind and wave load on the structure.



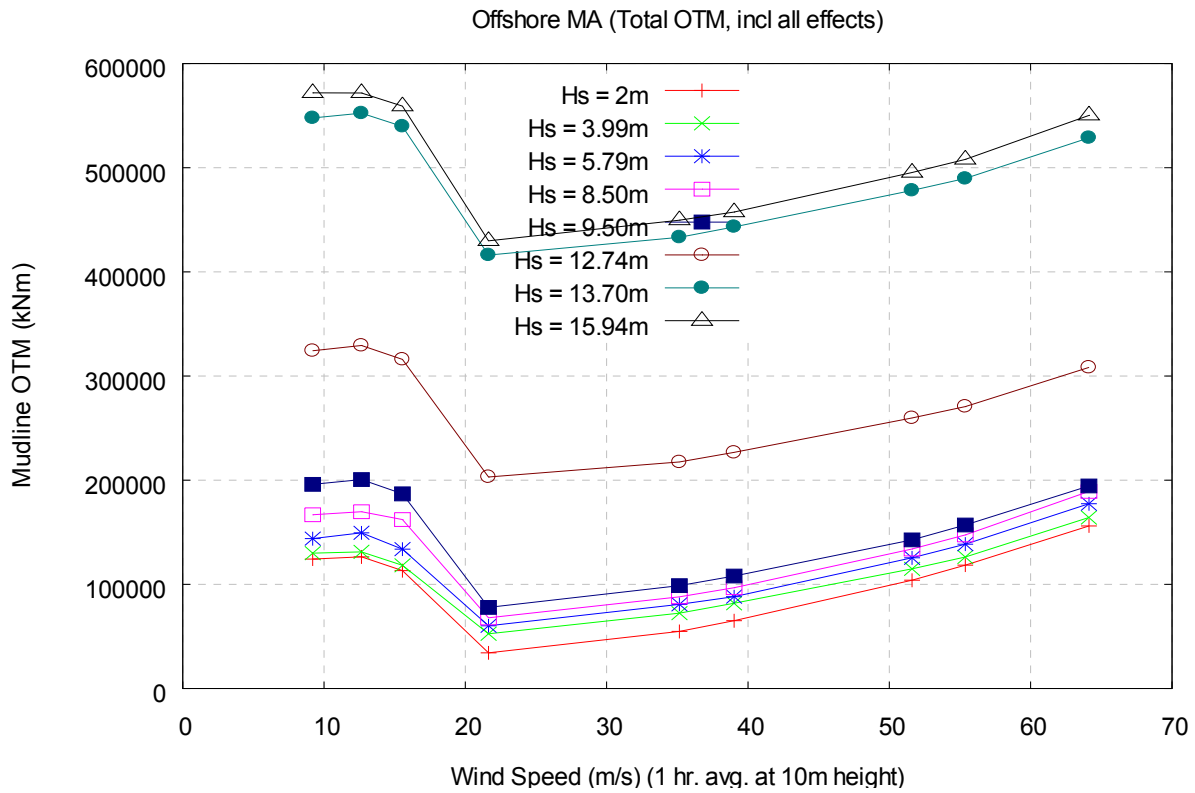
**Figure 27. Loads on blade and wave loads only as a function of  $W_s$ , shown for all  $H_s$  values analyzed**

In Figure 27, the uppermost three cases for  $H_s$  12.74 m (1000-year return period) and greater show much higher loads compared to smaller  $H_s$  values. These cases show prominent shallow-water wave kinematics for the larger storms. Note that the breaking wave effect is not yet included in these loads (these are included later).



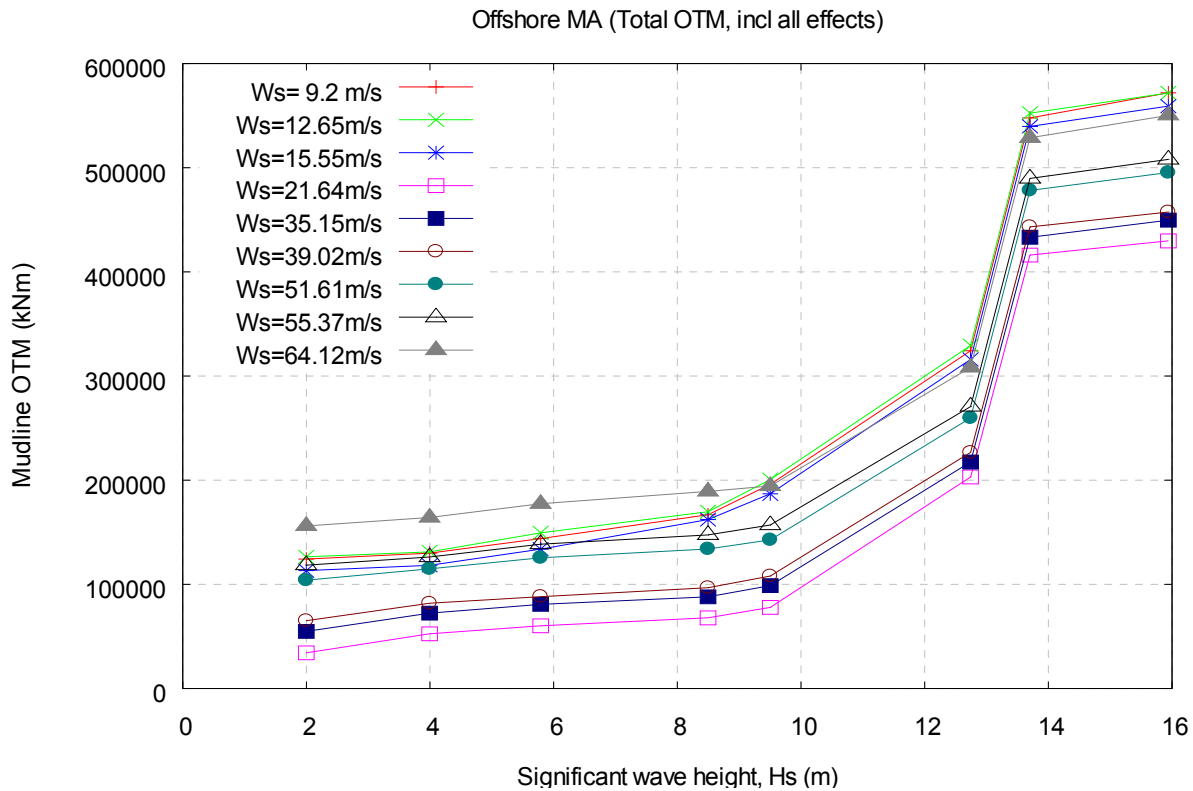
**Figure 28. Loads on blade and wave load as a function of  $H_s$**

Figure 28 is similar to the previous figure, except the metocean parameters are shown differently now. The variation of the load can be seen as a function of  $H_s$  for the different wind speeds analyzed.



**Figure 29. Total loads (including all applicable components) vs. wind speed. (1-hour average, at 10-m reference height.)**

In Figure 29, the upper set of  $H_s$  values result in much higher loads than the smaller  $H_s$  set, which is primarily due to the occurrence of breaking waves for storms with  $H_s \geq 13.70$  m. Now the slam load contribution from the breaking wave is included in the large storms, in addition to the wave kinematics from shallow-water depth effects.

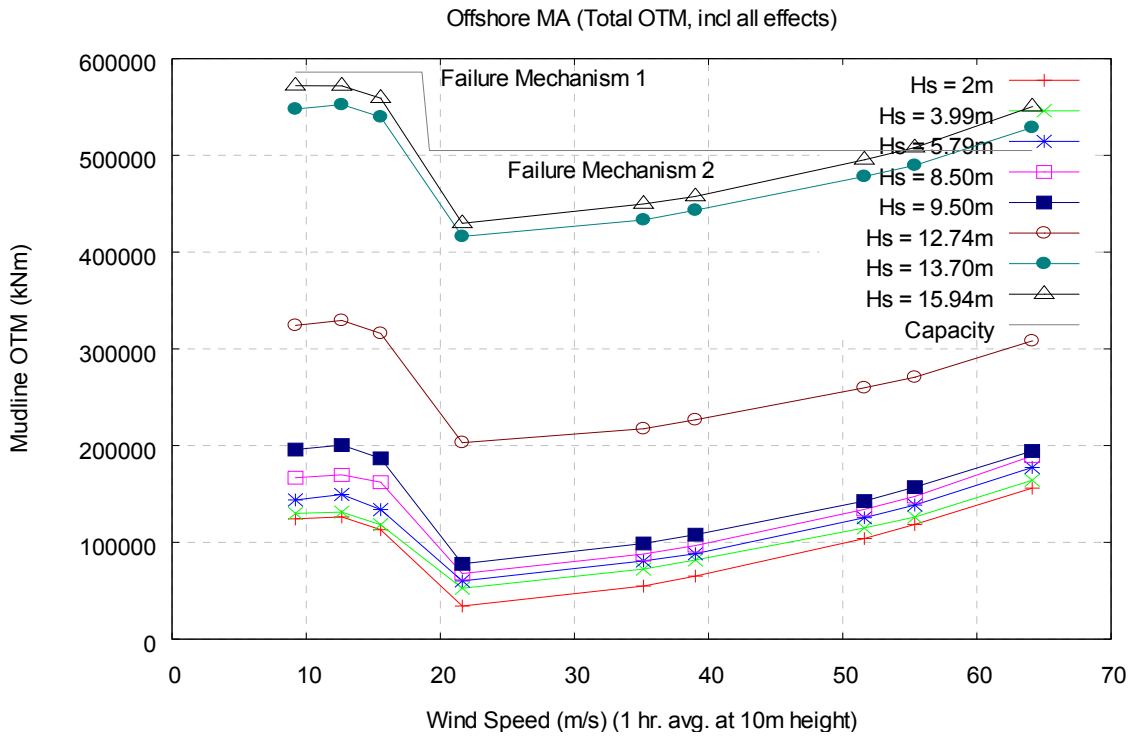


**Figure 30. Mudline overturning moment (including all load components) of monopile as a function of Hs**

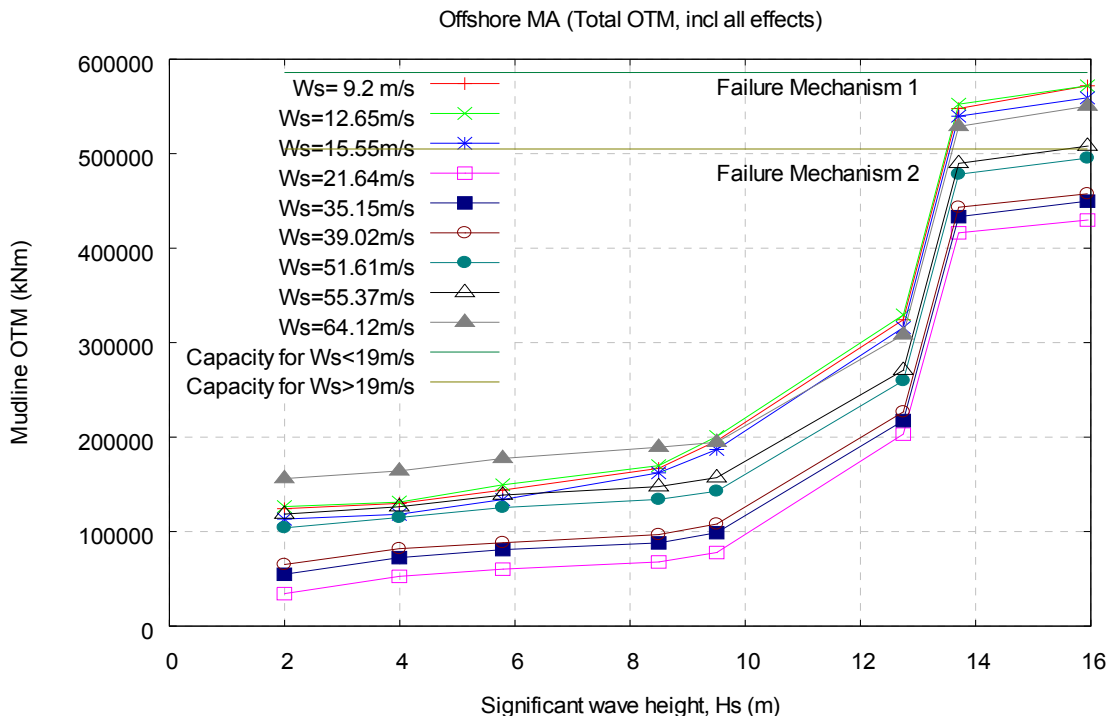
Once the breaking wave height ( $H_s \geq 13.7$  m) has been reached, the loads do not increase significantly because of the similarity of slam loads (Figure 30).

Figure 31 and Figure 32 present the capacity and total load, in terms of mudline overturning moment. The first figure shows how these values vary with an annual maximum 1-hour average wind speed. The second figure provides variation with an annual maximum significant wave height. The capacity of the system is different for the operating and parked conditions because of the different proportions of wave and wind load. This difference causes the plastic hinge to form (see Figure 24) at different elevations along the pile. The capacity is substantially greater than the loads at the 1,000-year level. The loads are higher than some of the likely  $H_s$  and wind speed combinations at the 10,000-year return period as well. Additionally, as noted earlier, the capacity-to-demand ratio indicates a very high reliability index for this design. This reliability is expected, given the small utilization ratios and large reserve-strength ratios for the monopile.

The 19 m/s value of the 1-hour average at 10 m translates to the 25 m/s cut-out speed for 10-min average at 90m (hub height). Employing the reliability formulation with the loads and capacities shown in Figure 32, along with their uncertainty values, the reliability index comes to 5.83, which corresponds to an annual failure probability of  $2.79 \times 10^{-9}$ . The ultimate strength-limit state does not govern the design of the monopile. The monopile design is controlled by the resonance avoidance requirement; therefore, the capacity far exceeds extreme loads for this monopile.



**Figure 31. Total load and capacity for monopile as a function of wind speed. (Failure mechanism is different for operating vs. parked modes.)**



**Figure 32. Total load and capacity for monopile as a function of significant wave height**

## 6 Jacket Substructure Analysis

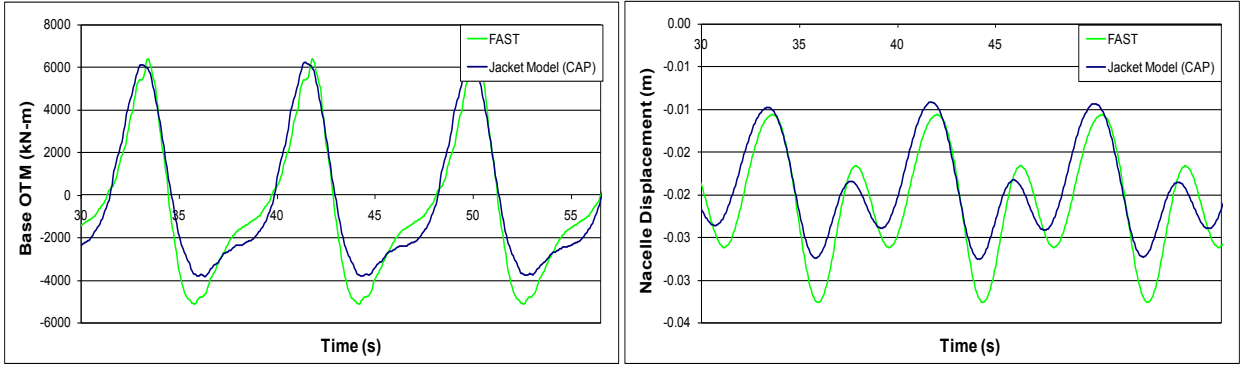
### 6.1 Design Requirements for Resonance Avoidance

As was the case with the monopile, the initial configuration of the jacket was developed to achieve the maximum 4-second period of vibration. The resonance avoidance requirement was initially assumed to control the design of the jacket-type substructure, both in terms of jacket elements and piles. Note that later, it was found that some jacket members were overstressed (utilization ratios were greater than 1.0) due to ultimate strength requirements and these members had to be redesigned. The conclusion appears to be that the jacket design was controlled by ultimate strength requirements in addition to resonance avoidance.

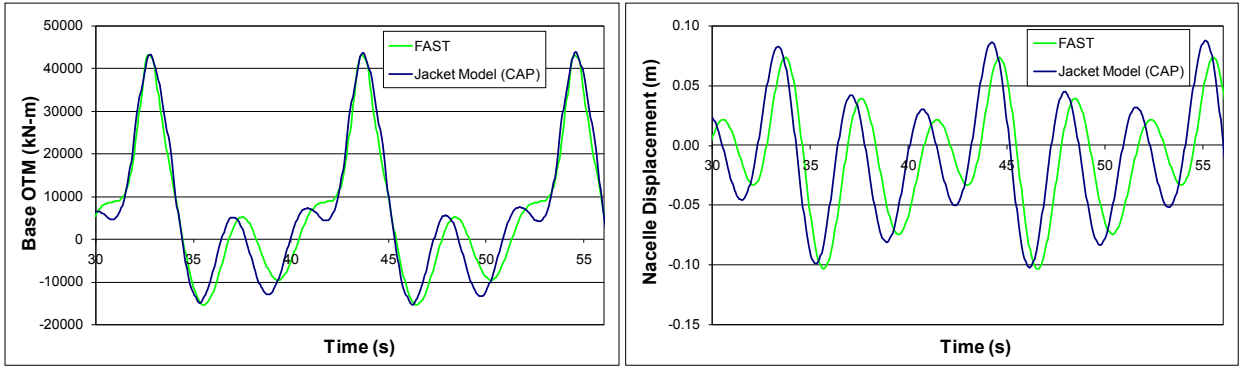
### 6.2 Wind and Wave Load Analyses with FAST

A representation of the jacket was developed as an equivalent monopile for input into the FAST program for wind and wave load analysis. In the case of the jacket, the equivalent monopile properties that were needed for the FAST analysis required additional effort. An equivalent monopile model was developed using the CAP program to properly represent the effect of the foundation, additional framing, and the variation of drag and inertia coefficients above and below water. The modulus of elasticity of the equivalent monopile model (including the tower) was scaled to set the period at 4 seconds. A series of analyses were performed to assess the best overall matching properties for an equivalent monopile in FAST in terms of total wave load and nacelle displacement.

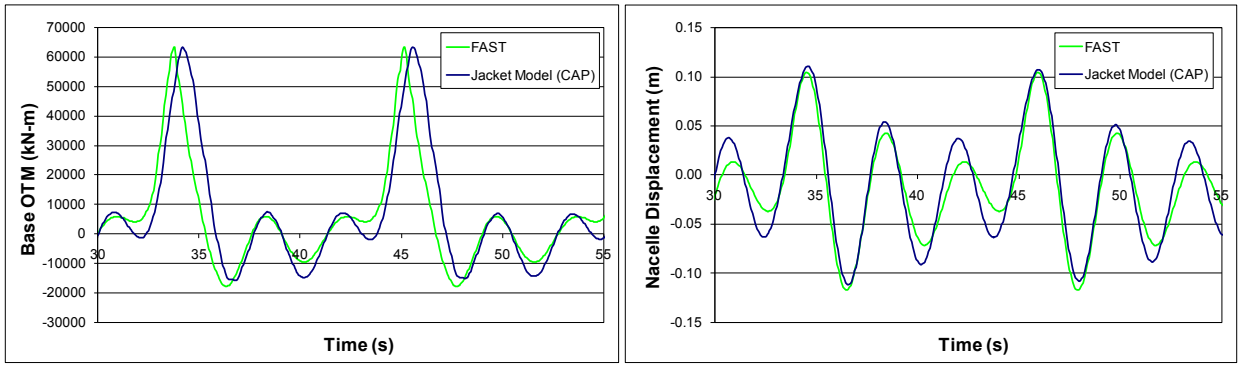
Figure 33 shows the effect of damping and the drag/inertia coefficients in the overturning moment and the nacelle displacement. The target nacelle displacement and the overturning moment time-histories were obtained by explicit CAP analysis. Parametric study for the damping values of the tower was performed by FAST analysis to replicate the target time histories. Priority was given to match the maximum (or minimum) values obtained from FAST and CAP analyses. In contrast to the monopile case, one damping value was not sufficient to obtain similar response values from CAP and FAST analyses for different wave heights. It was concluded that a 20% damping value up to a 100-year wave, a 30% damping value for a 100-year wave, and a 40% damping value beyond the 100-year wave were good representations of the damping in the system. Note again that damping is an overall tuning parameter to permit FAST to mimic the dynamic physical effects missing in FAST but available and modeled in CAP. As a result of parametric studies mentioned previously, equivalent monopile properties were used in the FAST analyses (Table 10).



**Operating Wave**



**50-Year Wave**



**100-Year Wave**

**Figure 33. Effect of damping on jacket structure**

**Table 10. FAST Input Data for Jacket Structure**

Monopile thickness (m)	0.067
Tower base outer diameter (m)	6
Tower base wall thickness (m)	0.03
Tower top outer diameter (m)	3.87
Tower top wall thickness (m)	0.02
Steel density (effective) (kg/m <sup>3</sup> )	8500
Steel Young's modules (E) (MPa)	1.995×10 <sup>5</sup>
Steel shear modulus (G) (MPa)	7.676×10 <sup>4</sup>
Water Depth, d (m)	25
Height monopile extends above MSL (m)	10
Length of Tower+Monopile (m)	112.6
C <sub>d</sub>	0.55 (<100 year) 0.60(=100 year) 0.70(>100 year)
C <sub>m</sub>	0.2
Damping	20%(<100 year) 30%(=100 year) 40%(>100 year)
Structural fore-aft period (s)	3.84

### 6.3 Total Wind and Wave Load Demand

Figure 34 presents the results of coupled wind and wave analyses with FAST in terms of base shear and overturning moment. A detailed discussion on the coupled wave and wind loading is provided for the monopile case after Figure 22. The main observation regarding the difference between the monopile and jacket responses is that both base shear and over turning moment decrease significantly in the case of the jacket-type structure. Base shear decreases almost by half because the projected area of the jacket structure is almost half that of the monopile. The overturning moment does not decrease by half because there are two components affecting the overturning moment: wave loading and wind loading times the height of the structure above the mudline. Although the overturning moment caused by wave loading decreases by half for the jacket structure compared to monopile, the effect of the wind loading and the height of the structure stays constant for both types of structures. Therefore, the decrease in the overturning moment is not by half for the jacket-type structure compared to the monopile. Table 11 provides the results for the metocean loads used in the design checks. These are nominal loads and do not include any load factors.

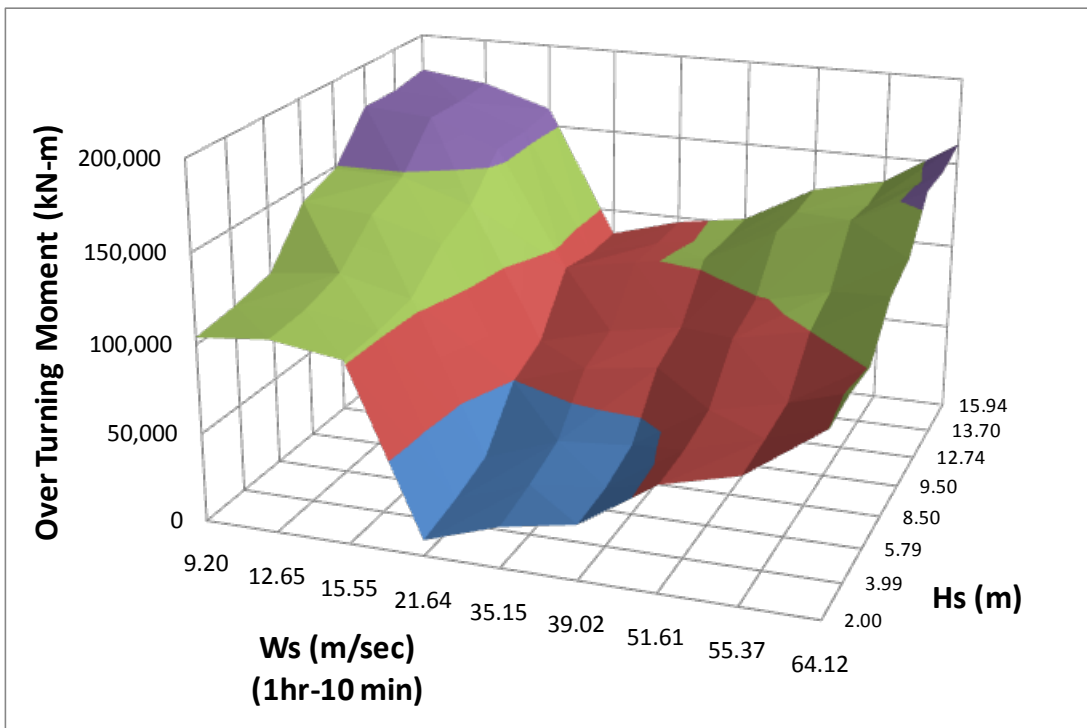
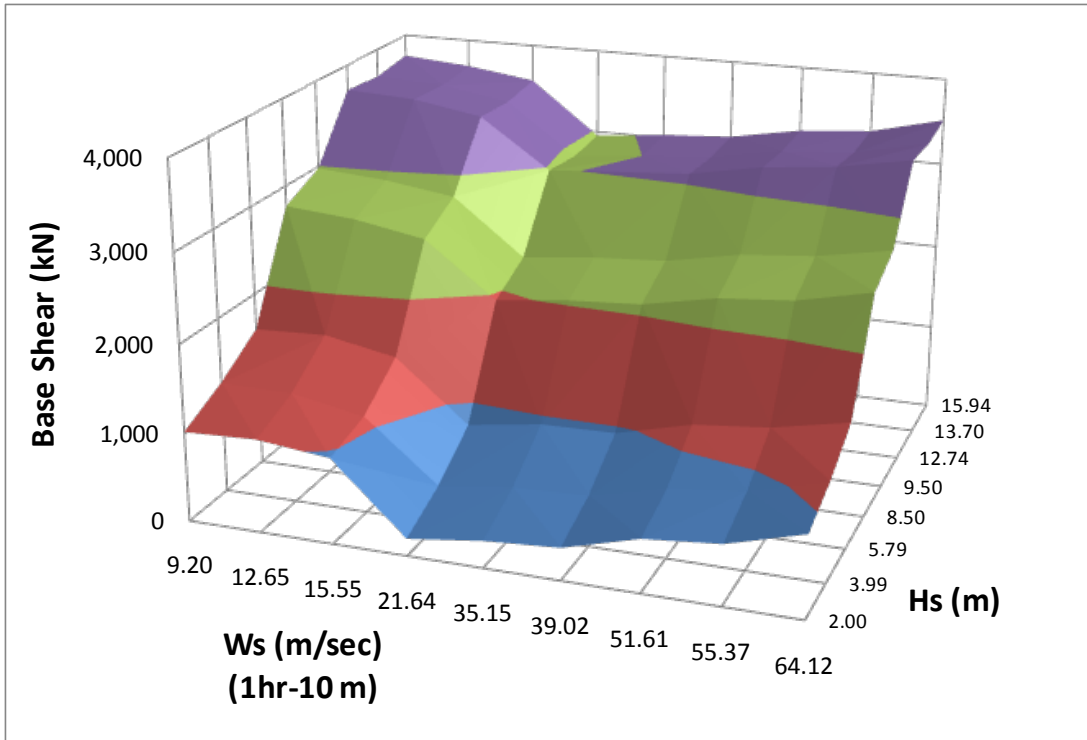


Figure 34. Coupled wind and wave loads (top-base shear, bottom-overturning moment) for a jacket-type structure for blade and hydrodynamic loads

**Table 11. Jacket Design Loads at Mudline Section**

<b>Base Shear (kN)</b>			
Storm Type	Coupled Wind-Wave	Tower Wind	Total*
Operating Storm	1,266	7.26	1,273
50-year Storm (Wind Driven)	1,632	117	1,749
50-year Storm (Wave Driven)	2,206	90	2,296
100-year Storm (Wind Driven)	2,043	145	2,188
100-year Storm (Wave Driven)	2,536	112	2,648
<b>Mudline Overturning Moment (MN-m)</b>			
Storm Type	Coupled Wind-Wave	Tower Wind	Total <sup>a</sup>
Operating Storm	107	0.51	107
50-year Storm (Wind Driven)	53	8.66	61
50-year Storm (Wave Driven)	61	6.64	68
100-year Storm (Wind Driven)	67	10.8	78
100-year Storm (Wave Driven)	75	8.3	83

\* Note: Breaking waves occur in storms larger than a 100-year storm

## 6.4 Strength Checks

Each unfactored base shear and overturning moment pair (at mudline) from Table 11 was converted into a shear-moment at the top of the jacket and applied to the jacket model in CAP (Figure 35). The analyses were repeated for three wave heading directions (0°, 90°, and 180° clockwise from north). In each analysis, the maxima of the axial load, shear, and bending moment demand on the main member types (central column, piles, legs, and braces) were obtained. The design checks showed that the preliminary design dimensions were sufficient according to both IEC and API.

Table 12 and Table 13 show the final member dimensions and the factored loads according to IEC and API, respectively. The maximum member utilization ratios are summarized for the API and IEC jacket designs in Table 14. In all of the cases, the pile elements were the ones to be most utilized.

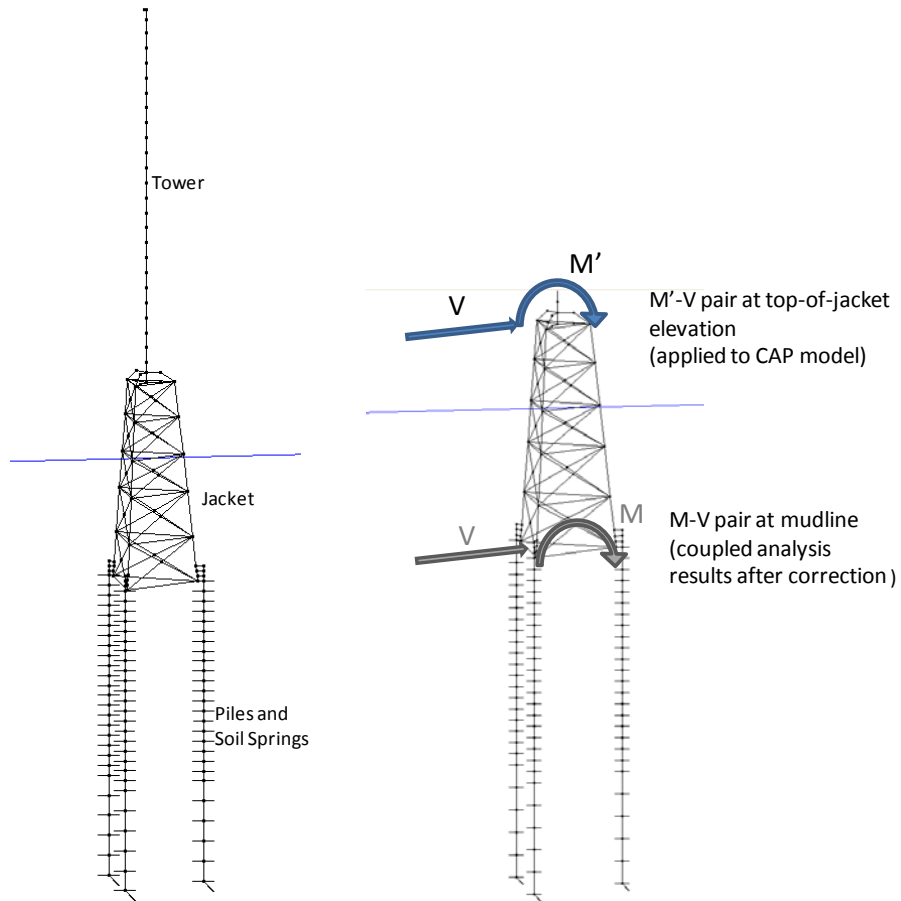


Figure 35. Jacket model in CAP. (Illustration from MMI Engineering)

Table 12. Jacket Design Loads per IEC/ISO

Jacket Design Checks per IEC/ISO	Diameter (m)	Thickness (m)	Operating Load Case (Factored Loads)				
			Axial Load (kN)	Bending Moment (kNm)	Shear, V (kN)	Utilization Ratio (N+M)	Utilization Ratio (V)
Vertical Brace	0.4	0.02	254	131	29	0.241	0.018
Horizontal Brace	0.3	0.01	134	18	6	0.243	0.01
Leg (below El. -16m)	1	0.05	11,939	4,677	920	0.813	0.09
Leg (above El. -16m)	0.9	0.045	12,485	2,244	430	0.774	0.052
Pile (below El. -31m)	1.2	0.04	9,514	871	173	0.376	0.017
Pile (above El. -31m)	1.2	0.045	11,397	5,450	1,298	0.711	0.116

Jacket Design Checks per IEC/ISO	Diameter (m)	Thickness (m)	50-Year Extreme Environmental Load Case (Factored Loads)				
			Axial Load (kN)	Bending Moment (kNm)	Shear (kN)	Utilization Ratio (N+M)	Utilization Ratio (V)
Vertical Brace	0.4	0.02	612	82	15	0.247	0.009
Horizontal Brace	0.3	0.01	190	19	8	0.318	0.012
Leg (below El.-16m)	1	0.05	8,273	2,037	391	0.451	0.038
Leg (above El. -16m)	0.9	0.045	5,241	1,071	204	0.341	0.025
Pile (below El.-31m)	1.2	0.04	11,397	5,450	1,298	0.363	0.01
Pile (above El.-31m)	1.2	0.045	8,676	6,530	1,816	0.707	0.162

**Table 13. Jacket Design Loads per API**

Jacket Design Checks per API	Diameter (m)	Thickness (m)	Operating Load Case				
			Axial Load (kN)	Bending Moment (kNm)	Shear (kN)	Utilization Ratio (N+M)	Utilization Ratio (V)
Vertical Brace	0.4	0.02	170	103	22	0.308	0.018
Horizontal Brace	0.3	0.01	110	16	7	0.327	0.015
Leg (below El.-16m)	1	0.05	9,272	3,936	715	0.989	0.096
Leg (above El. -16m)	0.9	0.045	9,607	1,754	336	0.91	0.056
Pile (below El.-31m)	1.2	0.04	7,425	662	138	0.426	0.019
Pile (above El.-31m)	1.2	0.045	8,887	4,262	1,006	0.863	0.123

Jacket Design Checks per API	Diameter (m)	Thickness (m)	50-Year Extreme Environmental Load Case				
			Axial Load (kN)	Bending Moment (kNm)	Shear (kN)	Utilization Ratio (N+M)	Utilization Ratio (V)
Vertical Brace	0.4	0.02	552	71	13	0.269	0.008
Horizontal Brace	0.3	0.01	171	17	7	0.346	0.012
Leg (below El.-16m)	1	0.05	7,474	1,854	356	0.471	0.036
Leg (above El.-16m)	0.9	0.045	4,560	942	178	0.343	0.022
Pile (below El.-31m)	1.2	0.04	6,566	1,483	88	0.371	0.009
Pile (above El.-31m)	1.2	0.045	7,853	5,897	1,639	0.761	0.151

**Table 14. Utilization Ratio Summary for Jacket**

Section	Dimensions		API				IEC/ISO			
			Power Production <sup>a</sup>		Parked/ Idling		Power Production <sup>b</sup>		Parked/ Idling	
	D (m)	t (m)	N+M	V	N+M	V	N+M	V	N+M	V
<b>Vertical Brace</b>	0.4	0.02	0.308	0.018	0.269	0.008	0.241	0.018	0.247	0.009
<b>Horizontal Brace</b>	0.3	0.01	0.327	0.015	0.346	0.012	0.243	0.01	0.318	0.012
<b>Leg (Lower)</b>	1	0.05	0.989	0.096	0.471	0.036	0.813	0.09	0.451	0.038
<b>Leg (Upper)</b>	0.9	0.045	0.91	0.056	0.343	0.022	0.774	0.052	0.341	0.025
<b>Pile (Lower)</b>	1.2	0.04	0.426	0.019	0.371	0.009	0.376	0.017	0.363	0.01
<b>Pile (Upper)</b>	1.2	0.045	0.863	0.123	0.761	0.151	0.711	0.116	0.707	0.162

<sup>a</sup> Without one-third allowable stresses increase factor

<sup>b</sup> With the same load and material factors from parked/idling condition

All utilization ratios are below 1.0, and most ratios are far below 1.0. This implies that factored strength is generally much greater than the factored loads in each design code. The largest ratio, 0.989, is for a leg member in power production condition. When weather severity pushes the structure beyond its elastic limit, the legs are mostly likely to be the first members to fail, given that the legs undergo the greatest utilization. The reliability indices for both API and IEC can be expected to come close to the safety levels implicit in these codes, especially for the legs that have utilization ratios close to 1.

## 6.5 Capacity Analysis

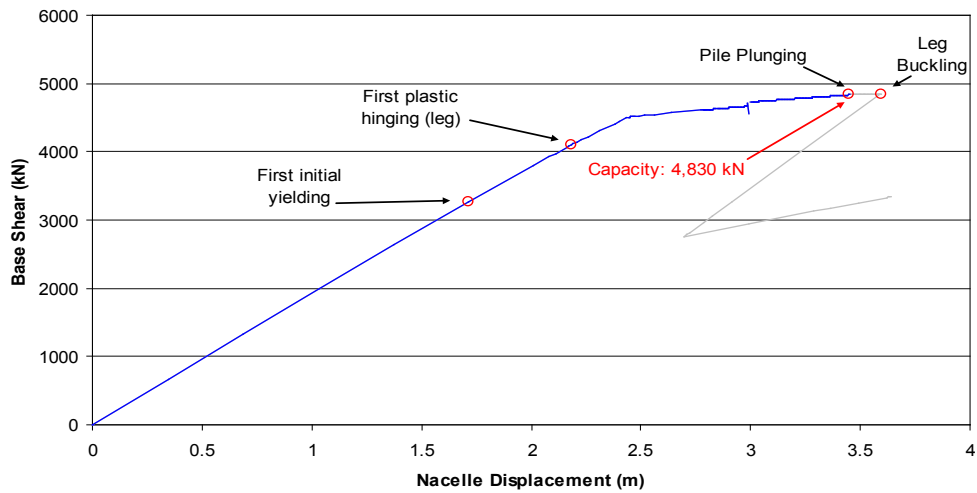
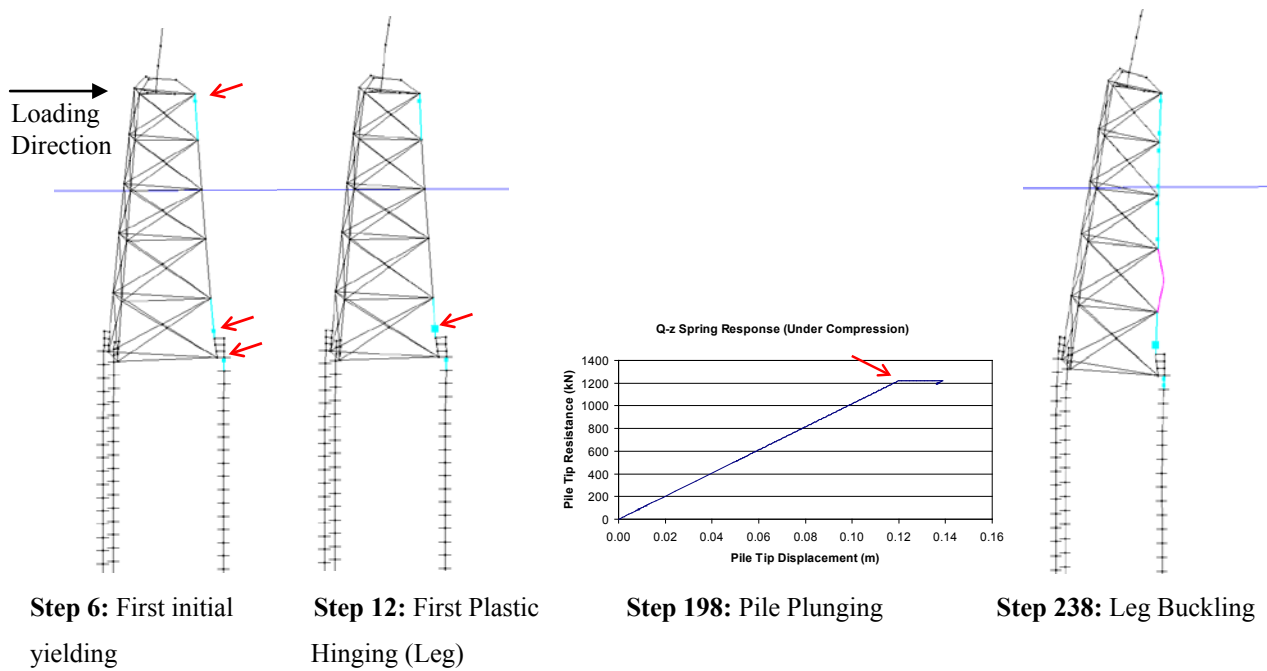
A nonlinear model of a jacket structure was developed using the CAP software and was used for capacity analyses. The analyses were repeated for each load case (i.e., operating, 50-year storm, 100-year storm). The model included soil-pile interaction explicitly.

Figure 36 summarizes the results of the analysis with the operating load case. As the lateral load on the structure is increased, initial yielding was observed at two locations on the compression leg and one location on the compression pile (Step 6). The lower spot on the compression leg became fully plastic (also referred to as a “plastic hinge”) at Step 12. Note that neither of these events caused a significant softening in the load-displacement curve. The structure softens because there are other locations along the compression leg reaching the initial yield level. The structure was assumed to reach the ultimate point when the compression pile plunged at Step 198. The lateral load on the structure at this step is the capacity used in the reliability analysis. Note that this is a conservative assumption because the structure could have been pushed further until the compression leg buckles at Step 238.

The response of the structure under storm loads (both 50-year and 100-year storms) is slightly different. The results of the capacity analysis with the 50-year storm load case are presented as an example in Figure 37 (results for the 100-year storm are similar and not shown in this report). In these analyses, the nonlinear events were concentrated mostly on the piles. The first plastic hinging was observed in the compression pile. This was followed by buckling of one of the horizontal braces at the mudline elevation. The structure was assumed to reach its capacity when the compression pile buckles. If the analysis is carried out further, the next significant event

would be the double hinging of the piles. Note that there was no significant increase in the lateral resistance after the pile plunging, as shown in the load-displacement plot.

The capacities based on these analyses are listed in Table 15.



**Figure 36. Results of a typical capacity analysis under operating storms (Bottom: load-displacement curve; Top: deflected shape with nonlinear events at important steps.)**

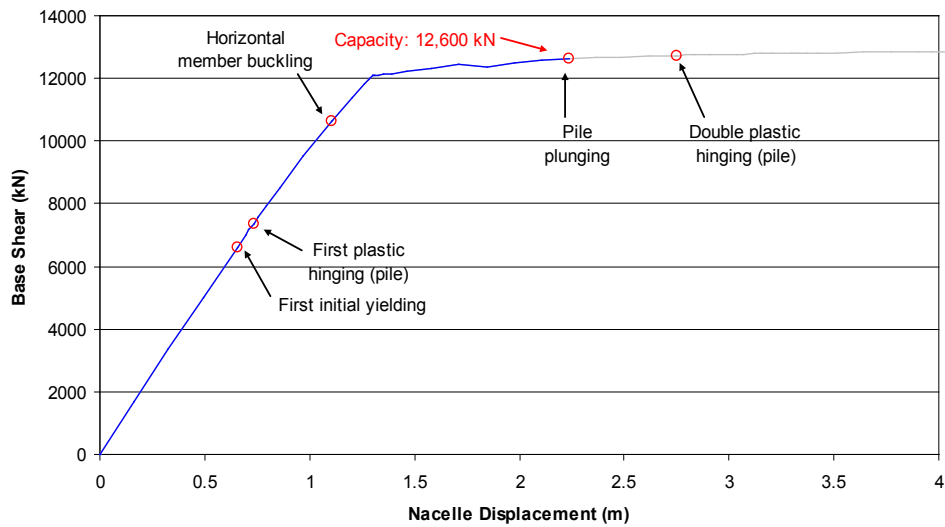
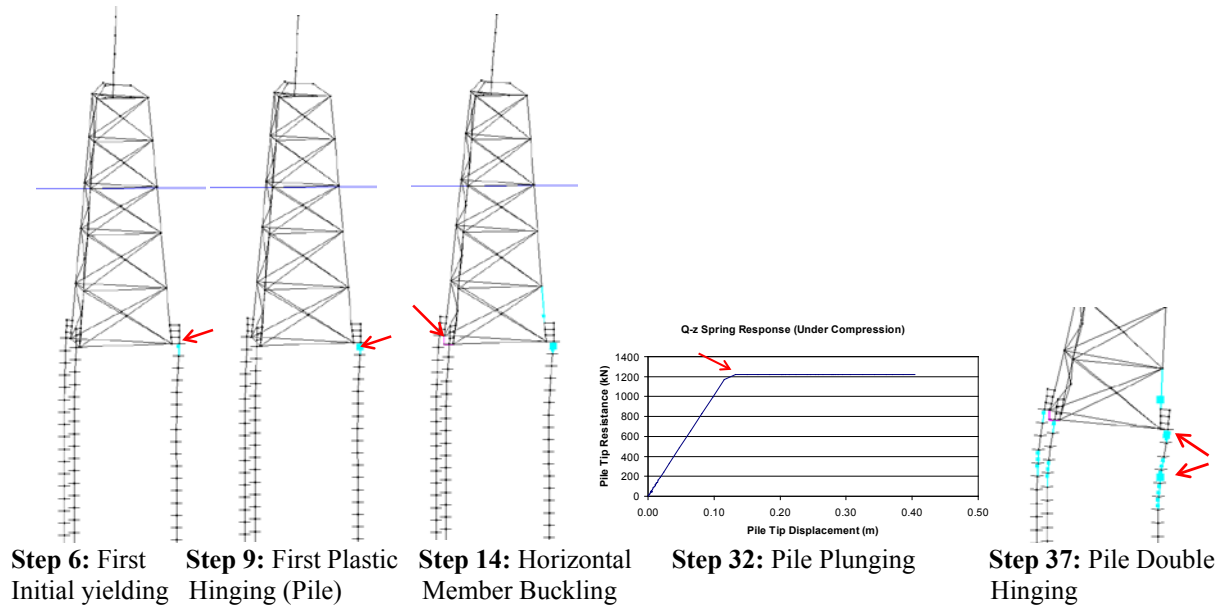


**Figure 37. Results of a typical capacity analysis for a 50-year wave (Bottom: load-displacement curve; Top: deflected shape with nonlinear events at important steps.)**

**Table 15. Capacity Analysis Results for Jacket**

Load Case	Demand		Capacity		Capacity/Demand Ratio	
	Base Shear (kN)	Base OTM (MN-m)	Base Shear (kN)	Base OTM (MN-m)	Base Shear	Base OTM
<b>Power Production</b>	1,273	107	4,833	419	3.8	3.92
<b>Parked (50-Year Metocean Criteria)</b>	2,296	68	12,644	400	5.51	5.88
<b>Parked (100-Year Metocean Criteria)</b>	2,648	83	12,611	400	4.76	4.82

The ratio of the capacity to the design loads provides an initial indication of reliability. Larger ratios imply greater levels of reliability for ultimate strength failure. The ratio for operating cases is 3.92. The IEC capacity-to-50-year-load ratio is 5.88 and the API capacity-to-100-year load is 4.82. The ratio of capacity to a reference load is commonly referred to as a reserve strength ratio (RSR). The API ratio is lower than the IEC ratio for the parked case because of the larger 100-year load compared to the 50-year load, and the capacity is the same for both designs. The ratio of the 100-year load to the 50-year load itself is about 1.15, while the capacities of the two designs are essentially the same. This implies that both IEC and API designs could be expected to result in levels of reliability that are higher than what is implicit in each code, given the relatively large reserve strength ratios (a high reserve strength ratio is expected to imply a high reliability, assuming the physics of the load and capacity do not change materially after the 100-year storm condition). A better indication of the reliability levels achieved in each design can be made by comparing the capacities to the same reference load.

## 6.6 Jacket Reliability Analysis

Figures 38 through 43 show the variation of the total mudline overturning moment with the annual maximum wind speed and with the annual maximum significant wave height. A comparison of the total load and the resulting capacity for the jacket is provided in Figure 44 and Figure 45.

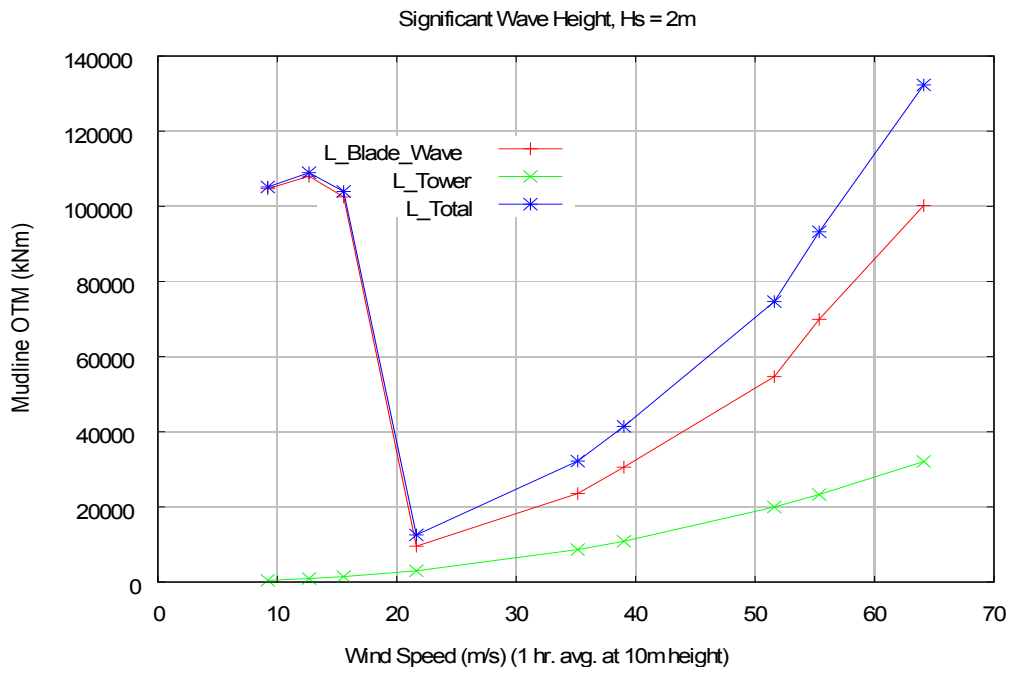


**Figure 38. Mudline overturning moment (OTM) versus wind speed for the smallest storm analyzed.**

(There is no breaking wave phenomenon for this small storm.)

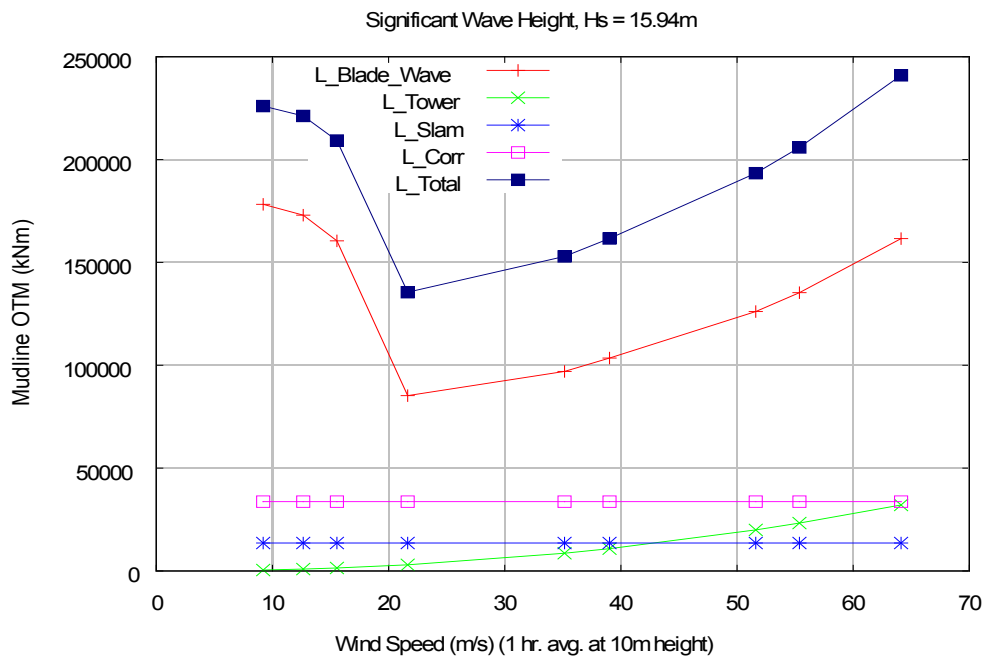


**Figure 39. Mudline OTM vs. wind speed for the largest storm analyzed. (Includes breaking wave effect.)**

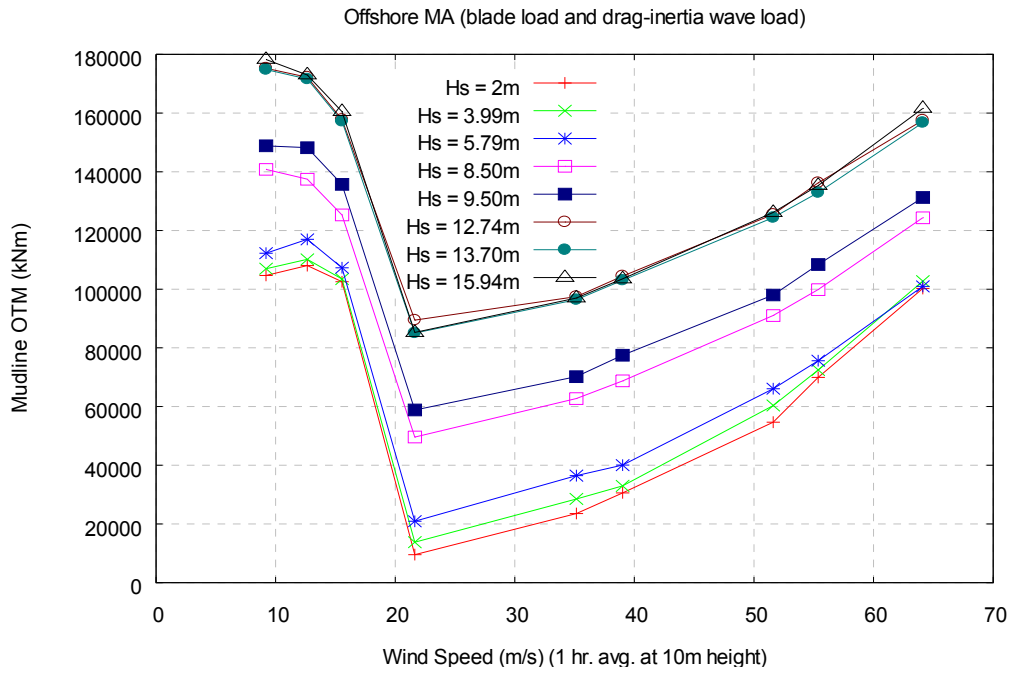


**Figure 40. Mudline overturning moment due to aerodynamic wind load and hydrodynamic wave loads. (No breaking wave effect included yet.)**

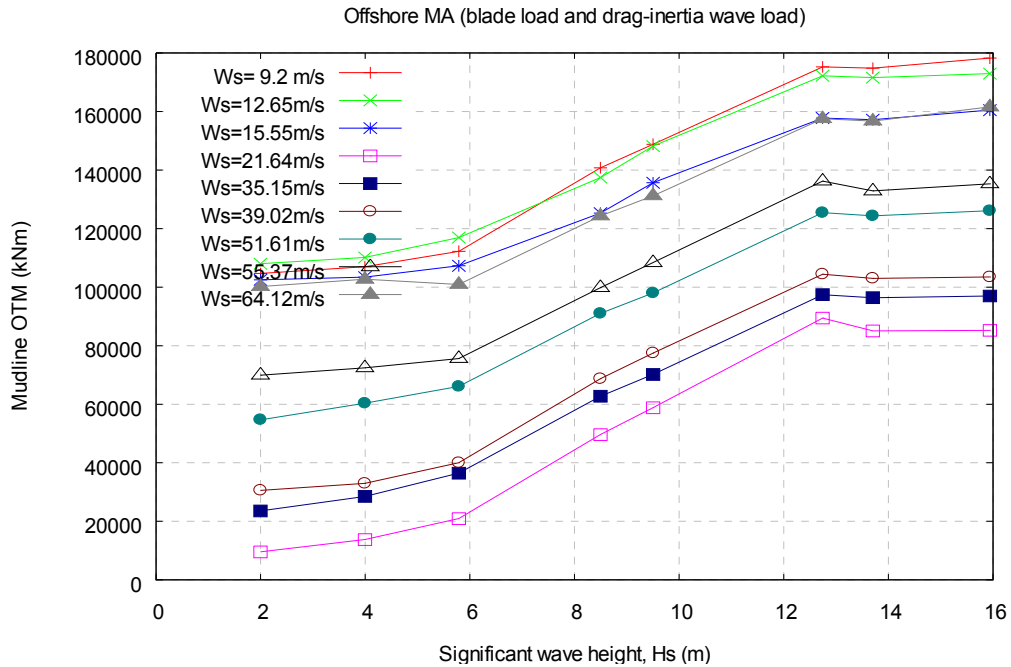


**Figure 41. Loads from aerodynamic and hydrodynamic effects (excluding breaking wave effects) vs. H<sub>s</sub>**

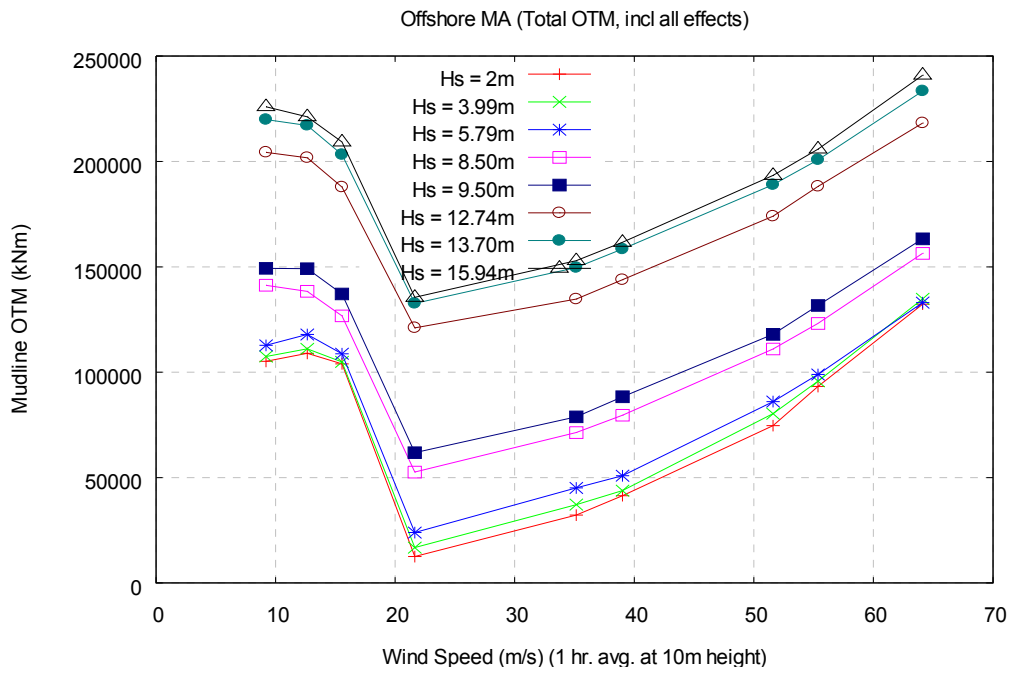


Figure 42. Total load (including all effects) vs wind speed for different  $H_s$  values

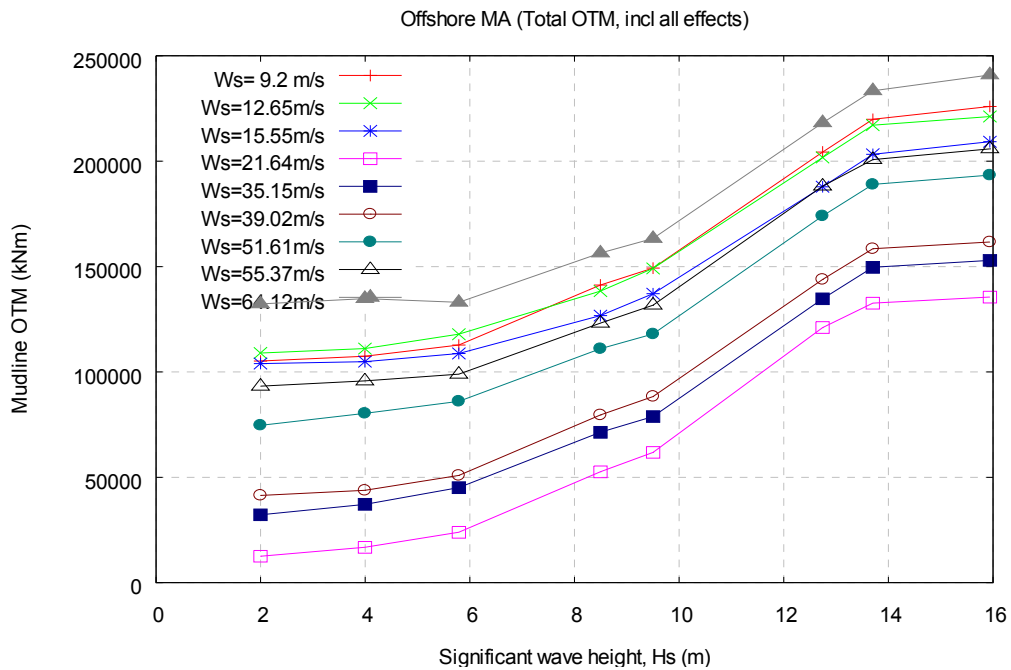
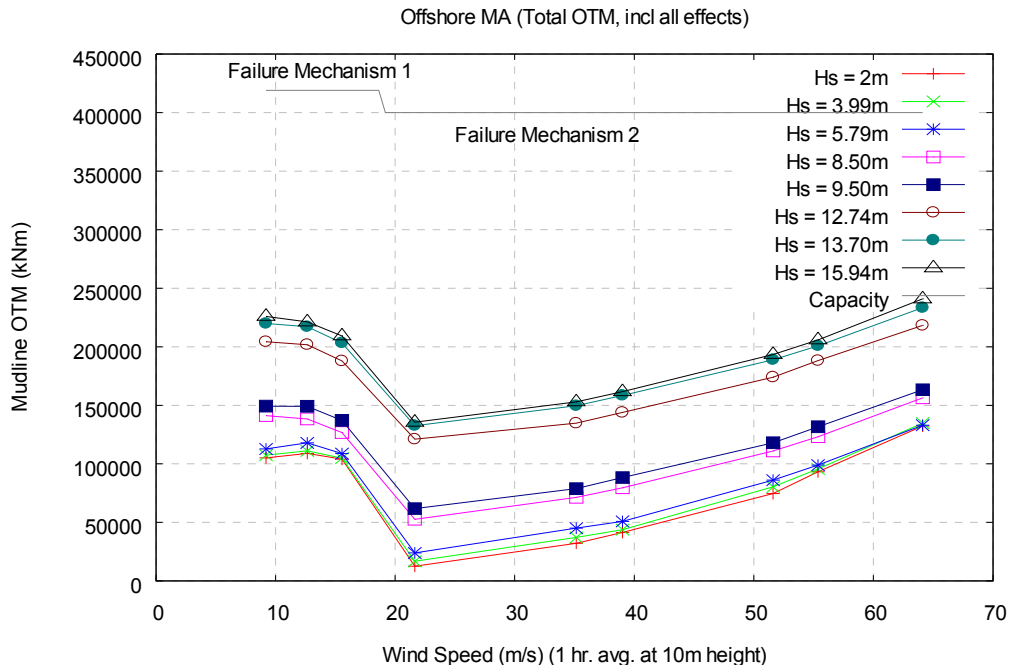


Figure 43. Total load (including all effects) vs  $H_s$  for different wind speed values



**Figure 44. Total load and capacity for jacket as a function of wind speed**

These figures are meant to show the variation of loads with different combinations of wind speeds and significant wave height. This does not address the likelihood of each  $W_s$  and  $H_s$  combination. The design codes use the 50-year and the 100-year storms as the basis for design development and these loads are much less than the capacity. The reliability index calculation<sup>11</sup> includes a range of  $H_s$  up to the 10,000-year value of 15.94 m. Note that the ultimate strength capacity of the structure is much larger than the loads, either in the operating or parked conditions for the blades.

<sup>11</sup> As additional insight, the pair that corresponds to the 1000-year  $W_s$  (60m/s) and the 1000-year  $H_s$  (13.13m) is likely to occur in a storm with a return period larger than 1000 years. This is due to the correlation between  $W_s$  and  $H_s$  which is less than 1. A correlation of 1 (100%) would result in the 1000-year storm having the 1000-year  $W_s$  value (independent of  $H_s$ ) and the 1000-year  $H_s$  value (independent of  $W_s$ ). A correlation less than 1 would result in a 1000-year storm having either  $W_s$  less than the 1000-year  $W_s$  or  $H_s$  less than the 1000-year  $H_s$ .

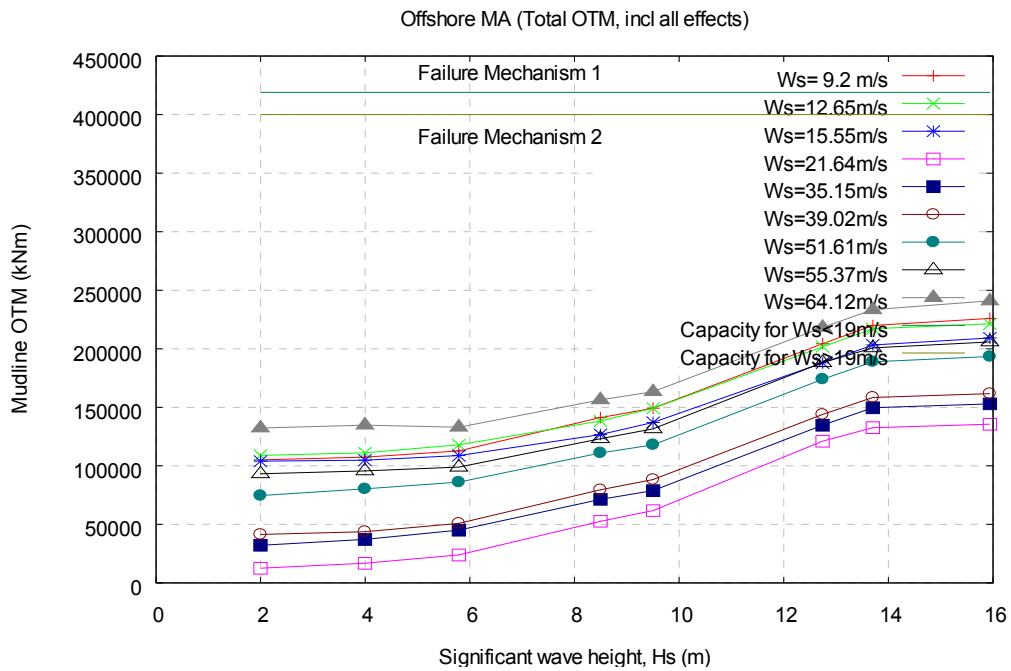


**Figure 45. Total load and capacity of jacket as a function of  $H_s$**

The reliability index is 5.45, which corresponds to an annual failure probability of  $2.51 \times 10^{-8}$ . The ultimate strength limit state does not govern the design of the jacket. The jacket design is controlled by the resonance avoidance requirement; and the capacity far exceeds extreme loads for this jacket.

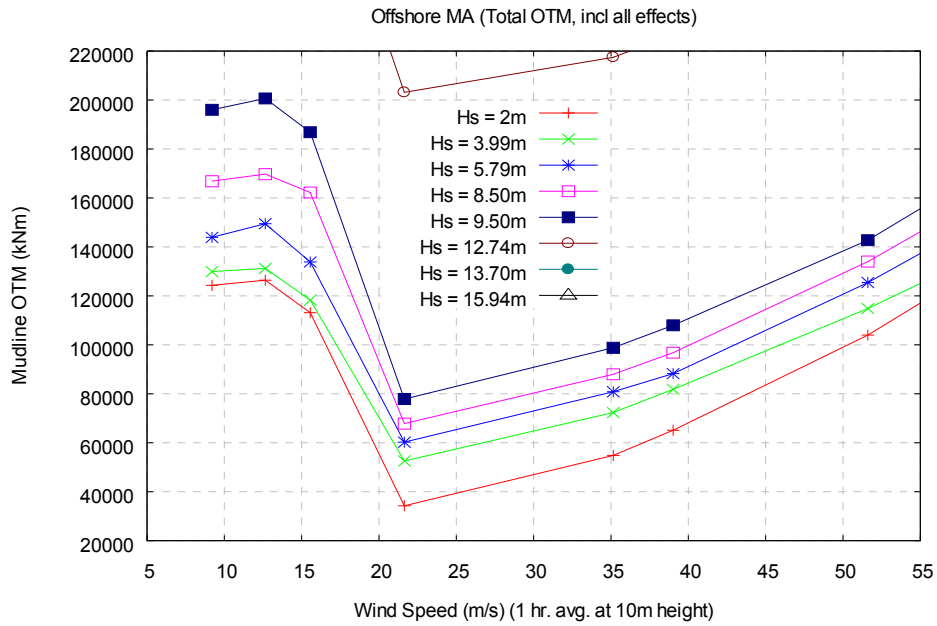
## 7 Comparison of Monopile and Jacket

This section presents some key comparisons of monopile to jacket results for the site analyzed at a water depth of 25 m, and a comparison of the monopile at the 15-m water depth from Phase I.

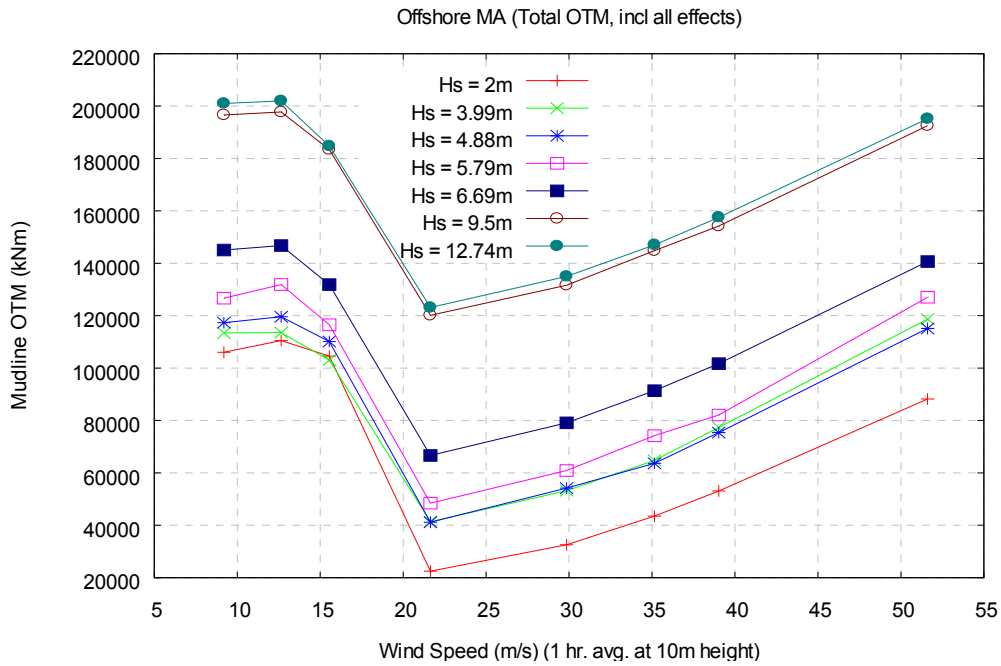
### 7.1 Monopile Results, 25-m versus 15-m water depth

Figure 46 compares the monopile total mudline overturning moments for the 25-m water depth case with the 15-m water depth case analyzed in Phase I. The 25-m results are shown for wind speed and moment ranges in the exhibit (a) to match those in exhibit (b) to permit direct comparison of the loads across similar  $H_s$  values. The following observations can be made from this figure:

- For a 2-m  $H_s$  storm, there are no breaking waves in either storm and the 25-m case results in slightly larger loads than the 15-m case due largely to the increased lever arm for the same aerodynamic loads on the blades in the two cases.
- Notice that for the 25-m depth case, the loads increase substantially in going from  $H_s$  9.5 m to 12.74 m, the onset of the breaking condition for the 25-m depth case. On the other hand, the onset of breaking happens earlier for the 15-m depth case (shallower depth causes breaking for smaller waves), as seen in the increase of loads going from  $H_s$  of 6.69 m to 9.5 m.
- For the same  $H_s$  value of 9.5 m, focus is on the loads around 52 m/s wind speed. The 15-m depth case indicates a larger OTM of 190 kN-m, compared to an OTM of 140 kN-m for the 25-m depth case. This larger OTM indicates the dominant effect of a breaking wave on the total overturning moment. (The breaking wave is present for the 15-m case, and absent for the 25-m case).



(a) Monopile at 25-m depth site (range shown corresponding to plot below, for convenience)



(b) Monopile at 15-m depth site

**Figure 46. Monopile loads for 15-m and 25-m depth as a function of wind speed and significant wave height**

Table 16 and Table 17 compare the specific design loads and the utilization ratio for the design loads for ultimate strength for the two water depth cases. Again, note that the design loads are

lower for the 25-m depth case for the 50-year and 100-year storms because of the absence of breaking loads for the 25-m case. The operating loads (about a 1-year storm) for the 25-m depth case are larger due to the larger level arm of the deeper case; note that the base shear is similar in magnitude because the hub height remains unchanged and the minor difference can be attributed to nominally larger hydrodynamic loads for the deeper water case. The utilization ratios are similar in the two depth cases, and this confirms the observation that the monopile design is largely driven by resonance avoidance and results in higher-than-needed ultimate strength per design loads.

**Table 16. Design Load Comparison for Monopile in 25-m Depth to 15-m Depth (from Phase I)**

Storm Type	Monopile 15-m water depth		Monopile 25-m water depth	
	Base Shear (kN)	Mudline Overturning Moment (MN-m)	Base Shear (kN)	Mudline Overturning Moment (MN-m)
Operating	2,450	113	2,549	130
50-year	6,740	142	4,136	99
100-year	6,910	153	5,264	112

**Table 17. Utilization Ratio Comparison for Monopile in 25-m Depth to 15-m Depth (from Phase I)**

	Based on API RP2A		Based on IEC / ISO	
	Power Production <sup>a</sup>	Parked/Idling	Power Production <sup>b</sup>	Parked / Idling
Monopile at 15-m water depth	0.570	0.605	0.433	0.595
Monopile at 25-m water depth	0.529	0.395	0.402	0.343

<sup>a</sup> Without one-third allowable stress increase factor

<sup>b</sup> With the same load and material factors from parked/idling condition

## 7.2 Jacket versus Monopile at 25-m water depth site

The next two figures, 47 and 48, show the mudline overturning moments for jackets (denoted “Jkt”) compared to monopile (denoted “Mp”) for a select set of return periods. The following observations can be made from these exhibits:

- The jacket loads are substantially smaller than the monopile loads for each return period.
- The 100-year jacket load is similar to the 1-year monopile loads, meaning again that jacket loads are much smaller than the monopile loads.
- The effect of shallow-water breaking waves appears much more pronounced for the monopile compared to the jacket. (Compare the large increase in the monopile load from  $H_s$  of 9.5 m to 13.7 m versus that of the jacket.)

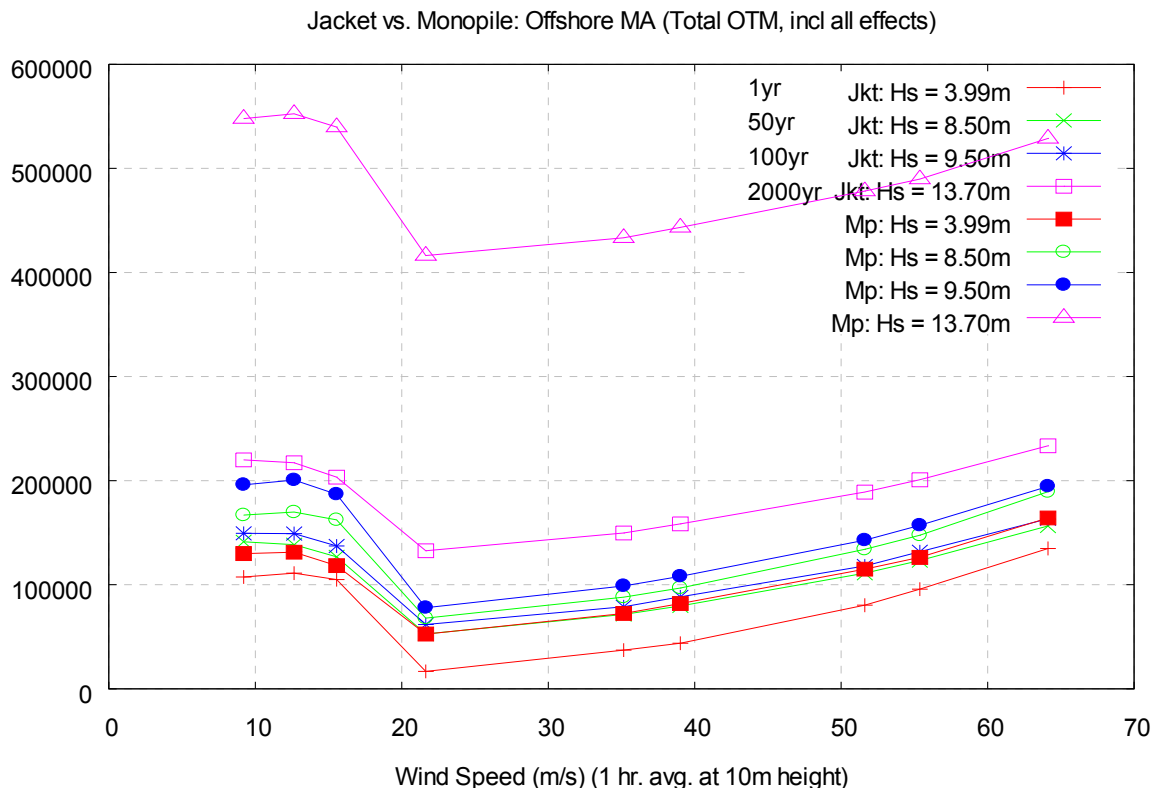


**Figure 47. Jacket vs. monopile loads for 25-m water depth for key return periods as a function of wind speed**

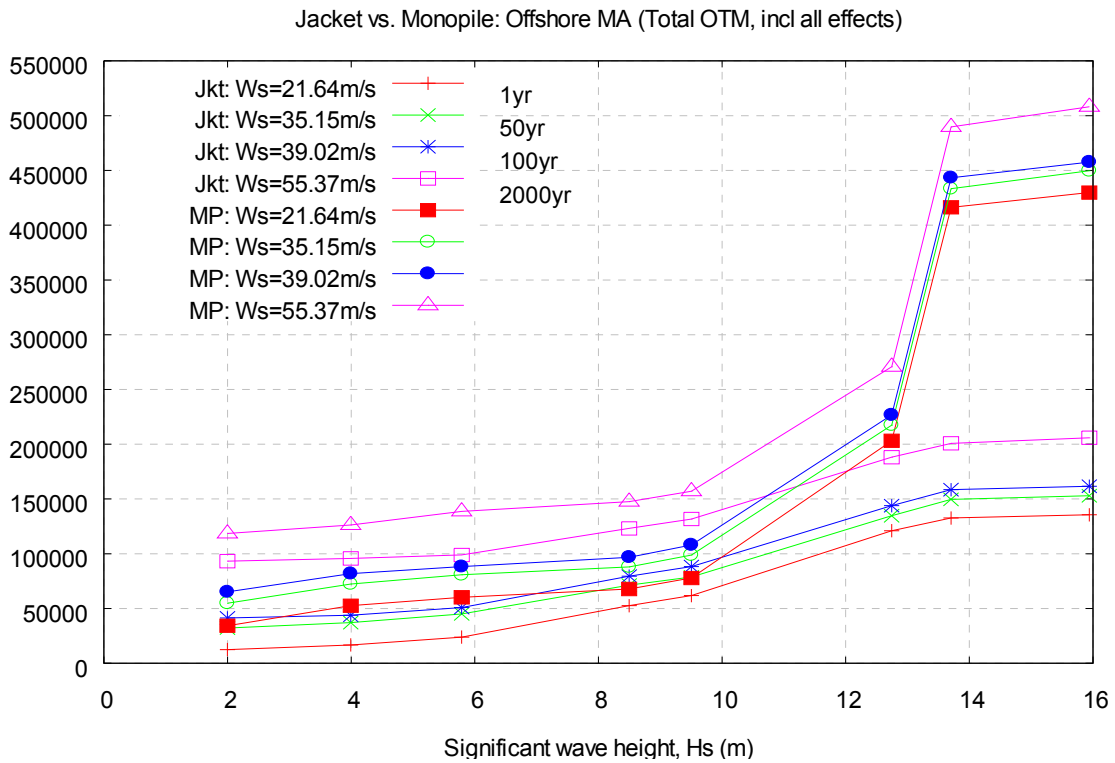


Figure 48. Jacket vs. monopile loads for 25-m water depth for key return periods as a function of significant wave height

### 7.3 Overall Comparison

Table 18. Comparison of reliability index of monopile to jacket

	Monopile	Jacket
Controlling Condition	Fatigue	Fatigue and strength
Utilization Ratio	0.5 (operating case/storm) 0.4 (parked case, extreme storm)	1.0 (operating case/storm) 0.8 (parked case, extreme storm)
Reliability Index, $\beta$	5.8	5.4
Conclusion	The monopile design likely <b>cannot</b> be optimized much due to fatigue resonance constraint	The jacket design <b>can</b> likely be optimized further to achieve $\beta=4$ (or an appropriate value) and still avoid resonance

## 8 Summary and Conclusions

This study has included a comparison of API RP-2A (the standard used by BSEE for the regulation of offshore structures in OCS waters) and the IEC 61400-3 (a new standard developed by an international committee specifically to address the design requirements for OWT support structures). This review has included a direct comparison of the standards in order to provide an assessment of their applicability to the design of typical wind turbine support structures in U.S. OCS waters.

### 8.1 Key Findings

#### 8.1.1 Effect of Breaking Waves

The shallow-water wave effects related to wave breaking occur in a much more severe storm for 25-m water depth compared to the 15-m depth. For the 25-m depth, wave breaking effects appear in a 1000-year storm versus wave breaking seen for only 25-year storms for the 15-m depth (in Phase I). At the 15-m depth site, wave breaking occurs in smaller storms compared to the 25-m site; owing to this effect, slam loads occur in smaller storms at the 15-m depth than at the 25-m depth. In these smaller storms, then, the total loads end up being larger at the 15-m depth than at the 25-m depth, implying the criticality of shallow-water effects on load calculation and the effect of water depth on the onset of wave breaking.

#### 8.1.2 Effect of Change in Water Depth on Monopiles

For the 25-m depth site, a longer pile penetration is generally needed to achieve resonance avoidance for the soil profile assumed (60 m for a 25-m water depth, versus 50 m for a 15-m depth in Phase I<sup>12</sup>). Additionally, a larger-diameter pile, was adopted for resonance avoidance (6.5 m for the 25-m depth, versus 6 m in Phase I). For smaller storms, the loads are similar for the two water depths, ignoring the difference in diameters for the monopiles used in the two phases. The design storm loads (i.e., for operating storms and for 50- and 100-year storms) have been reduced for the monopile because of the increase in water depth and the delay in the onset of breaking waves to storms with a return period 1000 years or greater. As compared to the phase I results, the 25-m monopile design was somewhat larger in diameter (6.5 m versus 6 m) to provide the stiffness required for resonance avoidance. The storm and operation wave load demands have been reduced from that of the more shallow-water case study because of the elimination of the breaking wave condition for the design event and because of some reduction in wave particle velocity for deeper water.

#### 8.1.3 Effect of Structure Type on Loads, Design, and Reliability

The design and extreme loads on the jacket structure are much less than on the monopile because of the jacket's more transparent profile. The primary difference between the jacket and monopile is in the load transfer mechanism between the structure and foundation. The jacket obtains its foundation fixity through compression and tension; the monopile achieves fixity through bending and soil bearing. In the storms with breaking waves, the jacket sees much smaller slam loads, again owing to its more transparent profile. The monopile design is predominantly constrained by resonance avoidance and cannot be optimized much for ultimate strength considerations (i.e.,

---

<sup>12</sup> Note that these pile penetration lengths are indicative of the design selected, and do not necessarily represent optimized designs in which the penetration length is optimized for minimal cost, for example.

the monopile ends up with high ultimate strength versus design loads). The jacket, however, can be optimized for both resonance avoidance and for ultimate strength to achieve a more “balanced” design for both of these design criteria.

## 8.2 Recommendations

The results of this study, complemented with the experience from the oil and gas industry, lead to the following recommendations for further study.

- Develop a comprehensive tool for use by the offshore wind industry to perform a coupled aerodynamic and hydrodynamic load analysis, including the effects of soil structure interaction and breaking wave effects (strength and fatigue).
- Develop recommendations for OWTs using a large-diameter monopile foundation for appropriate development of drag and inertia forces from hydrodynamic loads, for estimation of loads from breaking waves, and for appropriately characterizing the soil-structure interaction to include large-diameter effects.
- Quantify uncertainties associated with large pile/column effects (load and soil-pile interaction) for inclusion in an overall safety-level assessment.
- Study fatigue reliability for OWTs, especially from loads resulting from breaking waves for sites with shallow waters.
- Include fatigue reliability over the design life of the structure and ultimate strength reliability as part of a systems reliability assessment of OWTs.
- Develop an understanding of the implications of structural frequencies approaching blade frequency and other nacelle-related frequencies to be avoided. Assess the implications of uncertainty in installed OWT frequencies on structure dynamic behavior and the resulting change in safety levels.
- Study the effect of variation of turbine size for design loads and fatigue and ultimate strength to understand consequent effects on system reliability.
- Develop an appropriate safety level (reliability index) that would be acceptable by regulatory agencies and the offshore wind industry for OWTs in U.S. waters. This can be done via specification of safety factors in the design guidelines that would apply to U.S. waters.

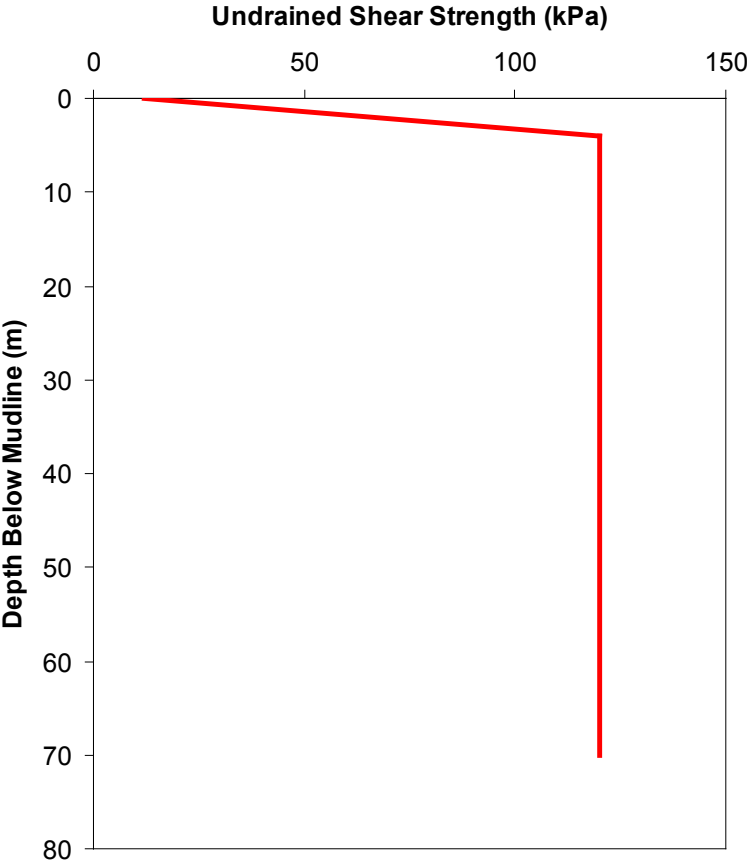
These recommendations are intended to be used to develop a comprehensive view of all of the engineering issues involved in OWT design, and then to develop a robust design guideline applicable to U.S. waters.

## References

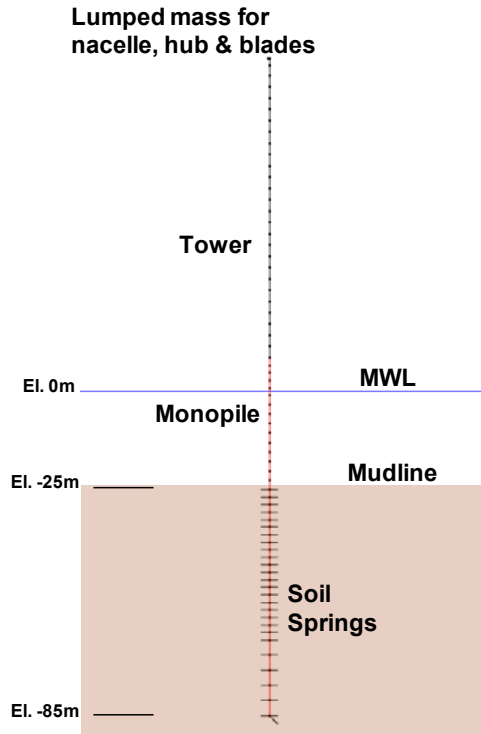
1. Jonkman, J., *Dynamics Modeling and Loads Analysis of an Offshore Floating Turbine*, National Renewable Energy Laboratory, Technical Report NREL/TP-500-41958, November 2007.
2. Argyriadis, K., Gill, L. and Schwartz, S., “Loads for Offshore Wind Turbines; the 2<sup>nd</sup> edition of the GL Wind Guideline”, 2004.
3. International Electrotechnical Commission (IEC), IEC 61400-3 Ed.1, Wind Turbines – Part 3: Design requirements of offshore wind turbines, IEC TC 88 WG3 Committee Draft, December 2005.
4. American Petroleum Institute (API), Recommended Practice for Planning, Designing and Constructing Fixed Offshore Platforms-Working Stress Design, API RP-2A-WSD, 21<sup>st</sup> Edition 2000.
5. Comparative Study of OWTG Standards (prepared for JIP sponsorship), MMI Engineering, March 2009.
6. A.K. Jha, W. Musial, C. Smith, D. Dolan. “On Hurricane Risk to Offshore Wind Turbines in US Waters”. Paper No. 20811. Offshore Technology Conference, Houston, Texas, 3-6 May, 2010.

# Appendix A: Soil Springs in the Analyses

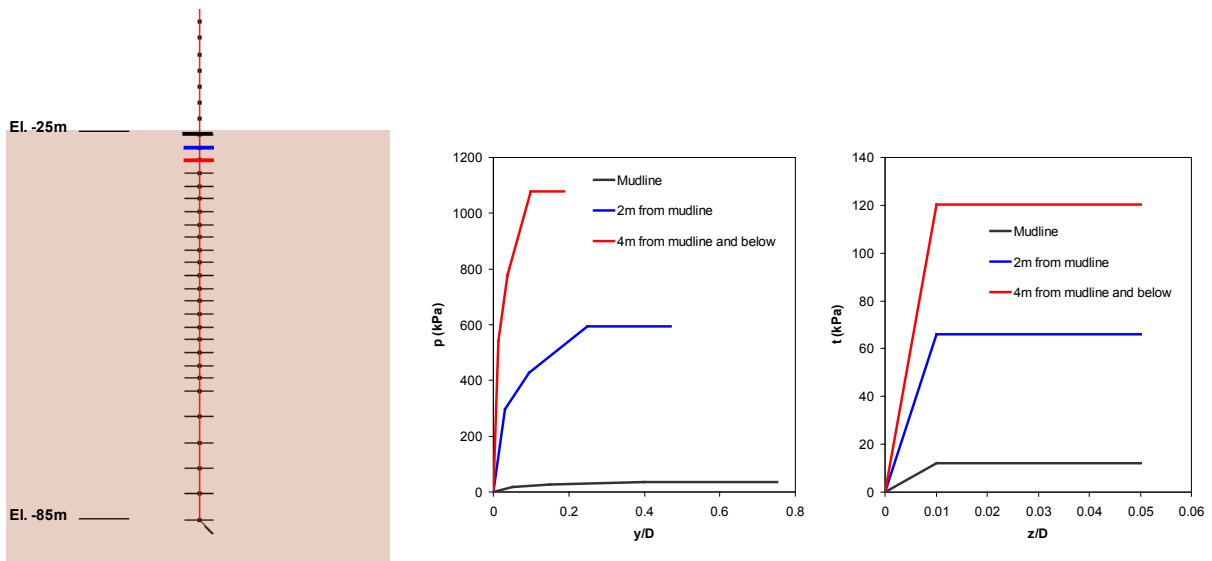
The shear strength profile used in this phase of the study is shown below. The profile belongs to a clay site where the shear strength linearly increases from 12 kPa to 120 kPa in the top 4-m portion and then remains constant below that. This profile was adopted from an earlier MMI project. Note that this is the same as the profile used in the earlier analyses.



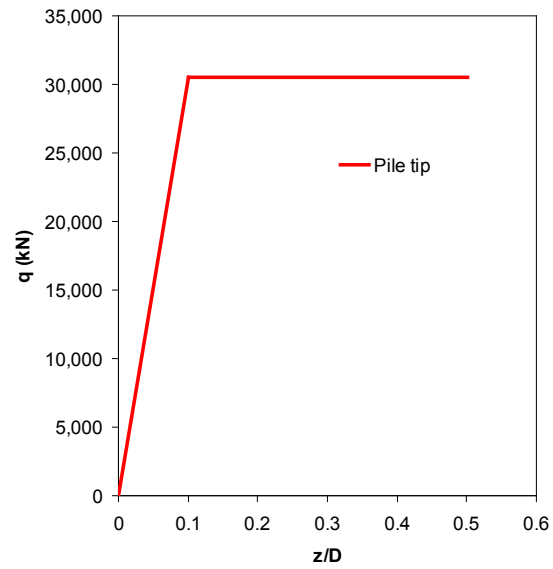
The monopile and the jacket models developed for this study include soil springs to properly capture the soil-structure interaction. There are two types of soil springs in the models: (1) lateral springs, commonly known as p-y springs; (2) vertical springs. These springs were distributed along the pile as shown below. The vertical springs along the pile are called t-z springs, whereas the spring at the bottom tip is called a q-z spring.



The properties of the soil springs were obtained using the equations provided in API RP2A 21<sup>st</sup> ed. The force-displacement curves of the top three lateral (p-y) and vertical (t-z) springs are provided below. Given the soil profile is uniform below 4 m under mudline, the spring properties also remain constant in that section.



The tip spring ( $q$ - $z$ ) is shown next. Note that the vertical axis is expressed in stress units in the  $t$ - $z$  plots, whereas it is expressed in force units in the  $q$ - $z$  plot.



## Appendix B: Drag and Inertia Coefficients for Large Diameter Turbine Components

The calculations below are performed using the approach outlined in API RP2A Section C2.3.1.b7.

Monopile diameter= 6.5 m

*Assumptions:*

- 25-m water depth
- 1.1-m surge
- 15-m wave height with 11 s period
- 0.4-m/s uniform current
- Above high-tide level (smooth), average peak-to-valley height of hard growth,  $k = 0.05 \text{ mm}$ ; relative surface roughness,  $e = k/D = 0.05\text{E-}3 \text{ m} / 6.5 \text{ m} = 8\text{E-}6$

Maximum water particle velocity normal to the cylinder axis,  $U_m = 10.2 \text{ m/s}$

Wave period,  $T = 11 \text{ s}$

Keulegan-Carpenter Number,  $K = U_m T / D = 10.2 \times 11 / 6.5 = 17.3$

*Below high-tide level (rough surface drag and inertia):*

$$C_{ds} = 1.0$$

$$K / C_{ds} = 17.3 / 1.0 = 17.3 \rightarrow C_d / C_{ds} = 1.4 \text{ (Figure C2.3.1-5)}$$

$$C_d = 1.4 \times 1.0 = 1.4$$

$$K / C_{ds} = 17.3 \rightarrow C_m = 1.2 \text{ (Figure C2.3.1-8, "rough" curve)}$$

*Above high-tide level (smooth):*

$$e = 8\text{E-}6 \rightarrow C_{ds} = 0.64 \text{ (Figure C2.3.1-4)}$$

$$K / C_{ds} = 17.3 / 0.64 = 27.0 \rightarrow C_d / C_{ds} = 1.2 \text{ (Figure C2.3.1-5)}$$

$$C_d = 1.2 \times 0.64 = 0.77$$

$$K / C_{ds} = 27.0 \rightarrow C_m = 1.6 \text{ (Figure C2.3.1-8, "smooth" curve)}$$

*Summary:*

	Rough	Smooth
$C_d$	1.4	0.77
$C_m$	1.2	1.6

*Equivalent Monopile Properties for FAST Analyses:*

A wave analysis (with 10-m wave with 10-s period) was performed in CAP using a model of a 6-m monopile with the actual  $C_d/C_m$  values calculated, shown previously, per API RP2A. The total base shear and the overturning moment histories are shown in the figures below as a target. Then the wave analysis was repeated for the cases of “ $C_d=1.0; C_m= 0$ ” and “ $C_d= 0; C_m=1.0$ ” . The results of these analyses are shown in the plots with the blue and the pink curves. The equivalent monopile with uniform properties was estimated to match the base shear and overturning moment histories. The unit  $C_d$  and the unit  $C_m$  analyses were added to each other in various proportions until the total overturning moment matched the target curve. The best result was obtained for the  $1.03C_d + 1.30C_m$  case (shown in the plots below). The maximum overturning moment was matched 100%. The maximum base shear is 5.6% below the target.

As a result, the drag and inertia coefficients that are applicable to the equivalent monopile analyses with FAST analyses are as follows:

$$C_d = 1.03$$

$$C_m = 1.30$$

## Appendix C: Study on Sensitivity of Load Results to the Number of Simulations

The coupled wave and wind load analysis was performed for a number of simulations because of the stochastic nature of the turbulent wind load. For each simulation, the maximum shear force and overturning moment were obtained throughout the time-history. The mean of these maximum values was used for the reliability assessment of the structure. The figures below show that, for all the operating wind speeds and all wave heights, enough accuracy is achieved after 10 simulations.

One can observe that after two simulations the variation is 4%, 5%, and 15% for the  $W_s=9.2$ , 12.7, and 15.6 m/s respectively. The variation drops to 2%, 3%, and 5% after five simulations. This level of variation was considered to be significant. Therefore, 10 simulations were performed to achieve an acceptable level of accuracy.

